

**TOUGHENING MECHANISMS IN COMPOSITES OF  
MISCIBLE POLYMER BLENDS WITH RIGID FILLER PARTICLES**

by

ROGER LOCKWOOD ARONOW

Bachelor of Science, Chemical Engineering  
University of California, Santa Barbara, California, 2000

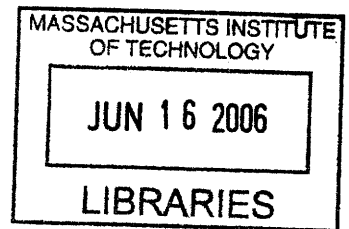
Master of Science, Chemical Engineering Practice  
Massachusetts Institute of Technology, Cambridge, Massachusetts, 2002

Submitted to the Department of Chemical Engineering  
in partial fulfillment of the requirements for the degree of

DOCTOR OF PHILOSOPHY IN CHEMICAL ENGINEERING

at the  
MASSACHUSETTS INSTITUTE OF TECHNOLOGY

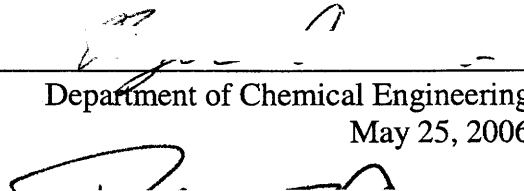
JUNE 2006



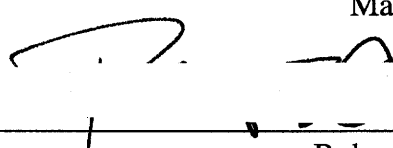
© 2006 Massachusetts Institute of Technology. All rights reserved.

ARCHIVES

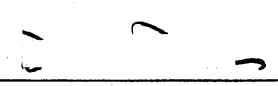
Signature of Author: \_\_\_\_\_

  
Department of Chemical Engineering  
May 25, 2006

Certified by: \_\_\_\_\_

  
Robert E. Cohen  
St. Laurent Professor of Chemical Engineering  
Thesis Advisor

Accepted by: \_\_\_\_\_

  
William M. Deen  
Carbon P. Dubbs Professor of Chemical Engineering  
Chairman, Committee for Graduate Students

# Toughening Mechanisms in Composites of Miscible Polymer Blends with Rigid Filler Particles

by  
Roger Lockwood Aronow

Submitted to the Department of Chemical Engineering on May 25, 2006  
in partial fulfillment of the requirements for the degree of  
Doctor of Philosophy in Chemical Engineering

## ABSTRACT

Fillers are often added to polymers improve stiffness at the cost of reduced toughness, but this tradeoff is not universal. Well-dispersed microscopic particles have been shown to improve toughness and stiffness simultaneously in some cases. The effect depends on interparticle distance as well as interfacial adhesion. This type of toughening has been more successful in semicrystalline than in amorphous systems.

An amorphous polymer blend was chosen to elucidate the effect of matrix properties on the toughening mechanism. The ternary blend of PMMA, PVC, and DOP (a common plasticizer) was characterized using TEM, and was found to be miscible over much of the PVC-rich domain. The blend  $T_g$ 's fit well to an empirical model, which was used to predict a constant- $T_g$  ( $\sim 40^\circ\text{C}$ ) blend series. Mechanical testing showed a wide, systematic variation in properties among these blends, although all were brittle in tension.

The blend 90% PVC / 10% DOP was mixed with barium sulfate filler and evaluated for toughness in slow tension. In general, the composites showed decreasing toughness with increasing filler content. However, several specimens at 5 vol% filler exhibited a large increase in ductility and toughness ( $\sim 19$ -fold). SEM examination of tough specimens revealed several important findings: (1) Filler is present both as micron-scale agglomerates and as well dispersed particles. (2) Well-dispersed particles remain bonded to the matrix even for large deformations. (3) Filler agglomerates are prone to debonding and internal fracture, creating void space and enabling deformation.

Base blend properties significantly affect the response to filler. The blend 8% PMMA / 80% PVC / 12% DOP showed small increases in ductility for 5 and 10 vol% filler, with the best result being a 10 vol% specimen showing a 6-fold toughness increase over the neat-blend average. This specimen showed similar microscopic behavior to the 90/10 blend, i.e. agglomerate debonding and fracture, but to a lesser degree. The blend 16% PMMA / 70% PVC / 14% DOP, showed no significant toughening. Also investigated were high- $T_g$  ( $\sim 70^\circ\text{C}$ ) blends, which were brittle and became weaker with filler, and low- $T_g$  ( $\sim 30^\circ\text{C}$ ) blends, which were intrinsically ductile and were not toughened by filler.

Thesis Supervisor: Robert E. Cohen, St. Laurent Professor of Chemical Engineering

## ACKNOWLEDGEMENTS

I am deeply grateful for the unfailing support of my advisor, Prof. Robert Cohen. Through the ups and downs of this project, he was always ready with new ideas and words of encouragement. My thesis committee, Profs. Mary Boyce, Gareth McKinley, Paula Hammond, and Kenneth Beers, have all provided useful advice that made this thesis the best it could be.

I am greatly indebted to my mentors within the Cohen group. Jeff Abes and Tom Wang helped introduce me to grad student life even before I joined the group. Doctors Pam Bryant, Young Jun Lee, Russell Gorga, and Chunxia He provided invaluable assistance during their stays. And of course, Yonathan Thio taught me vital skills in the lab and has served as my example of what a graduate researcher ought to be.

My lab mates Ed, Michelle, Heejae, Prem, Adam, Sharon, Ben, Daeyeon, Ryan, and Andy have all helped in various ways large and small. They taught me techniques, kept me up to date with the literature, helped me find what I needed, and generally made the lab a pleasant place to work. Thanks also to mechanical engineers Adam Mulliken, Ethan Parsons, Nuo Sheng, Nici Ames, and Sai Sarva, and to Dr. Anuj Bellare of Brigham and Women's Hospital, for their assistance and advice.

Sincere thanks are due to MIT Staff members Tim McClure, Tony Garratt-Reed, Mike Frongillo, Patrick Boisvert, Fred Cote, Peter Morley and the entire Central Machine Shop, Jeff Baur, Steve Kooi, Cathy Byrne, Joanne Maxwell, Elaine Aufiero, Janet Fischer, Suzanne Easterly, Mary Wesolowski, Iris Chang, Patsy Sampson, Alina Haverty, Danielle Delgado, Carrie Casado, Una Sheehan, Annie Fowler, and Steve Wetzal. If I tried to list the ways they have helped me, this would be the longest chapter in my thesis.

I could not have remained sane through all this without a great group of friends. I feel I have made more lasting friendships at MIT than in any other stage of my life. My thanks and curses to Chopster, who dragged me into the world of poker, and to Sparky, Karlaj, G Money, and the rest of the Boston Poker Tour, who took my money until I got the hang of it. Practice School companions Heather, Nick, Yue, Ben, Bharat, Jamie, and Zhendi helped me make the best of a painful process. Fellow first-years Tom, Paul, Meegan, Brian, and Frank commiserated with me over late-night problem sets and bore with me when I got cranky. Floorball friends Jari, Mats, Ron, Knut, Ole, Amelia, Anton, Liz, Wojtek, and Sami taught me a great new sport and kept me in shape. And Sanj, Kristin, Myrn, Theis, and Jake have provided the moments of fun and weirdness that make life worthwhile.

Finally, I am thankful for the love and support of my family. My parents Abraham and Alice, my brother Adam, and my grandmother Jane have provided with me outstanding role models for my life. My East Coast family, aunt Rita, uncle Nadav, and cousins Amitai and Rebecca have made me feel at home here in New England. And Mary Beth, thank you for sharing the good times and sticking with me in the bad.

This work was funded by the AFOSR DURINT program.

# CONTENTS

<b>ABSTRACT.....</b>	<b>2</b>
<b>1. INTRODUCTION.....</b>	<b>8</b>
1.1. Overview of Polymer Property Improvement.....	8
1.2. Mechanisms of Polymer Toughening .....	11
1.2.1. Critical Ligament Thickness .....	11
1.2.2. Plastic Resistance and Preferential Matrix Crystallization .....	12
1.2.3. Adhesion and Debonding.....	14
1.3 Amorphous Matrix Properties.....	16
1.4. Thesis Outline .....	18
<b>2. CHARACTERIZATION OF PMMA – PVC – DOP TERNARY BLEND SYSTEM .....</b>	<b>19</b>
2.1. Introduction .....	19
2.2. Experimental .....	20
2.2.1. Material Preparation.....	20
2.2.2. Thermomechanical Characterization.....	21
2.2.3. Mechanical Property Measurement.....	21
2.3 Results .....	23
2.3.1. Preliminary Experiments.....	23
2.3.2. Model Validation.....	31
2.3.3. Constant-T <sub>g</sub> Blend Series .....	32
2.4. Discussion .....	37
2.4.1 Blend Miscibility and Phase Structure.....	37
2.4.2 Property Prediction and Variation.....	39
<b>3. HARD-PARTICLE TOUGHENING .....</b>	<b>42</b>
3.1. Hard-Particle Toughening Criteria.....	42
3.1.1. Particle Dispersion .....	42
3.1.2. Debonding .....	44
3.1.3. Particle Size Effect on Debonding .....	44
3.2. Experimental .....	46
3.2.1. Material Preparation.....	46
3.2.2. Thermomechanical Characterization.....	46
3.2.3. Mechanical Property Measurement.....	47
3.2.4 Electron Microscopy and Particle Size Analysis .....	47
3.3. Results .....	50
3.3.1 Thermomechanical Characterization.....	50
3.3.2 Mechanical Property Measurement.....	51
3.3.3 Electron Microscopy and Particle Size Analysis .....	55
3.4. Discussion .....	61
3.4.1 Effect of Well-Dispersed Particles.....	61
3.4.2 Effect of Agglomerates .....	63
3.4.3 Contrast between Compressive and Tensile Behavior.....	63

<b>4. MATRIX PROPERTY INFLUENCE .....</b>	<b>65</b>
4.1. Effect of Matrix Properties on Toughenability .....	65
4.2. Experimental .....	68
4.2.1. Material Preparation.....	68
4.2.2. Thermomechanical Characterization.....	68
4.2.3. Mechanical Property Measurement.....	69
4.2.4 Electron Microscopy and Particle Size Analysis .....	69
4.3 Results .....	70
4.3.1 Middle- $T_g$ Series .....	70
4.3.2 High- $T_g$ Series .....	76
4.3.3 Low- $T_g$ Series.....	81
4.3.4 Peculiarities of High-PMMA Ternary Blends .....	83
4.4 Discussion .....	90
<b>5. CONCLUSION .....</b>	<b>92</b>
5.1. Summary of Thesis Contributions .....	92
5.2. Future Work .....	94
<b>BIOGRAPHICAL NOTE .....</b>	<b>96</b>
<b>REFERENCES.....</b>	<b>97</b>

## INDEX OF FIGURES

Figure 1-1: Uniaxial Tension Experiment.....	8
Figure 1-2: Izod Impact Experiment .....	9
Figure 1-3: Impact Strength of Nylon-Rubber Blends .....	12
Figure 2-1: Phase Diagram for PMMA-PVC-DOP System .....	24
Figure 2-2: Transmission Electron Micrographs of Binary Blends .....	25
Figure 2-3: DSC Traces for Binary Blends .....	26
Figure 2-4: Transmission Electron Micrographs of Ternary Blends with ~5 wt% DOP .....	27
Figure 2-5: DSC Traces for Ternary Blends with ~5 wt% DOP .....	28
Figure 2-6: Transmission Electron Micrographs of Ternary Blends with ~10 wt% DOP .....	29
Figure 2-7: DSC Traces for Ternary Blends with ~10wt% DOP .....	30
Figure 2-8: Constant-T <sub>g</sub> Blends Shown on Ternary Phase Diagram .....	32
Figure 2-9: Transmission Electron Micrographs of Constant-T <sub>g</sub> Blend Series .....	33
Figure 2-10: DSC Traces for Constant-T <sub>g</sub> Blends.....	33
Figure 2-11: Compression Stress-Strain Curves for Constant-T <sub>g</sub> Blends.....	34
Figure 2-12: Compression Properties for Constant-T <sub>g</sub> Blends .....	35
Figure 2-13: Tensile Properties for Constant-T <sub>g</sub> Blends .....	36
Figure 3-1: Example of Particle Size Analysis.....	49
Figure 3-2: DSC Results for Filled Blends.....	50
Figure 3-3: DMA Results for Filled Blends .....	51
Figure 3-4: Compression Results for Filled Blends .....	53
Figure 3-5: Tension Curves for Filled Blends .....	53
Figure 3-6: Tensile Properties for Filled Blends .....	54
Figure 3-7: SEM Images of Cryo-Fractured Strand, 5 vol% Composite.....	55
Figure 3-8: SEM Images of Cryo-Fractured Composite Strands.....	56
Figure 3-9: Characterization of Well-Dispersed Filler Particles .....	57
Figure 3-10: Histogram of Agglomerate Sizes in Composite Materials.....	58
Figure 3-11: SEM Views for Mechanical Test Specimens.....	59
Figure 3-12: SEM Photos of Brittle Tensile Specimens, 5 vol% Composite .....	59
Figure 3-13: SEM Photos of Ductile Tensile Specimens, 5 vol% Composite.....	60
Figure 3-14: SEM Photos of Compression Specimen, 5 vol% Composite.....	60
Figure 3-15: Tensile Moduli vs. Guth Model Predictions .....	62
Figure 3-16: Comparison of Compressive and Tensile Moduli for Filled Blends.....	64
Figure 4-1: Tensile Results for Composites of Blend 7.8/80/12.2.....	72
Figure 4-2: SEM of Tensile Specimens – 10 vol% Composite of Blend 7.8/80/12.2.....	72
Figure 4-3: Tensile Results for Composites of Blend 15.6/70/14.4.....	73
Figure 4-4: Tensile Properties for Middle-T <sub>g</sub> Composites .....	74
Figure 4-5: Compressive Properties for Composites of Blend 7.8/80/12.2 .....	74
Figure 4-6: Compressive Properties for Composites of Blend 15.6/70/14.4 .....	75
Figure 4-7: Compressive Properties for Middle-T <sub>g</sub> Composites .....	75
Figure 4-8: Tensile Properties for Composites of PVC.....	77
Figure 4-9: Compressive Properties for Composites of PVC.....	78
Figure 4-10: Tensile Properties for Composites of Blend 36/57.5/6.5 .....	78
Figure 4-11: Compressive Properties for Composites of Blend 36/57.5/6.5 .....	79
Figure 4-12: Tensile Properties for High-T <sub>g</sub> Composites.....	80
Figure 4-13: Compressive Properties for High-T <sub>g</sub> Composites .....	80
Figure 4-14: Tensile Curves for Composites of Blend 0/85/15.....	82
Figure 4-15: Tensile Properties for Composites of Blend 0/85/15 .....	82
Figure 4-16: Compressive Properties for Composites of Blend 0/85/15 .....	83
Figure 4-17: Morphology of High-PMMA Blends .....	84
Figure 4-18: Morphology of High-PMMA Composite .....	84
Figure 4-19: Effect of Processing Conditions on Morphology.....	85
Figure 4-20: PMMA Beads.....	87
Figure 4-21: Characterization of Dark Regions.....	87
Figure 4-22: Effect of Processing Conditions on MDSC Behavior.....	88
Figure 4-23: Morphology of Heavily-Filled Composites .....	89
Figure 4-24: Tensile Behavior of Heavily-Filled Composites.....	89

## INDEX OF TABLES

Table 1-1: Critical Thickness Values for Various Polymers.....	11
Table 2-1: Polymer Properties .....	20
Table 2-2: DSC Results for PMMA-PVC Blends.....	24
Table 2-3: DSC Results and Model Predictions .....	31
Table 2-4: Model Parameters.....	31
Table 2-5: Model Confirmation.....	31
Table 2-6: Constant- $T_g$ Blend Series .....	32
Table 2-7: Predicted values for entanglement molecular weight in constant- $T_g$ blend series .....	40
Table 3-1: Compressive Properties for Filled Blends .....	52
Table 3-2: Tensile Properties for Filled Blends .....	54
Table 3-3: Characteristics of Well-Dispersed Filler Particles .....	56
Table 4-1: Properties of Middle- $T_g$ Blends.....	71
Table 4-2: Mechanical Properties of Middle- $T_g$ Composites.....	71
Table 4-3: Properties of High- $T_g$ Blends .....	76
Table 4-4: Mechanical Properties of High- $T_g$ Composites .....	77
Table 4-5: Properties of Low- $T_g$ Blends .....	81
Table 4-6: Properties of Composites Based on Blend 0/85/15 .....	81

# 1. INTRODUCTION

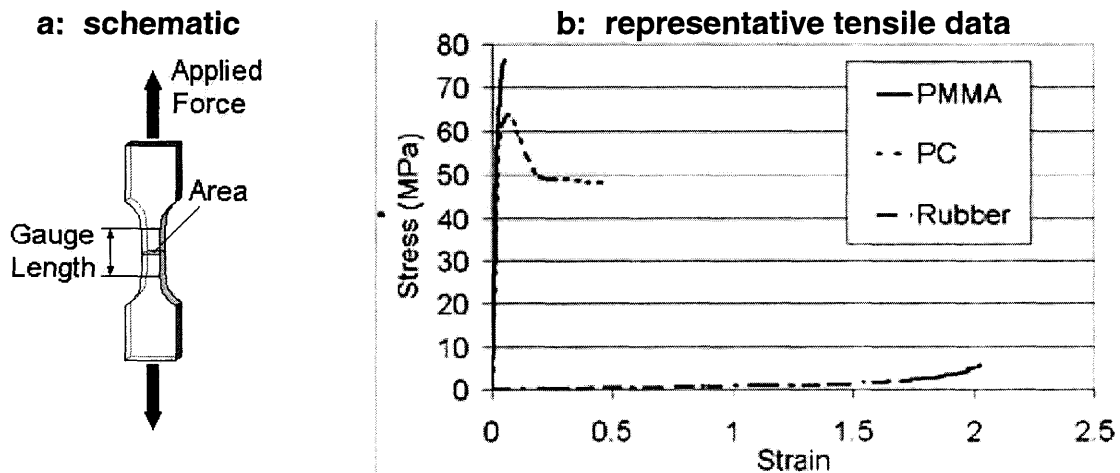
## 1.1. Overview of Polymer Property Improvement

Improvement of polymer properties is an area of ongoing practical interest. Polymeric materials are used in an extremely diverse range of applications, ranging from adhesives to gas separation membranes to structural components. With each application comes a different set of required properties, and product developers must be able to either modify existing materials or synthesize new materials to meet these requirements. For the former option, a thorough understanding of structure-property relationships is essential. Countless investigators have worked to elucidate these relationships.

Several figures of merit are used to characterize the mechanical properties of materials. Young's modulus is a measure of stiffness, the amount of stress needed to create a small recoverable (elastic) deformation. Yield strength is the stress needed create an irrecoverable (plastic) deformation. Flow stress is that needed to steadily stretch the material beyond the yield point. Figure 1-1a shows a schematic of a tensile experiment, and Figure 1-1b shows typical measurements for brittle (PMMA), ductile (PC), and rubbery polymers in tension.

**Figure 1-1: Uniaxial Tension Experiment**

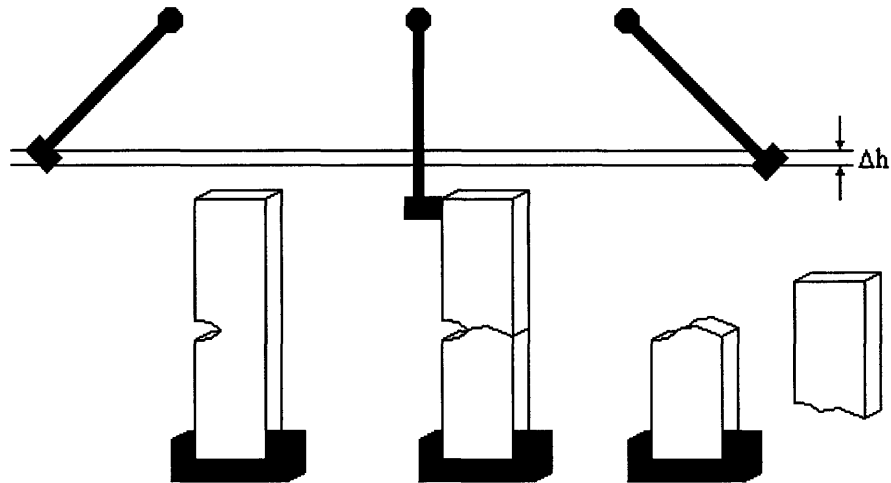
PMMA [1], PC [2], and Rubber [3]





Toughness expresses the amount of energy needed to fracture a specimen of material. It is highly dependent not only on material properties, but on strain rate, temperature, sample geometry, and pre-existing flaws. For this reason, many different techniques are used to measure it. At one end of the spectrum, toughness can be measured in a low-rate experiment such as that illustrated in Figure 1-1a. In this case, toughness is computed from the area under the stress-strain curve. Hence, even though the glassy polymer reaches higher stresses during deformation, the ductile polymer is much tougher. Toughness can also be measured at high rate to simulate impact conditions. Figure 1-2 illustrates the Izod test, one common measurement for high-rate fracture behavior. In this method, a pendulum hammer impacts a notched specimen of material; the difference in potential energy is used to calculate the amount of energy absorbed by the material.

**Figure 1-2: Izod Impact Experiment**



In many cases, the most efficient method for modifying polymer properties is by mixing them with other materials. They can be mixed with different polymers to create a blend, with

small molecules called plasticizers, or with nonpolymeric particles or fibers to create a composite. Particulate fillers are generally more rigid than the polymers to which they are added, thus enhancing the overall modulus, but also tend to make the material more brittle, reducing the toughness. Plasticizers make polymers softer and more flexible, reducing the modulus while increasing toughness.

Polymer blends can be either homogeneous or heterogeneous. In homogeneous blends, the polymer chains mix intimately to form a single phase, and the properties are generally in between those of the homopolymers. However, homogeneous polymer blends are rare due to thermodynamic factors. Mixing of small molecules is primarily driven by an entropy increase, which results from the addition of possible configurations. A polymer molecule, when considered as an interconnected chain of small molecules, clearly has fewer possible arrangements than for the case of unconnected units. Even if the chain is put into a sea of small molecules, it does not gain many possible configurations since the units must remain within the proximity dictated by the size of the polymer. For this reason, polymer molecules have little entropic driving force for mixing with one another, and so only polymer pairs with strong enthalpic interactions between their functional groups will form a homogenous blend. More commonly, the blend will separate into multiple phases, and the morphology of a heterogeneous blend has strong implications for its properties. Most often the less abundant component will form spherical droplets dispersed in a matrix of the more abundant polymer, and the size of these droplets will depend on both thermodynamic (e.g., interfacial energy) and kinetic (e.g., mixing time) factors. By forming chemical bonds between polymer chains of different types (e.g., block copolymers), the blend can be forced to assume a cylindrical, lamellar, or bicontinuous morphology.

## 1.2. Mechanisms of Polymer Toughening

### 1.2.1. Critical Ligament Thickness

One common technique for modifying the properties of a hard thermoplastic is the addition of soft particles, e.g. rubber, to form a second phase in the material. Well-dispersed rubber particles have long been known to increase the toughness of relatively brittle polymers, such as polystyrene, albeit at the cost of reduced stiffness. Wu [4] demonstrated in a nylon-rubber blend that the crucial factor for toughening was the average interparticle distance, rather than interfacial area or particle concentration. The blends in the study exhibited a sharp increase (~10-fold) in toughness and a visible (via SEM) change in microscopic deformation behavior as particle size was decreased. This transition from brittle to tough behavior occurred at different particle sizes  $d$  for different rubber concentrations, but collapsed to a single abscissa value when toughness was plotted against interparticle distance  $t$  (see Figure 1-3), as computed from

$$t = d \left\{ \left( \pi / (6\phi_r) \right)^{1/3} - 1 \right\}$$

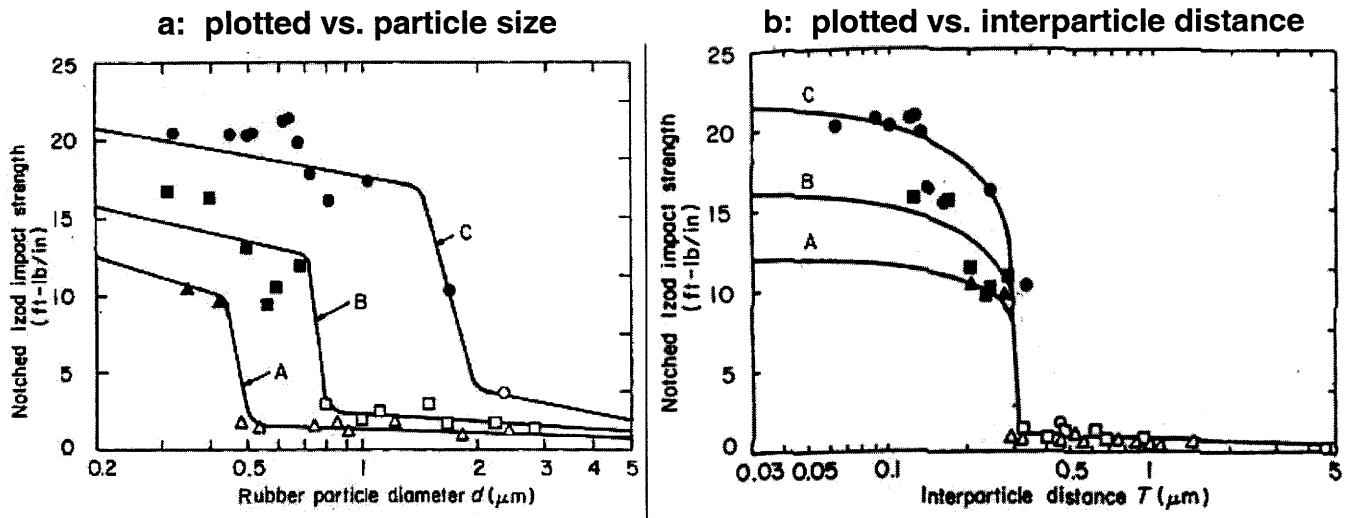
The critical value for the ligament thickness has been shown to be a property of the thermoplastic matrix. Some literature values of  $t_c$  are listed in Table 1-1.

**Table 1-1: Critical Thickness Values for Various Polymers**

Polymer	Critical Thickness in $\mu\text{m}$	Source
Nylon-6,6	0.304	[4]
Polystyrene	0.05	[5]
High-Density Polyethylene	0.6	[6]
Polypropylene	0.27	[7]

**Figure 1-3: Impact Strength of Nylon-Rubber Blends**

Curve A: 10wt% rubber; Curve B: 15wt%; Curve C: 25wt% [4]



The importance of interparticle distance has also been demonstrated in polymers filled with hard particles. Bartczak et al. [8] investigated HDPE modified alternately with hydrocarbon rubber particles and with calcium carbonate particles. In both general cases and for all particle sizes, it was observed that impact toughness increased sharply when the average ligament thickness dropped below  $0.6 \mu\text{m}$ . This reinforces the assertions that (1) interparticle distance is the primary factor determining toughness in particle-modified thermoplastics; and (2) the critical value of interparticle distance, below which material behavior becomes tough, is a material property of the matrix, and is independent of the particle properties or the particle-matrix interaction.

### 1.2.2. Plastic Resistance and Preferential Matrix Crystallization

It is generally accepted that in order for particle toughening of a brittle polymer to be successful, one must effect a widespread reduction in plastic resistance [9]. Wu [4] hypothesized that the critical interparticle distance he observed in rubber-modified nylon was due to a strong

overlap of the stress fields surrounding the rubber inclusions, which would lead to enhanced yielding. He later proposed an alternative explanation for cases of small interparticle distance, in which the proximity of rubber particles shifts the stress state of the matrix from plane strain to plane stress. Muratoglu et al. [10] argued that both explanations are insufficient because they rely on changes in geometrical ratios which depend only on rubber volume fraction and geometrical dispersion, and not on particle size.

Muratoglu et al. [10] showed using transmission electron microscopy and X-ray scattering that at the nylon-rubber interface, the crystalline lamellae tend to orient perpendicular to the particle surface. In regions far from particles, the lamellae are randomly oriented, as is the case in bulk nylon. Hence, in blends with widely spaced rubber particles, the matrix morphology is largely unaffected by the presence of the inclusions, and so the overall behavior is similar to bulk nylon, i.e. brittle. However, when the particles are closely spaced, the oriented-lamellar morphology dominates the matrix behavior. It has been shown that the (001) plane has by far the lowest slip resistance in nylon 6 crystallites [11]. This plane is oriented perpendicular to the longitudinal axis of the lamella and parallel to the surface of the rubber particle. Thus, when oriented lamellae percolate the matrix, the interparticle matrix ligaments are able to yield and stretch much more readily than in bulk nylon.

The observation of preferential crystallization gives a clear mechanism to explain the phenomenon critical thickness in semicrystalline polymer systems, but it does not explain why the critical thickness also applies in amorphous systems such as polystyrene [5]. From Table 1-1, we see that semicrystalline polymers tend to have higher critical thickness values than amorphous polymers, and that in general the critical thickness seems to drop as the chains become less regular. HDPE is simply a hydrocarbon backbone, nylon adds functional groups,

and PP and PS add progressively bulkier side groups. This may imply that similar aspects of chain mobility influence both crystallization and particle toughening, or that toughening occurs more readily in the presence of oriented crystallites. In any case, some other mechanism must be occurring to facilitate toughening in polystyrene and other amorphous polymers.

### 1.2.3. Adhesion and Debonding

Sources disagree as to the importance of interfacial adhesion for toughening behavior in polymer-filler systems. Wu [4] argues that strong adhesion is necessary to ensure toughness, and shows as evidence that in nylon filled with non-adhering rubber, no tough behavior was observed, while use of adhering rubber led to toughening of 25- to 60-fold over unmodified nylon. The concentrations of the two rubber types were similar (approx 10, 15 , and 25 weight %), but the particle size range was much smaller for the non-adhering particles ( $d_n$  ranged from 24 to 26  $\mu\text{m}$  for non-adhering rubber and 0.31 to 2.42  $\mu\text{m}$  for adhering rubber). Using adhering particles, Wu estimated the critical interparticle distance to be approximately 0.3  $\mu\text{m}$ . As the interparticle distances for non-adhering rubber blends did not drop below 1  $\mu\text{m}$ , this argument is not convincing.

Contradictory evidence is presented by van der Sanden and coworkers [5], who investigated blends of polystyrene with two different types of core-shell rubber. The weakly adhering rubber (PMMA shell, SBR core) was used successfully to toughen PS, while strongly adhering rubber (PS shell, SBR core) did not toughen PS significantly at similar volume fractions and particle sizes. These results suggest that particles that adhere too tightly to the matrix can actually prevent toughening. Since the true source of toughness in such systems is

plastic drawing of the interparticle ligaments, it is plausible that factors impeding ligament stretching, e.g. strong adhesion of inclusions, would tend to reduce toughness.

Similar evidence for hard particle filled systems is presented by Thio [12]. In this study, polypropylene was modified with three different varieties of glass beads, each with a different surface treatment. Hydrocarbon-modified glass adhered strongly to the matrix, and did not give measurable toughening. Fluorocarbon-modified glass adhered weakly, and gave significant toughening. Glass modified with a mixture of hydrocarbon and fluorocarbon gave an intermediate result. Using dilatometry in conjunction with a tensile testing, it was shown that significant volume strain developed as the fluorocarbon-glass composites were stretched. This suggests that the particles were detaching, or debonding, from the polymer matrix, and that voids were forming around them. These voids left the material as a network of thin polymer ligaments stretching independently.

### 1.3 Amorphous Matrix Properties

Polymers that do not readily crystallize are classified as amorphous. Common examples include polystyrene, poly(methyl methacrylate), and poly(vinyl chloride). Instead of a sharp transition from solid to liquid as temperature increases, linear amorphous polymers undergo a gradual change from solid-like (“glassy”) to viscoelastic (“rubbery”) behavior. The characteristic temperature at which this transition occurs is a material property denoted as the glass transition temperature, or  $T_g$ . Common methods for measuring  $T_g$  include differential scanning calorimetry (DSC), which distinguishes the change in heat capacity that occurs at the glass transition, and dynamic mechanical analysis (DMA), which shows a drop in stiffness at the glass transition. The  $T_g$  value depends strongly on the method used, as well as test parameters such as DSC temperature ramp rate and DMA oscillation frequency. In general, higher rates and frequencies allow the material less time to respond to the stimulus, and hence tend to shift the appearance of  $T_g$  to later in the experiment.

A bulk sample of linear amorphous polymer can be pictured as a spaghetti-like mass of flexible molecules. Although they do not have crystallites or chemical crosslinks to hold the structure together, they exhibit cohesion due to the points where chains cross one another, or entanglements. The molecular weight between entanglements, denoted  $M_e$ , is another important material property, reflecting the looseness of the chain network.  $M_e$  is inversely proportional to the plateau modulus  $G_N^0$ , which reflects the cohesiveness of the material, by the relation

$$M_e = \frac{\rho RT}{G_N^0}$$

where  $\rho$  is the density,  $R$  is the gas constant, and  $T$  is the temperature [13]. Plateau modulus is commonly measured via shear rheology.



The properties of the amorphous matrix have a strong effect on the toughening behavior in composite materials. Meijer et al. [14] investigated a series of polystyrene-poly(2,6-dimethyl-1,4-phenylene ether) blends modified with rubber particles. They showed that the entanglement density of the PS-PPE blend varies in a roughly linear fashion over the composition range, and that the critical interparticle distance follows a similar trend. A polymer blend could similarly be used as a matrix for the study of hard-particle toughening. The primary advantage of this approach is the ability to vary the properties of the amorphous matrix in a systematic way without otherwise changing the nature of the material.

## **1.4. Thesis Outline**

This thesis explores the issue of toughening in amorphous polymer blends using rigid filler particles. The objective is to utilize the versatility of the blend system in order to identify the matrix properties that have the strongest effects on toughenability. The polymer matrix is a ternary blend of poly(vinyl chloride), poly(methyl methacrylate), and dioctyl phthalate, a plasticizer. The filler is submicron, roughly spherical barium sulfate particles coated with citrate to reduce agglomeration. Chapter 2 shows characterization and empirical modeling of the blend system. Chapter 3 focuses on a single blend composition with various proportions of filler. Chapter 4 expands the investigation to include several different matrix materials with widely varying mechanical and thermal properties. Chapter 5 concludes and gives possible directions for future work in this area.

## **2. CHARACTERIZATION OF PMMA – PVC – DOP TERNARY BLEND SYSTEM**

### **2.1. Introduction**

The miscibility of the poly(methyl methacrylate) (PMMA) – poly(vinyl chloride) (PVC) blend has been extensively studied in the past several decades. The system is of interest because both components are used extensively as commercial thermoplastics. The dominant factors dictating their miscibility are the tacticity of the PMMA and the thermal treatment used in making the blend. Most studies have found that isotactic PMMA is incompatible with PVC [15, 16], although some found limited compatibility for i-PMMA with lower MW and/or moderate concentrations of iso-triads [17, 18]. Syndiotactic and atactic PMMA can be successfully blended with PVC either through solution blending or through melt mixing below the system's lower critical solution temperature [15-19].

Plasticizers are small-molecule compounds added to thermoplastics in order to impart greater flexibility. Di(2-ethylhexyl) phthalate, better known as dioctyl phthalate (DOP), is commonly used to plasticize PVC. In this study, DOP is added to the PMMA-PVC system to form a ternary blend. Some recent work has been published on the miscibility, mechanical properties, and degradation behavior of this system [20].

The utility of this ternary blend derives from the extra degree of freedom in composition space. This allows the creation of a series of blends with, for example, constant  $T_g$  and widely varying mechanical properties. The present chapter focuses on characterizing the miscibility and mechanical properties of this system. Later chapters will investigate the effect of properties such as yield strength, strain hardening, and entanglement density on the hard-particle toughenability of amorphous polymers.

## 2.2. Experimental

### 2.2.1. Material Preparation

The research-grade PMMA and PVC used in this study were produced by Scientific Polymer Products, and the properties provided by the manufacturer are listed in Table 2-1. The PVC discussed below is actually a blend of 97 wt% as-received polymer and 3 wt% organotin heat stabilizer (Thermolite 890F, generously provided by Atofina Corp). The DOP was obtained from Sigma-Aldrich.

**Table 2-1: Polymer Properties**

Provided by manufacturer					
Polymer	Form	$M_w$ (g/mol)	Density (g/cm <sup>3</sup> )	$T_g$ (°C)	Solubility Parameter
PVC	powder	90,000	1.40	85	9.53
PMMA	beads	35,000	1.20	105	9.3

All blends produced in this study were made by first hand-mixing PVC powder with stabilizer, hand-mixing this blend with appropriate quantities of PMMA beads and liquid DOP, and then compounding the mixture in a bench-scale twin-screw extruder (Daca MicroCompounder with co-rotating screws, screw speed 100 RPM, 2 min mixing time, temperature approximately  $T_g + 120^\circ\text{C}$ ). The extruded strands were used directly for differential scanning calorimetry (DSC) and transmission electron microscopy (TEM). Extruded material was also compression molded into dumbbell-shaped specimens for uniaxial tension, and into plaques, which were then machined to make cylindrical plugs for uniaxial compression. Compression molding was done at approximately the extrusion temperature and 10,000 psi.

### 2.2.2. Thermomechanical Characterization

Modulated DSC (MDSC) was performed on a TA Instruments DSC Q1000. A thorough explanation of MDSC is provided by Thomas [21]. The operating principle is that by superimposing an oscillation on a standard DSC temperature ramp, the instrument can distinguish between reversible and non-reversible heat effects. Reversible heat effects are identified as changes in the baseline heat capacity of the material (i.e., glass transitions), while non-reversible heat effects are identified as kinetic events (e.g., crystallization, decomposition, chain relaxation). Thus, when measuring the glass transition temperature ( $T_g$ ) of these blends, only the reversible heat flows were considered.

All MDSC runs began with an annealing step at least  $10^\circ\text{C}$  above the highest component  $T_g$  (PVC  $\sim 70^\circ\text{C}$ , PMMA  $\sim 117^\circ\text{C}$ ) for 20 min, followed by rapid cooling to sub-ambient temperature and then a temperature ramp. The ramp rate was  $2^\circ\text{C}/\text{min}$ , the period of the oscillation was 60 sec, and the amplitude was automatically set to  $0.32^\circ\text{C}$  to maintain heat-only mode.

The homogeneity of several blends was confirmed via using a JEOL 200CX transmission electron microscope. Extruded polymer strands were sectioned using a diamond knife and then mounted on copper grids. It has been shown previously [22] that the phase structure of PMMA-PVC blends can be seen in TEM without addition of contrast agents, presumably due to the high electron density of chlorine atoms in PVC.

### 2.2.3. Mechanical Property Measurement

Uniaxial compression experiments were performed on a servohydraulic Zwick/Roell Z010 mechanical tester. Compression-molded, machined plugs approximately

3 mm in height and 6 mm in diameter were placed between plates lubricated with a thin layer of hydrocarbon oil, compressed at constant engineering strain rate to the maximum allowable load (9000 N), and then unloaded at the same strain rate.

Uniaxial tension testing was performed on the same instrument. An extensometer was used to monitor the length of the gauge section while the specimens were pulled at a constant engineering strain rate. The specimens were compression-molded dumbbells with a gauge section approximately 1.5 mm thick, 4 mm wide, and 13 mm long.

## 2.3 Results

### 2.3.1. Preliminary Experiments

In order to map out the PMMA-PVC-DOP phase space, a small number of blends were first produced and characterized. A combination of TEM and DSC data allowed the creation of the schematic phase diagram shown in Figure 2-1. For comparison, results from a literature source [20] are plotted as well. The results are qualitatively similar, but disagree somewhat as to the border of the two-phase region.

$T_g$  measurements of miscible blends from MDSC were used to develop an empirical model of the form

$$T_g = C_0 + C_1 F_{\text{PMMA}} + C_2 F_{\text{PVC}} + C_3 (F_{\text{PMMA}})^2 + C_4 (F_{\text{PVC}})^2 + C_5 F_{\text{PMMA}} F_{\text{PVC}} \quad (2-1)$$

where  $\{F_i\}$  are polymer weight fractions in the blend and  $\{C_j\}$  are model parameters. The dependence on DOP content is implicit in the model, since  $F_{\text{DOP}} = 1 - F_{\text{PMMA}} - F_{\text{PVC}}$ . The equation may be rearranged as

$$T_g = (C_0 + C_1 + C_3) + (-C_1 + C_2 - 2C_3 + C_5) F_{\text{PVC}} + (-C_1 - 2C_3) F_{\text{DOP}} \\ + (C_3 + C_4 - C_5) (F_{\text{PVC}})^2 + C_3 (F_{\text{DOP}})^2 + (2C_3 - C_5) F_{\text{PVC}} F_{\text{DOP}}$$

to show the dependence explicitly. This model was used to predict several series of blends with constant  $T_g$ . The compositions and  $T_g$ 's of the initial blends are listed in Table 2-3, and the model parameters are listed in Table 2-4.

**Figure 2-1: Phase Diagram for PMMA-PVC-DOP System**

Squares are TEM results; × & + are DSC results from ref [20]

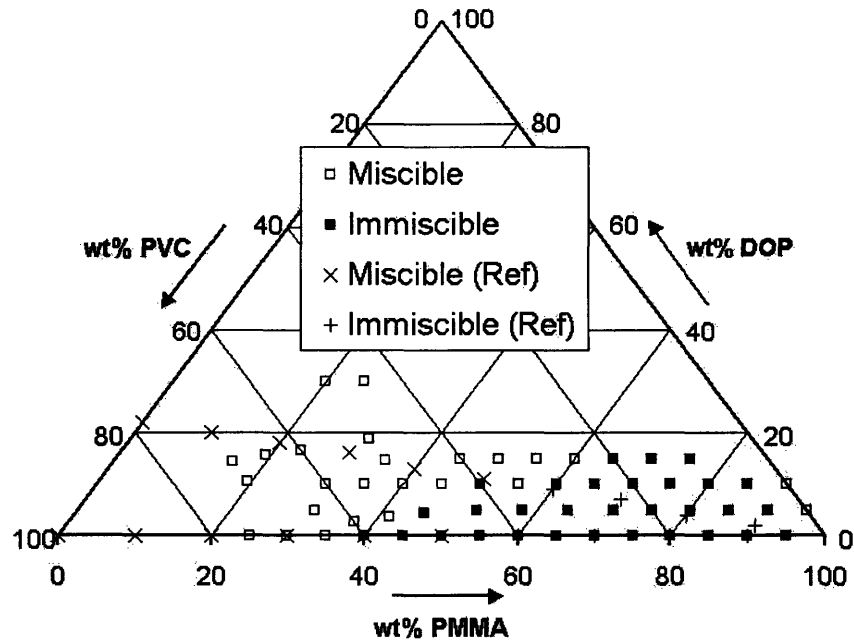


**Table 2-2: DSC Results for PMMA-PVC Blends**

Ref results are from [20]

PMMA	PVC	$T_g(1)$	by	$T_g(1)$	by	$T_g(2)$	by	$T_g(2)$
wt%	wt%	°C	MDSC	°C	DSC (ref)	°C	MDSC	°C
0	100	74.63		83.00		-		-
10	90			84.00				-
20	80			84.50				-
25	75	85.21				-		
30	70	87.79		85.00		-		-
35	65	90.06				-		
40	60	90.59		85.80		-		-
45	55	92.40				-		
50	50	94.26		96.00		-		-
55	45	94.17				-		
60	40	93.86		88.70				112.40
65	35	94.73				116.88		
70	30	95.30		96.00		116.91		113.00
75	25	94.84				117.52		
80	20	93.87		100.50		115.27		113.60
85	15	95.76				116.22		
90	10	95.69		103.50		116.32		114.50
95	5	97.71				115.60		
100	0	-		-		117.80		115.00



### Figure 2-2: Transmission Electron Micrographs of Binary Blends

Labels are composition in wt% PMMA/PVC; each image shows a 1-micron square.

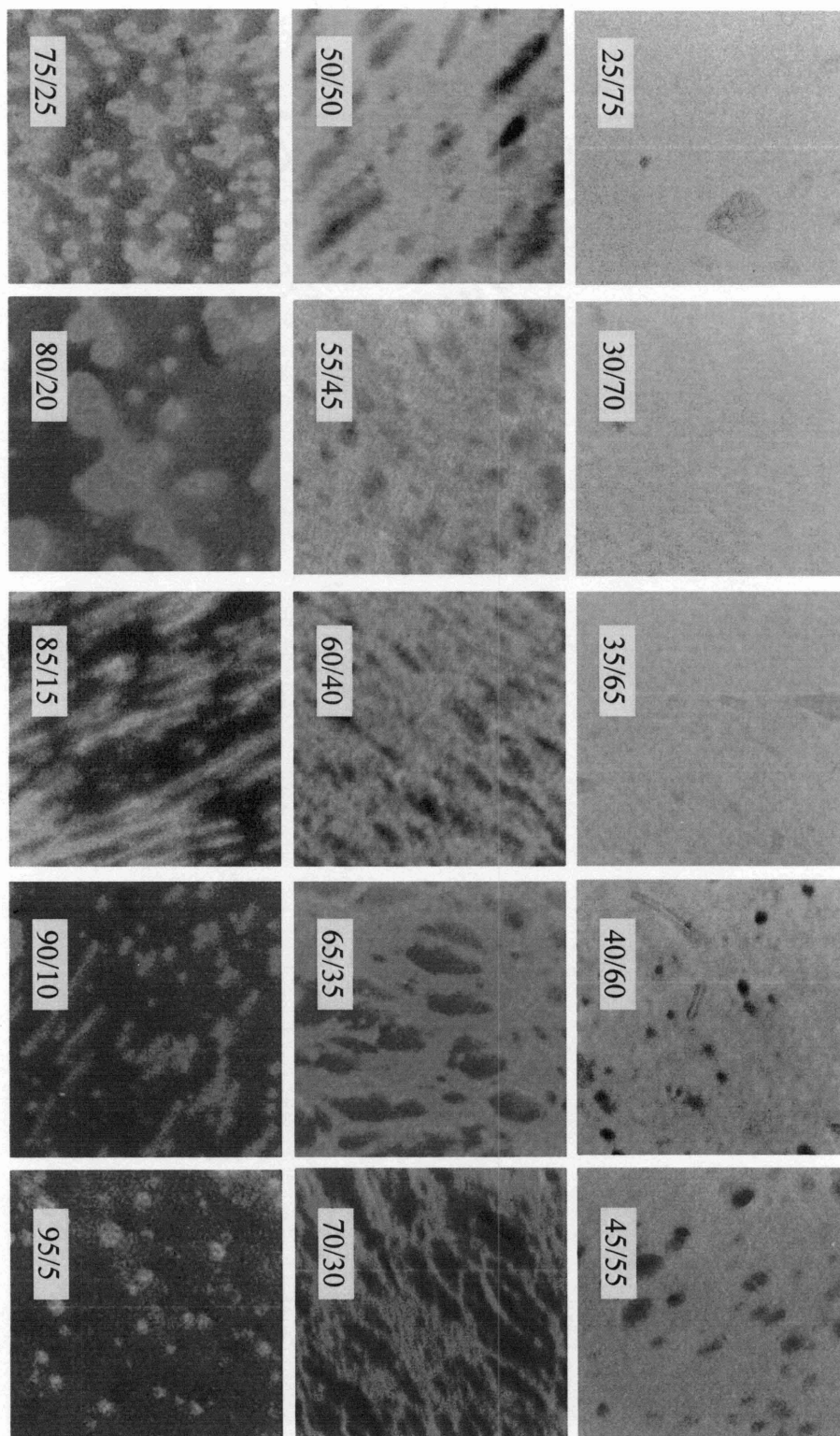


### Figure 2-3: DSC Traces for Binary Blends

Labels are composition in wt% PMMA/PVC; all tests carried out at 2°C/min, with an initial annealing step (see Methods).

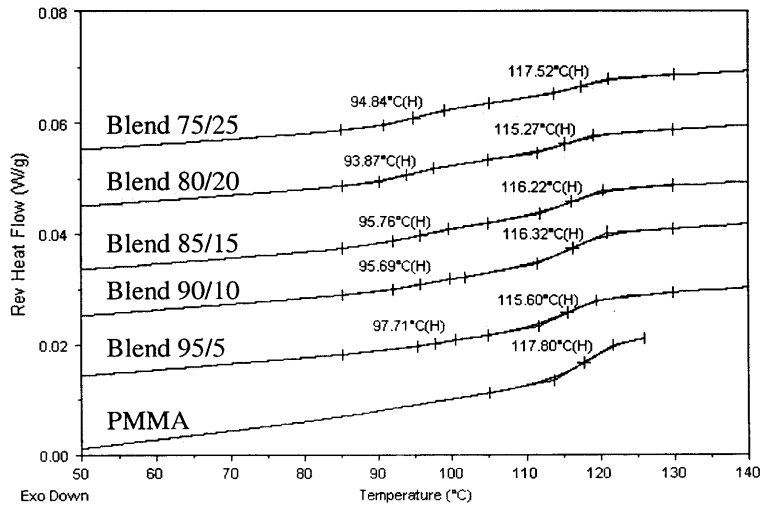
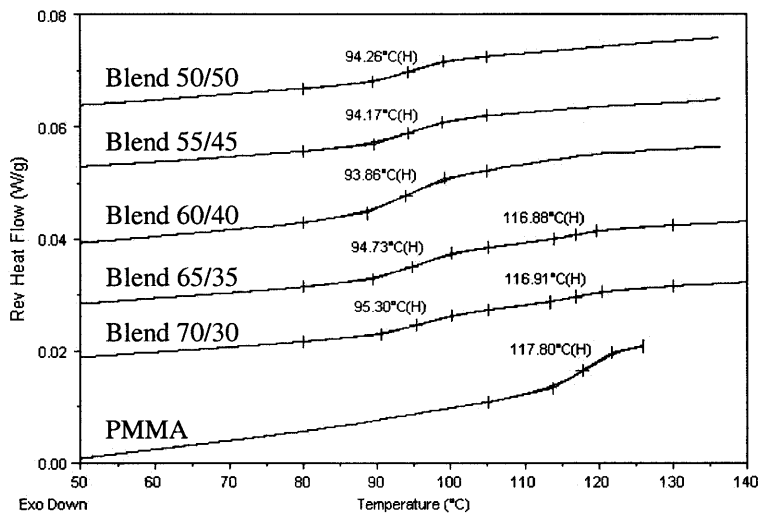
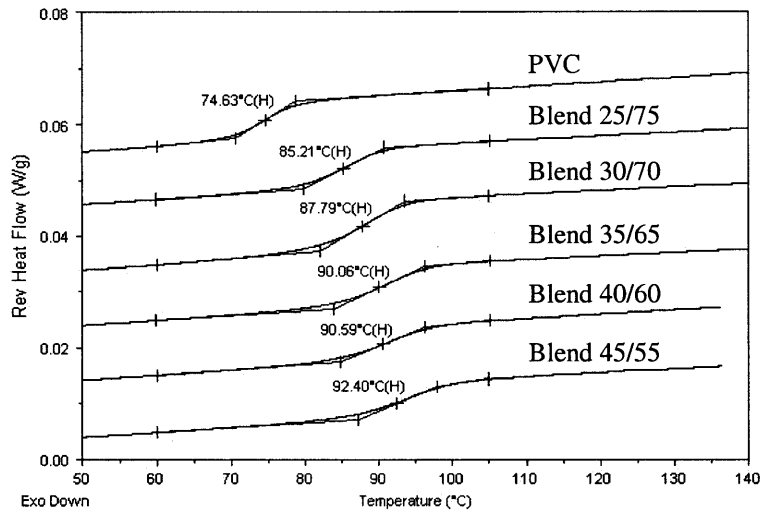


**Figure 2-4: Transmission Electron Micrographs of Ternary Blends with ~5 wt% DOP**  
Labels are composition in wt% PMMA/PVC/DOP; each image shows a 1-micron square.

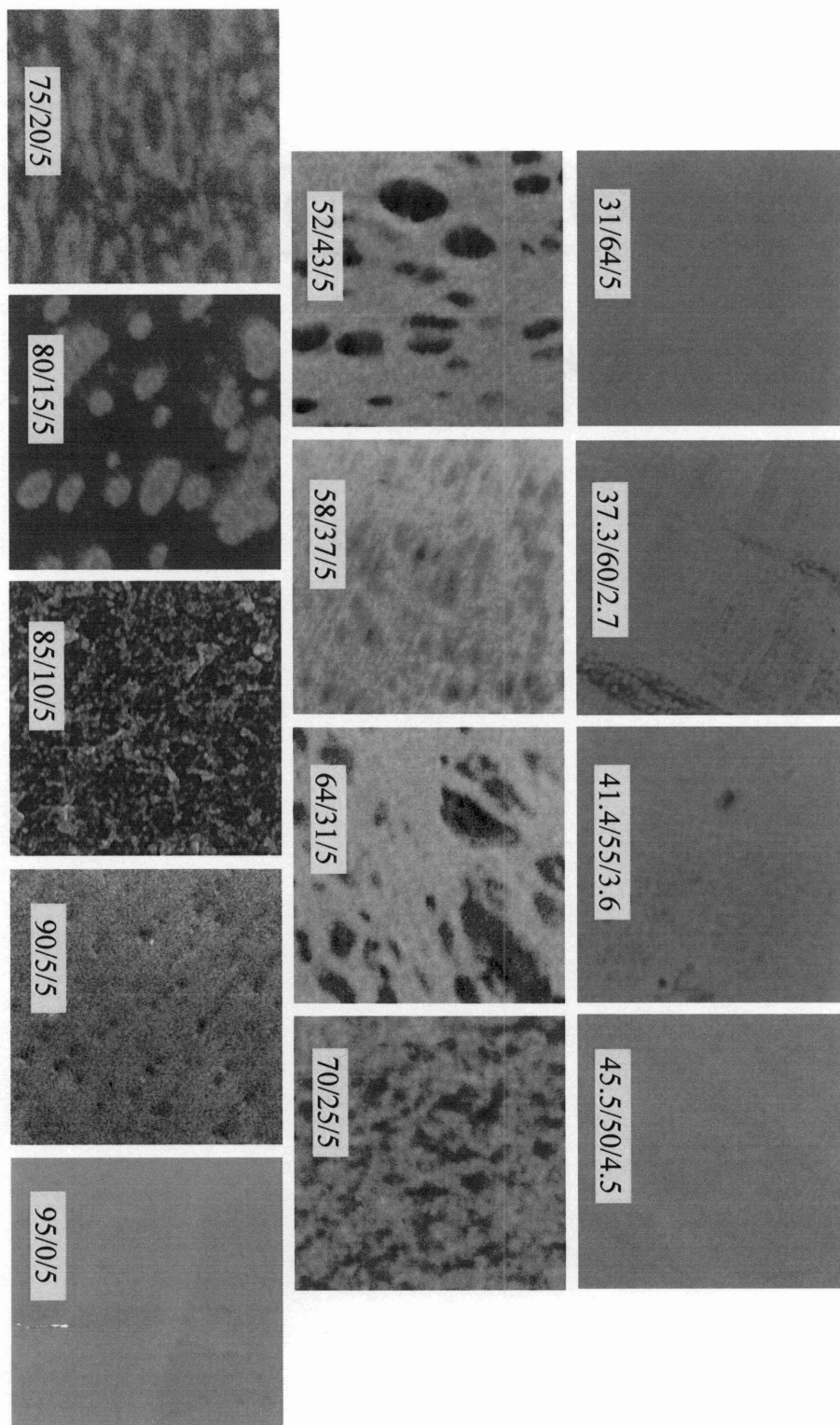


### Figure 2-5: DSC Traces for Ternary Blends with ~5 wt% DOP

Labels are composition in wt% PMMA/PVC/DOP; all tests carried out at 2°C/min, with an initial annealing step (see Methods)

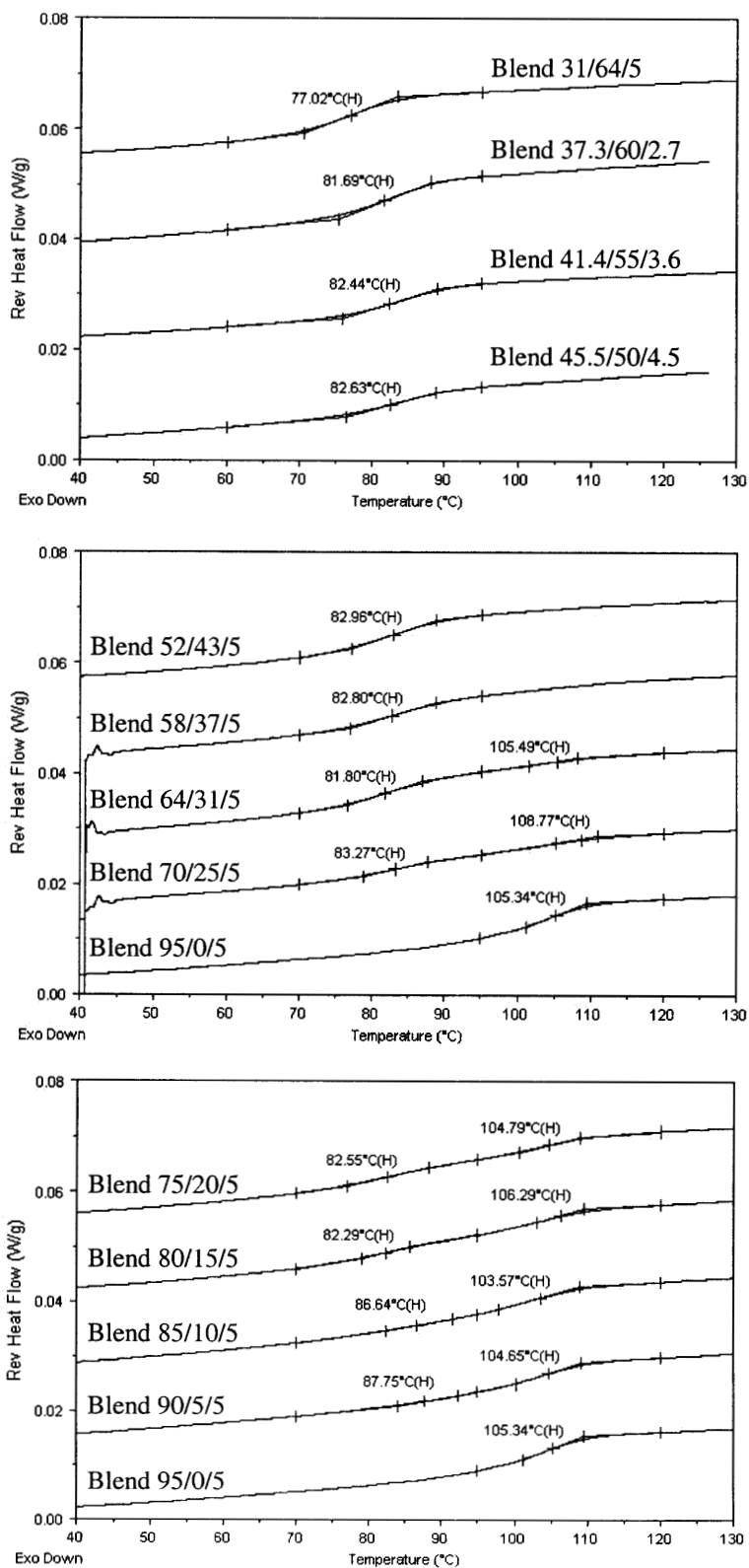


**Figure 2-6: Transmission Electron Micrographs of Ternary Blends with ~10 wt% DOP**

Labels are composition in wt% PMMA/PVC/DOP; each image shows a 1-micron square.

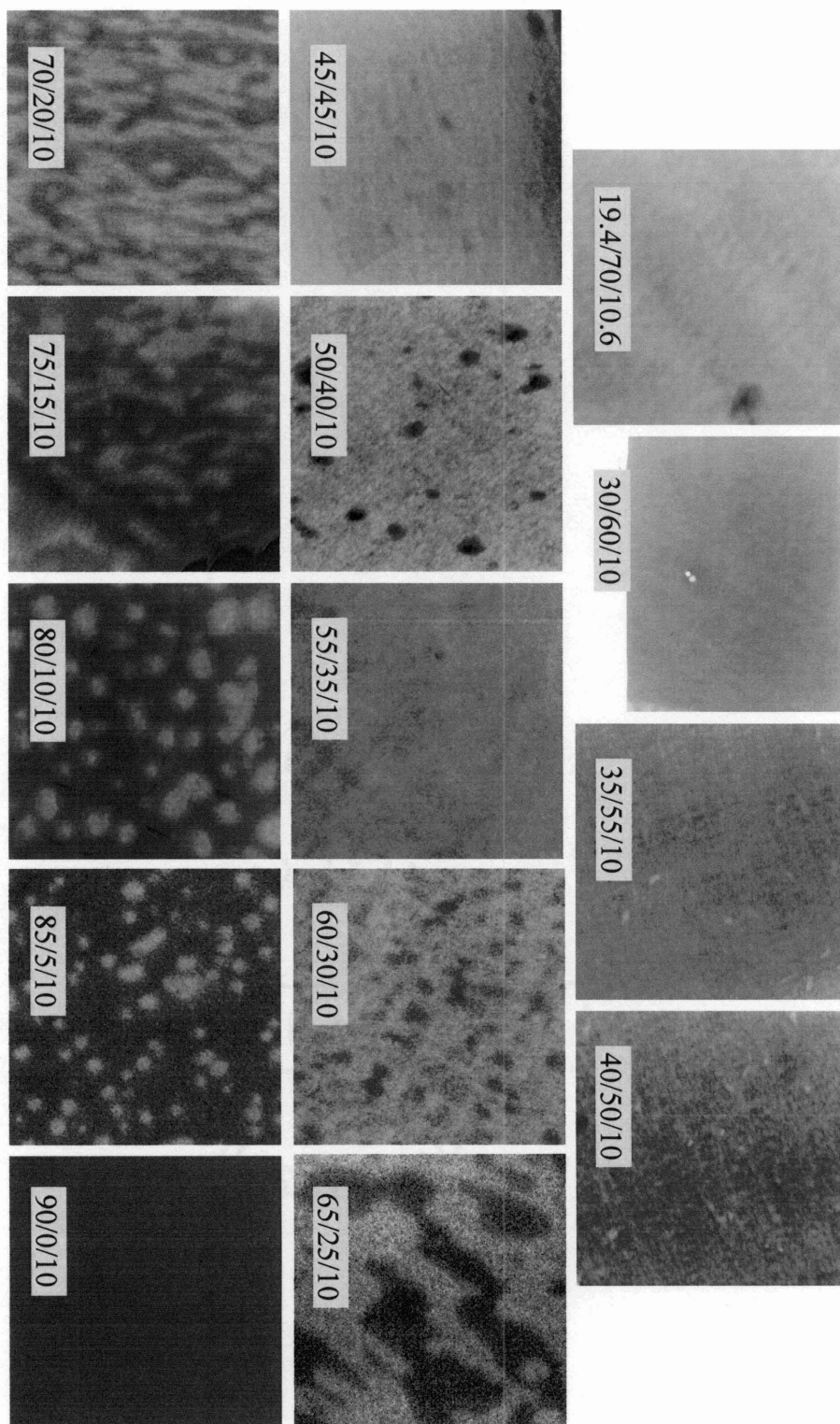


**Figure 2-7: DSC Traces for Ternary Blends with ~10wt% DOP**

Labels are composition in wt% PMMA/PVC/DOP; all tests carried out at 2°C/min, with initial annealing step (see Methods)

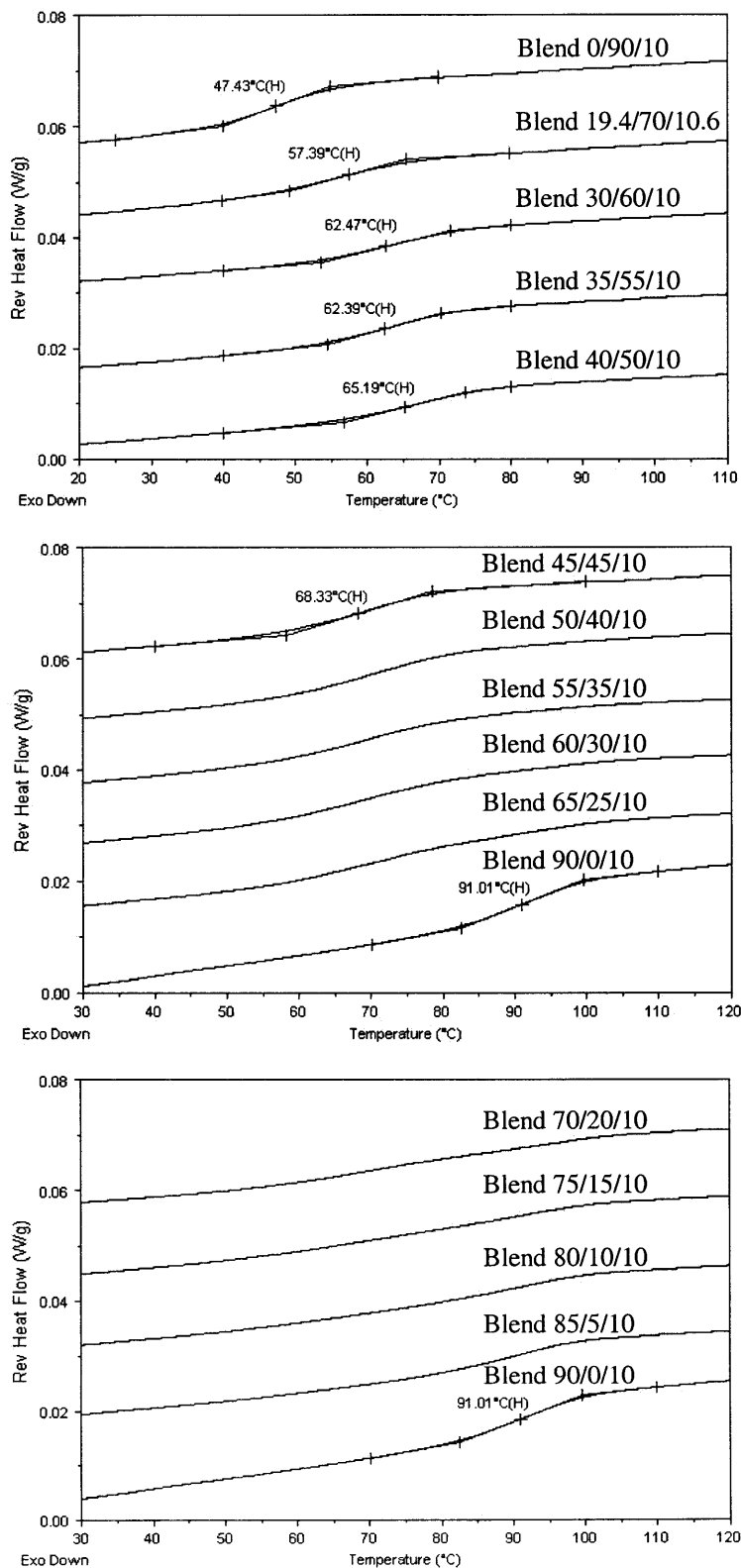


**Table 2-3: DSC Results and Model Predictions**

F <sub>PMMA</sub>	F <sub>PVC</sub>	T <sub>g</sub>	Std Dev of T <sub>g</sub>	Model T <sub>g</sub>	Sq Residual
%	%	°C	°C	°C	(°C) <sup>2</sup>
0	100	69.9	1.4	68.9	0.96
25	75	83.2	0.2	84.1	0.89
100	0	117.3	0.4	116.3	1.05
0	90	43.5	0.7	43.8	0.08
0	80	18.7	1.1	20.8	4.25
0	70	0.2	1.2	-0.2	0.12
90	0	89.4	1.1	90.6	1.53
40	60	91.2	0.3	92.2	0.99
8	80	45.3	0.6	44.4	0.80
25	60	49.6	2.0	48.3	1.64
33	50	49.7	2.0	48.7	1.02
Sum Sq Resid					13.33

**Table 2-4: Model Parameters**

Parameter	Value
C <sub>0</sub>	-87.3
C <sub>1</sub>	1.45
C <sub>2</sub>	0.506
C <sub>3</sub>	0.00587
C <sub>4</sub>	0.0106
C <sub>5</sub>	0.0182

### 2.3.2. Model Validation

In order to validate the model formulated above, several new blends were mixed and their T<sub>g</sub>'s measured via DSC (Table 2-5).

**Table 2-5: Model Confirmation**

F <sub>PMMA</sub>	F <sub>PVC</sub>	Meas T <sub>g</sub>	Std Dev of T <sub>g</sub>	Model T <sub>g</sub>	Diff
%	%	°C	°C	°C	°C
0	75	11.5	0.7	10.0	1.5
3.7	70	11.0	0.9	10.0	1.0
9	70	20.7	0.8	24.9	-4.2
19.4	70	56.2	0.9	55.0	1.3
35.3	50	53.6	1.6	55.0	-1.4
37.3	60	82.3	0.9	84.1	-1.8
45.5	50	82.2	0.6	84.0	-1.8

### 2.3.3. Constant- $T_g$ Blend Series

Using the model equation (2-1), the compositions of several different constant- $T_g$  blend series were computed. The resulting trajectories are superimposed on the ternary phase diagram in Figure 2-8. The series matching the  $T_g$  of a blend of 90% PVC and 10% DOP was selected for further study, and so the blends listed in Table 2-6 were formulated and analyzed (DSC traces shown in Figure 2-10). As a check for blend miscibility, several of these blends were viewed in TEM. It has been shown previously [22] that phase structure PMMA-PVC blends can be seen in TEM without addition of contrast agents. As shown in Figure 2-9, very little contrast was visible in these micrographs.

**Figure 2-8: Constant- $T_g$  Blends Shown on Ternary Phase Diagram**

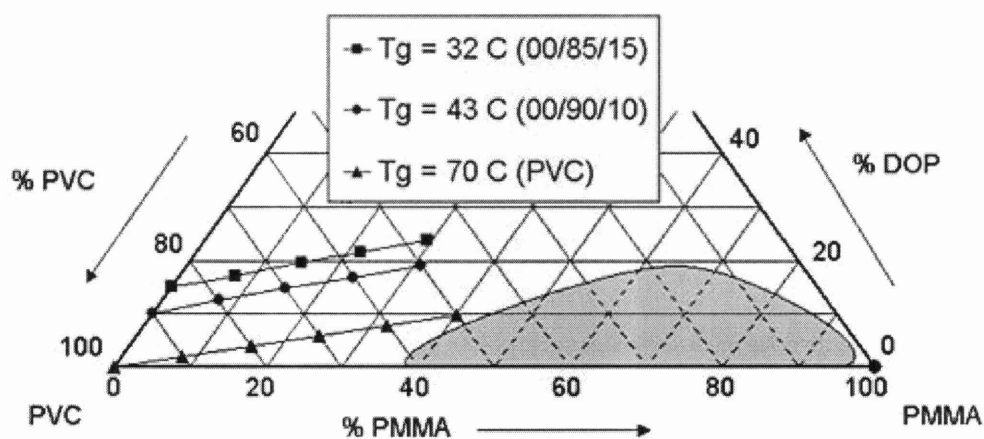


**Table 2-6: Constant- $T_g$  Blend Series**

$F_{PMMA}$	$F_{PVC}$	Meas $T_g$	Std Dev of $T_g$	Model $T_g$	Diff
%	%	$^{\circ}C$	$^{\circ}C$	$^{\circ}C$	$^{\circ}C$
7.8	80	43.9	0.77	43.8	0.1
15.6	70	42.0	0.71	43.8	-1.8
23.4	60	43.3	2.57	43.8	-0.5
31.2	50	42.7	1.54	43.8	-1.1



**Figure 2-9: Transmission Electron Micrographs of Constant-T<sub>g</sub> Blend Series**  
 Labels are composition in wt% PMMA/PVC; each image shows a half-micron square.

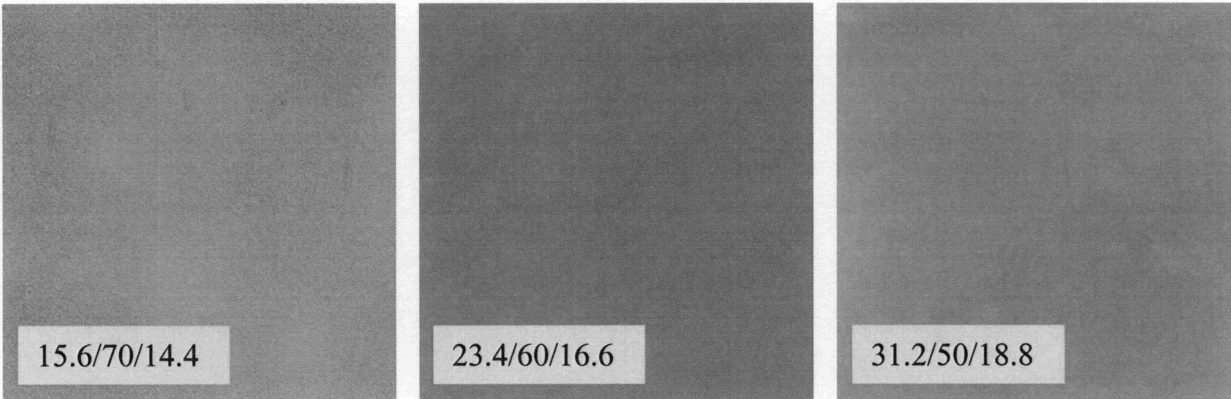
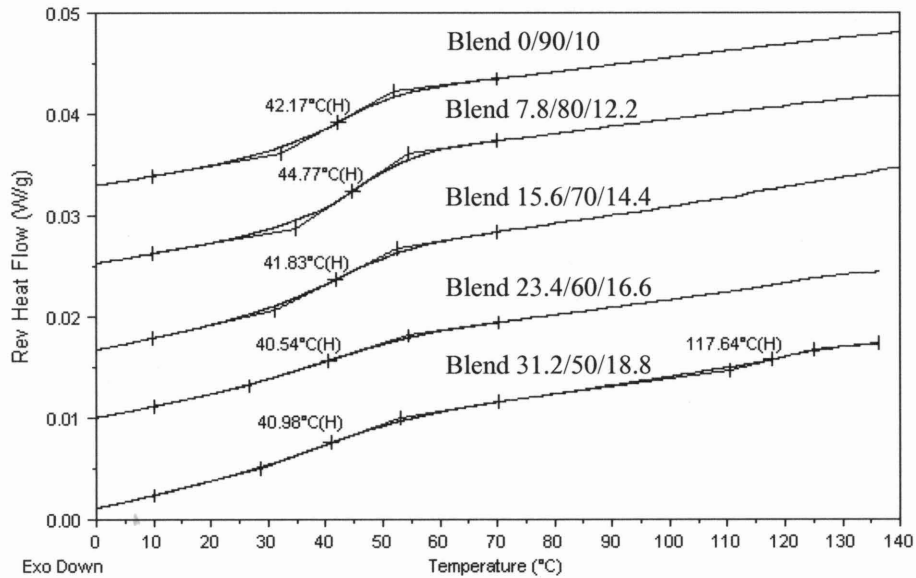


**Figure 2-10: DSC Traces for Constant-T<sub>g</sub> Blends**  
 Labels are composition in wt% PMMA/PVC/DOP; all tests carried out at 2°C/min, with initial annealing step (see Methods)



Several samples of each blend were tested in compression. The data were converted to true stress vs. true strain via an assumption of constant total volume:  $A_i L_i = A_0 L_0$ . Since the nominal (engineering) stress and strain are defined as:

$$\sigma = \frac{F}{A_0} \text{ and } \varepsilon = \frac{L_0 - L_i}{L_0}$$

And true stress and strain are defined as:

$$\sigma_{true} = \frac{F}{A_i} \text{ and } \epsilon_{true} = \ln\left(\frac{L_0}{L_i}\right)$$

Then we can write the relations:

$$\sigma_{true} = \frac{F}{A_0} \left(\frac{L_i}{L_0}\right) = \sigma(1 - \epsilon)$$

$$\epsilon_{true} = \ln\left(\frac{1}{1 - \epsilon}\right)$$

Using these relations, we can easily convert the nominal stress-strain data into true stress-strain curves, shown in Figure 2-11. The trends in the compressive modulus (calculated from the steepest portion of the initial stress increase), yield stress (taken as the local maximum following the initial rise), and flow stress (taken as the local minimum following the yield) are shown in Figure 2-12.

**Figure 2-11: Compression Stress-Strain Curves for Constant-T<sub>g</sub> Blends**

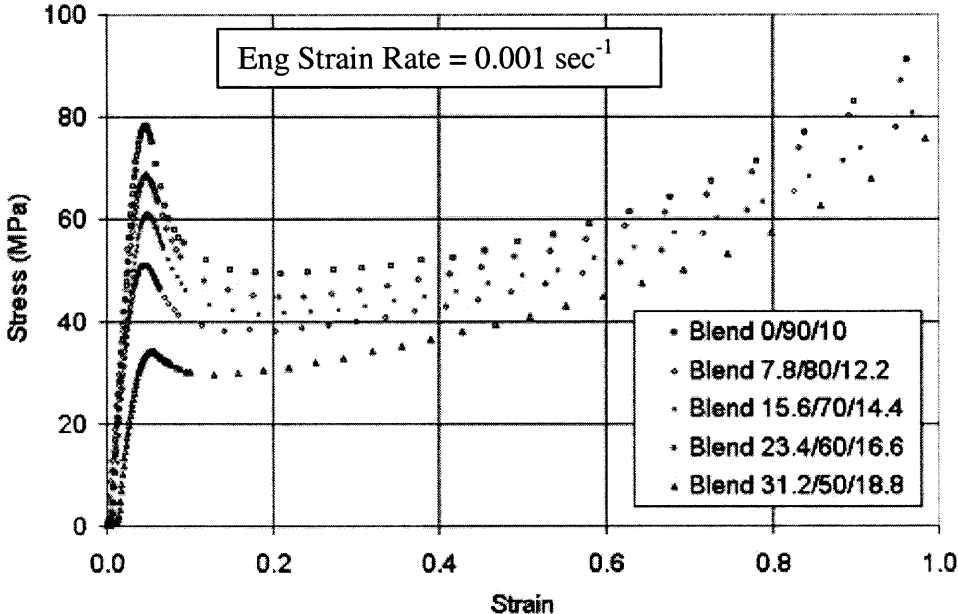
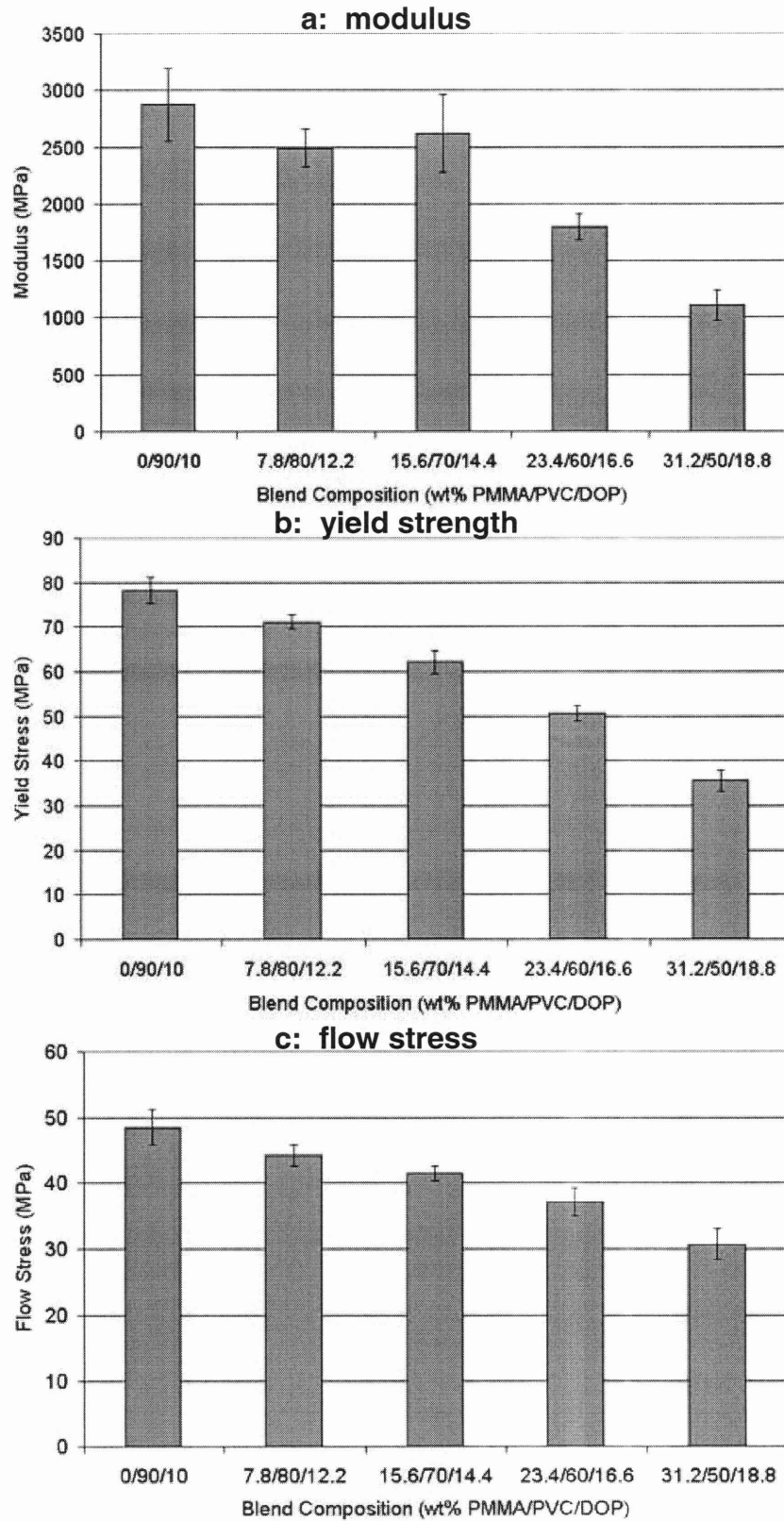
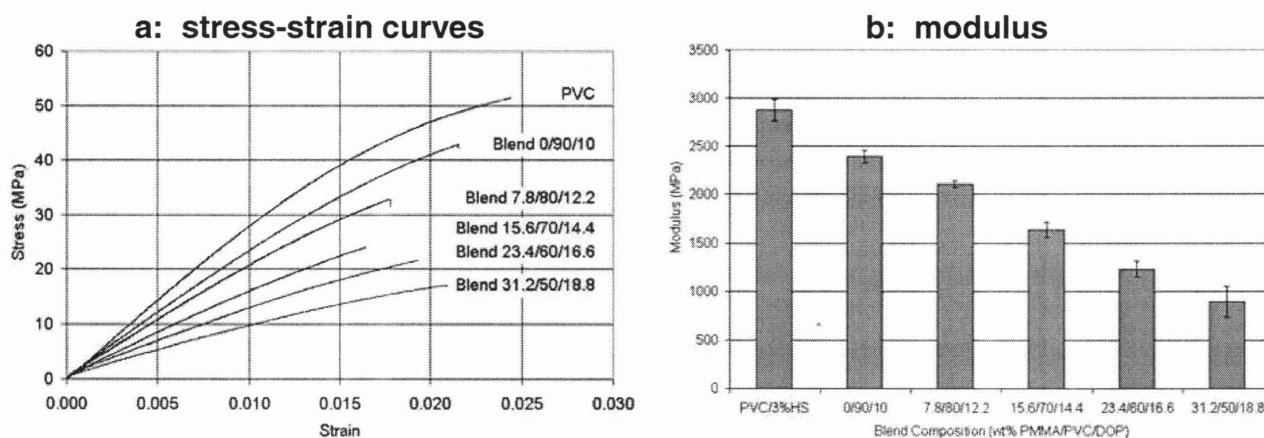


Figure 2-12: Compression Properties for Constant-T<sub>g</sub> Blends



Blend specimens were also tested in uniaxial tension, along with neat PVC for comparison. All of the blends failed in a brittle manner, so no measurements could be made of yield or flow stresses. Tensile stress-strain curves are shown in Figure 2-13a, and modulus values are plotted in Figure 2-13b.

**Figure 2-13: Tensile Properties for Constant- $T_g$  Blends**



## 2.4. Discussion

### 2.4.1 Blend Miscibility and Phase Structure

Examining the TEM photos (Figure 2-2) and DSC traces (Figure 2-3) for the binary PMMA/PVC system, it seems clear that miscibility is highly dependent on the technique used to observe it. TEM shows clear evidence of phase separation at PMMA fractions as low as 40 wt%, while DSC begins to show two-phase behavior around 60 wt% PMMA. Since TEM shows more sensitivity to phase separation, it was the primary source for miscibility data used in the ternary phase diagram (Figure 2-1).

In the TEM images showing multiple phases, the bright regions are assumed to be rich in PVC. Such regions would contain large amounts of chlorine, which has high electron density, and hence would be expected to scatter incident electrons more strongly than PMMA-rich regions. Since these are negative images, regions of higher electron density would appear brighter.

For the binary PMMA/PVC blends, phase separation occurs at compositions of 40 wt% PMMA and higher, where dark spots begin to appear in TEM (Figure 2-2). The PVC-rich (bright) phase is the continuous phase through 65 wt% PMMA. The phases invert at approximately 70 wt% PMMA, and the PMMA-rich phase is continuous for 75 wt% PMMA and higher. Multiple phases are distinguishable even when only 5 wt% PVC remains, confirming that the miscibility of PVC in PMMA is much lower than the reverse. In DSC (Figure 2-3), the phase behavior is unchanged from 65 wt% to 95 wt% PMMA, with an almost pure PMMA phase ( $T_g \sim 115^\circ\text{C}$ ) and a PVC-rich phase saturated with PMMA ( $T_g \sim 95^\circ\text{C}$ ). From 60 wt% to 45 wt% PMMA, only one transition is visible in DSC. However, the  $T_g$  value does not vary significantly

from the saturated value of 95°C, implying that a pure PMMA phase is still present, and this is consistent with the TEM results.

The addition of DOP to the system appears to improve the miscibility of the polymers. For blends containing approximately 5 wt% DOP, PMMA must make up at least 50 wt% of the blend before phase separation appears in TEM (Figure 2-4). The miscibility limit for PVC in PMMA is still below 5 wt%, but the phase structure is very faint in this case. This may be due to a high dilution of the PVC-rich phase with PMMA and DOP, leading to reduced contrast. In other words, the phase structure is similar to the binary case, with the phase inversion again occurring at approximately 70 wt% PMMA. The behavior observed in DSC is also very similar to the binary case. Two transitions coexist at roughly constant  $T_g$  values until PMMA drops below 64 wt% of the blend, and thereafter there is a single transition roughly equal to the saturated value until the PMMA fraction drops to about 30 wt%. The transition temperatures of both the PMMA-rich and PVC-rich phases are lower than the values for the binary case, approximately 105°C and 80°C, respectively. Hence it appears that the DOP added to the system is being partitioned between the two phases. This is unsurprising, since TEM and DSC both show PMMA blending homogeneously with DOP at 5 wt%. Furthermore, since the  $T_g$ 's of the two phases remain roughly constant as PVC is added, DOP appears to blend with both phases with equal affinity.

TEM results for blends containing 10 wt% DOP (Figure 2-6) are similar to the above cases. PMMA blends homogeneously with 10 wt% DOP, but the addition of even 5 wt% PVC leads to clear phase separation. Once again, the phase inversion occurs at approximately 70 wt% PMMA, below which the PVC-rich phase is continuous. The miscible blend 55/35/10 interrupts the trend, since both 50/40/10 and 60/30/10 show two phases. Blends with 45 wt% PMMA and

below are miscible. As seen in Figure 2-7, the DSC results for this series are difficult to interpret because the transitions have become too broad to distinguish.

As noted previously, the results presented here disagree somewhat with miscibility results from the literature. Belhaneche-Bensemra and coworkers [20] reported that binary PMMA-PVC blends are miscible for 50 wt% or less of PMMA, whereas the TEM results showed phase separation for 50, 45, and 40 wt% PMMA (Fig 2-2). Also, they reported that a blend of approximately 50 wt% PMMA, 40 wt% PVC, and 10 wt% DOP was miscible, but TEM results show clear phase separation in this blend (Fig 2-6). These differences are most likely due to the fact that the literature source used only DSC to characterize miscibility; from the results, it appears that DSC is less sensitive than TEM for this purpose. The  $T_g$ 's measured by DSC also differ somewhat between this study and the literature (Table 2-2), especially for neat PVC. This difference is most likely due to the different type of heat stabilizer (lead bibasic phosphate) and possibly different grades of polymer used in that study.

#### 2.4.2 Property Prediction and Variation

The phase diagram (Figure 2-1) gives a schematic map of the homogenous composition space that this system makes available. As shown in the results, the  $T_g$ 's of PMMA-PVC-DOP blends can be predicted quite accurately using a simple empirical model. This creates the potential for making a series of blends for which the  $T_g$  is held constant and mechanical properties are allowed to vary. This allows one to readily compare the blends at a constant fictive temperature, or difference of temperature from  $T_g$ .

This blend is also expected to show a broad variation in entanglement network density, which has strong implications for the mechanical properties. Although the nonlinear rheological

behavior of PVC and its blends prevented the direct measurement of plateau moduli, entanglement densities can be predicted using molecular simulation techniques. Using the Synthia Module, part of the Accelerlys Molecular Simulations package, pure component  $M_e$  values were predicted to be 4320 g/mol for PVC and 10,440 g/mol for PMMA. In order to predict  $M_e$  values for the blends, it was assumed that (1) the mixing of PVC and PMMA is athermal and (2) a geometric mixing rule applies for the plateau moduli of PMMA-PVC blends, such that the simplified form of the Tsengoglou equation may be used [23]:

$$\sqrt{G_{NB}^0} = v_1 \sqrt{G_{N1}^0} + v_2 \sqrt{G_{N2}^0}$$

$$M_e = \frac{\rho RT}{G_N^0}$$

It was further assumed that (3) when plasticizer is added to a polymer blend, the  $M_e$  varies as the inverse of the volume fraction of polymer in the final mixture [13]. Thus  $M_e$  values were predicted for the constant- $T_g$  blend series discussed above (Table 2-7).

**Table 2-7: Predicted values for entanglement molecular weight in constant- $T_g$  blend series**

Composition (wt% PMMA/PVC/DOP)	$M_e$ (g/mol)
0/90/10	4830
7.8/80/12.2	5400
15.6/70/14.4	6060
23.4/60/16.6	6580
31.2/50/18.8	7190

The test results confirm that this blend system allows a wide range of mechanical behavior, even when the  $T_g$  is held constant. Moving along the trajectory  $T_g \sim 44^\circ\text{C}$  from 90 wt% PVC to 50 wt% PVC, the compressive modulus, yield strength, and flow stress all drop



by roughly a factor of two (Figure 2-11). Similarly, in tension (Figure 2-12), the modulus drops by more than a factor of two across this series. All of the blends fractured in a brittle manner in tension, so parameters such as yield strength and flow stress could not be measured.

This ability to vary the plastic resistance of the material is vitally important for a particle toughening study. The polymer matrix must yield before the point of brittle failure and flow to a large extension, but it must also resist enough to dissipate a large amount of energy in the process. Ideally the particles should carry part of the load for small elastic strains, but beyond that point they should simply act as placeholders that detach from the matrix and separate the ligaments from one another. The interplay between yield stress, flow stress, and debonding stress will be explored in the following chapters.

### **3. HARD-PARTICLE TOUGHENING**

#### **3.1. Hard-Particle Toughening Criteria**

Hard fillers have historically been added to thermoplastics and rubbers in an effort to impart stiffness, strength, color, and other properties. For example, calcium carbonate is used to strengthen PVC in piping applications. In addition, a filler material is often so much less expensive than the base polymer that it reduces the overall price. It is generally accepted that filler addition will tend to embrittle the material. However, several recent studies have shown that under certain conditions, hard fillers can vastly increase polymer toughness while maintaining or improving stiffness.

The majority of successes in hard-particle toughening of polymers have come in semicrystalline polymer systems. For example, the impact toughness of high-density polyethylene can be increased at least fifteen fold through the addition of calcium carbonate particles, while the modulus simultaneously increases by 50% [8]. With proper surface treatment, calcium carbonate can increase the toughness of polypropylene in low-rate deformation by a factor of 3 [12]. Some of the mechanisms thought to be responsible for these improvements, such as the critical ligament thickness and preferential matrix crystallization, apply for both hard and soft fillers, and are discussed in detail in Section 1.2. Several factors of key importance for hard fillers are discussed below.

##### **3.1.1. Particle Dispersion**

One of the most important requirements for hard-particle toughening is that the particles be dispersed well in the polymer matrix. Good dispersion actually includes two different conditions: particles must completely permeate the matrix so that polymer ligaments will be

below the critical thickness needed for toughening, and there must not be any large agglomerates present to initiate premature failure.

As discussed in Section 1.2.1, a key parameter in particle toughening, either with soft or hard inclusions, is the average interparticle distance. Studies have shown that a sharp increase in toughness is observed as particle volume fraction increases, and that the concentration at which this transition occurs depends strongly on the particle size [8]. However, when toughness is plotted against the average interparticle distance, the point of toughness increase converges to a single matrix-dependent critical thickness [4]. The precise mechanism for this dependence is a matter of ongoing debate, as discussed previously, but it seems apparent that some altered polymer morphology is induced by the presence of the particles, and penetrates a certain distance into the matrix. This morphology appears to favor shear yielding over brittle failure, so it must percolate the matrix in order for the material as a whole to yield and stretch readily.

Large agglomerates are a major source of early failure in particle-modified polymers, as demonstrated in several studies [24, 25]. In Griffith fracture theory, a morphological flaw or second-phase inclusion in a bulk solid tends to act as a point of stress concentration. The stress field is distorted in the vicinity of this point, and the triaxiality can lead to an effective stress many times greater than the macroscopic value [26]. The larger the flaw is, the greater the local stress will be. If this local stress exceeds the stress of brittle fracture before the material can yield macroscopically, then the crack will propagate and the specimen will fail in a brittle manner. For this reason, the formation of large agglomerates must be prevented.

### 3.1.2. Debonding

As discussed above, in order to achieve toughening through particle addition, the particles must induce a polymer morphology that favors shear yielding and stretching. In addition, the particles must not hold the matrix back and prevent it from stretching. For soft particles, this is generally not an issue; even if they bind strongly to the matrix, they will yield at a lower stress, and affect the matrix deformation only minimally. Hard particles, in contrast, generally do not fail before the matrix yields. If they bind strongly to the matrix, they will severely restrict the matrix and prevent significant stretching. If the particles detach, or debond, from the matrix short of the yield point, then the interparticle ligaments will be free to stretch once they yield.

However, since one of the project goals is to either maintain or increase the modulus, or stiffness, the particles must carry part of the load at small deformations. If the particles are completely loose from the matrix, then they effectively act as voids within the material, and the modulus will be diminished by an amount proportional to the particle volume fraction. If they do bind tightly at small strains, then they will carry part of the load, and since they are stiffer than the matrix, the overall modulus will increase. For these reasons, the adhesion between the particles and the matrix must be of intermediate strength in order to accomplish the goal of simultaneous stiffening and toughening.

### 3.1.3. Particle Size Effect on Debonding

Zhuk and coworkers have shown a strong dependence of the stress required for debonding on the inclusion diameter. Experiments were performed on polypropylene and high-density polyethylene filled with glass beads ranging in mean diameter from 8  $\mu\text{m}$  to 360  $\mu\text{m}$ .

The debonding stress increased monotonically as particle size decreased, changing by nearly a factor of two across the observed range [27]. Hence, it is expected that debonding will be even more difficult for sub-micron scale inclusions.

## 3.2. Experimental

### 3.2.1. Material Preparation

The polymer (PVC), stabilizer (Themolite 890F), and plasticizer (DOP) are described in Section 2.2.1. Citrate-coated barium sulfate filler (grade HU-D, quoted mean size of 100 nm) was generously provided by Sachtleben. Before use, the filler was vacuum-dried and stored in a dessicator.

All composites in this study used a base blend of 90 wt% PVC and 10 wt% DOP. They were made by first hand-mixing PVC powder with stabilizer, hand-mixing this blend with liquid DOP, hand-mixing the appropriate amount of filler, and then compounding the mixture in a bench-scale twin-screw extruder (Daca MicroCompounder with co-rotating screws, screw speed 100 RPM, 2 min mixing time, temperature approximately 170°C). The extruded strands were used directly for differential scanning calorimetry (DSC), dynamic mechanical analysis (DMA), and scanning electron microscopy (SEM). Extruded material was also compression molded into dumbbell-shaped specimens for uniaxial tension, and into plaques, which were then machined to make cylindrical plugs for uniaxial compression. Compression molding was done at approximately the extrusion temperature and 10,000 psi.

### 3.2.2. Thermomechanical Characterization

Modulated DSC (MDSC) was performed on a TA Instruments DSC Q1000; see Section 2.2.2 for a description. All runs began with an annealing step at 140°C for 20 min, followed by rapid cooling to sub-ambient temperature and then a temperature ramp. The ramp rate was 2°C/min, the period of the oscillation was 60 sec, and the amplitude was automatically set to 0.32°C to maintain heat-only mode.

Dynamic mechanical analysis was performed on a TA Instruments DMA Q800. Extruded strand samples approximately 1 cm long and 2 mm in diameter were tested in single-cantilever mode for small-amplitude 1 Hz and 10 Hz oscillations during a temperature ramp of 2°C/min.

### 3.2.3. Mechanical Property Measurement

Uniaxial compression was performed on a servohydraulic Zwick/Roell Z010 mechanical tester. Compression-molded, machined plugs approximately 3 mm in height and 6 mm in diameter were placed between plates lubricated with a thin layer of hydrocarbon oil, compressed at constant engineering strain rate to the maximum allowable load (9000 N), and then unloaded at the same strain rate.

Uniaxial tension testing was performed on the same instrument. An extensometer was used to monitor the length of the gauge section while the specimens were pulled at a constant engineering strain rate. The specimens were compression-molded dumbbells with a gauge section approximately 1.5 mm thick, 4 mm wide, and 13 mm long.

### 3.2.4 Electron Microscopy and Particle Size Analysis

Scanning electron microscopy (SEM) was used to examine the filler particle distribution in extruded strand specimens, as well as for post-fracture analysis of compression and tension specimens. SEM samples were notched with a razor blade, cooled in liquid nitrogen for at least 30 minutes, and fractured at the notch using a blunt edge. Specimens were then mounted using carbon tape and sputter-coated with a thin layer of gold. The microscope used was a JEOL JSM-6060.

For characterization of well-dispersed filler particles, appropriate (agglomerate-free) regions were cropped from SEM images at a magnification of 2000. A Kuwahara edge-preserving filter was run twice on each image in order to reduce noise. A histogram was used to find the mean and standard deviation of image brightness. A threshold was then applied to the image; pixels above the threshold brightness value were turned black, while those below were turned white. The threshold was set at two standard deviations above the mean for each image. A particle analysis routine was then run, with a minimum particle size appropriate to the scale (see below). This routine outputs a list of all particles with size, as well as an outline map of counted particles. The map is used to eliminate any obvious extraneous features (ridges, etc.), and the list of remaining particles is used to characterize the material. In summary:

1. Crop agglomerate-free region from 2000X SEM image.
2. Apply Kuwahara filter, repeat.
3. Compute brightness histogram.
4. Set brightness threshold at mean + 2 std dev.
5. Run particle analysis (minimum size  $0.01 \mu\text{m}^2$ ).
6. Eliminate obvious non-particle features.
7. Export particle size list for analysis.

Steps 2-5 were implemented using the ImageJ software package, provided free of charge by the National Institutes of Health, with an addition plugin that contains the Kuwahara filter. An example of the process is illustrated in Figure 3-1.

Agglomerates of filler particles were characterized by a similar procedure. The differences were as follows:

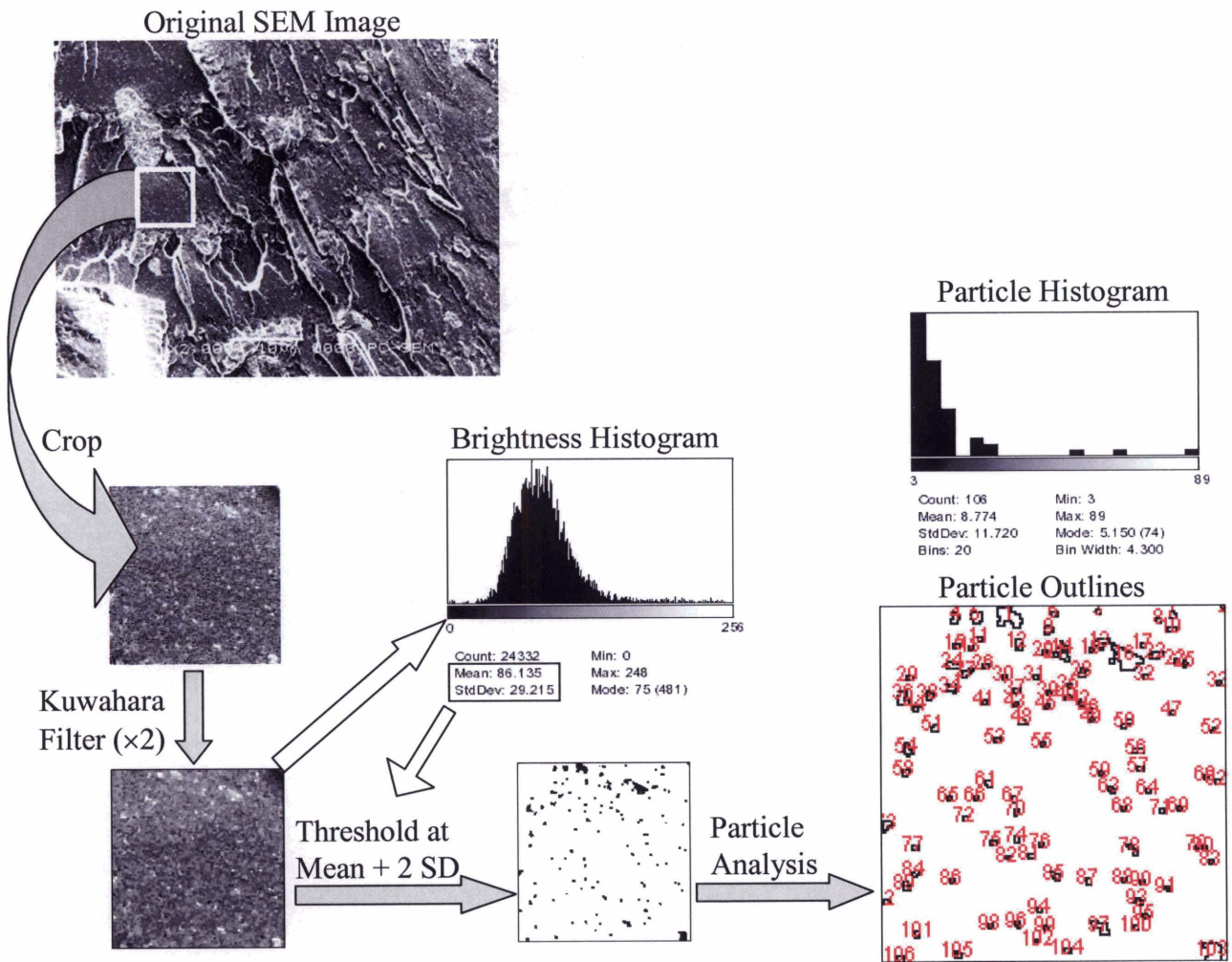
1. Crop *any* region from 500X SEM image.



4. Set brightness threshold at mean + 1 *std dev*.
5. Run particle analysis (minimum size 1  $\mu\text{m}^2$ )

The brightness threshold was set lower in Step 4 due to greater variation in the shading of the agglomerates than the well-dispersed particles.

**Figure 3-1: Example of Particle Size Analysis**

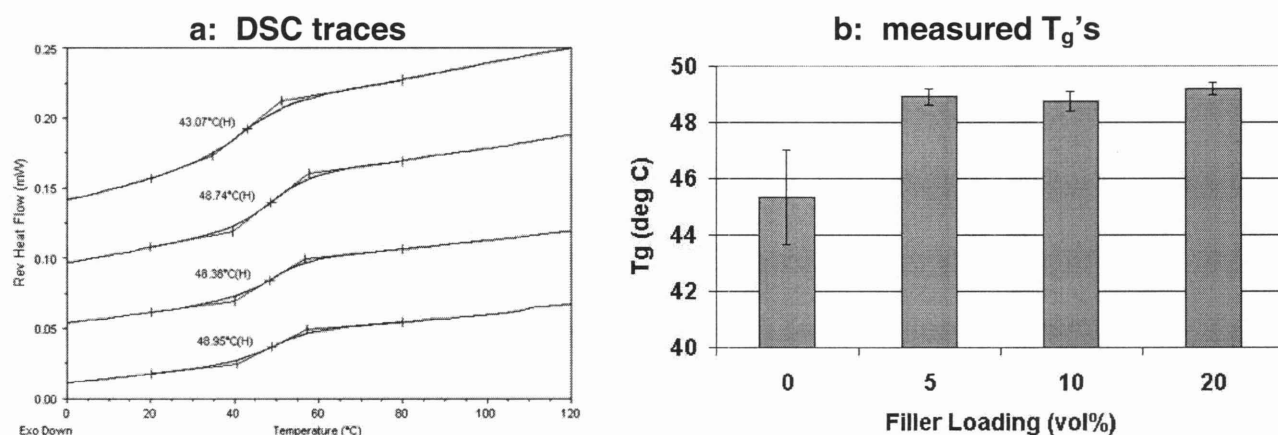


### 3.3. Results

#### 3.3.1 Thermomechanical Characterization

The neat blend and its filled composites were analyzed via modulated DSC at a ramp rate of 2°C/min. Two tests were run for each material; representative traces are shown in Figure 3-2a. Due to variability in the position of the  $T_g$  for different search limits, four measurements were taken from each trace, and eight total measurements were averaged to give the  $T_g$  values shown in Figure 3-2b.

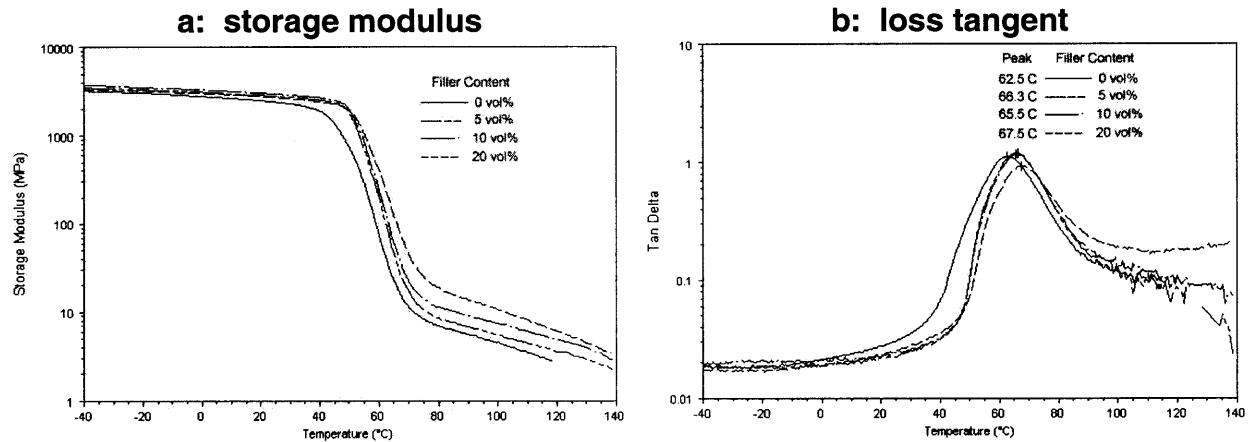
Figure 3-2: DSC Results for Filled Blends



Dynamic mechanical measurements were taken for each material in single-cantilever mode for a small-amplitude 1 Hz oscillation and a temperature ramp of 2°C/min. The elastic component of the response is shown in the storage modulus traces (Figure 3-3a), and the relative viscous component is shown in the loss tangent traces (Figure 3-3b). The loss tangent is the ratio of the loss modulus to the storage modulus, and its peak position is generally taken as a measurement of the glass transition temperature.

Both techniques show a significant rise in  $T_g$  with the introduction of filler, but relatively little effect from the amount of filler. DMA also shows a steady rise in the high-temperature storage modulus with increasing filler content.

**Figure 3-3: DMA Results for Filled Blends**



### 3.3.2 Mechanical Property Measurement

The neat blend and its filled composites were tested in uniaxial compression at a constant nominal strain rate of  $0.001 \text{ sec}^{-1}$ . Representative stress-strain curves are shown in Figure 3-4a, and the compressive properties, averaged from at least 3 tests of each material, are shown in Figures 3-4b (modulus), 3-4c (yield strength), and 3-4d (flow stress). The modulus was measured via a linear fit of the slope in the steepest portion of the initial increase (approx. 10 - 25 MPa), the yield strength was taken to be the early peak stress, and the flow stress was taken to be the local minimum stress following the yield point.

The materials were tested in uniaxial tension, again at a constant nominal strain rate of  $0.001 \text{ sec}^{-1}$ . Here a large difference in behavior was seen for a small number of specimens. While specimens of the neat blend and its 10 vol% and 20 vol% composites all failed in a brittle manner with no significant whitening, some of the 5 vol% composite specimens reached large

extensions with significant whitening before failure. Representative tensile results are shown in Figure 3-5a, while the range of behavior seen for the 5 vol% composite is demonstrated in Figure 3-5b. Because of this large qualitative difference, the ductile and brittle 5 vol% specimens are treated as separate groups for the calculation of tensile properties. Various properties are plotted in Figure 3-6. Modulus was computed from the slope of the stress-strain curve from 8-12 MPa, as this range was shown to give the most consistent results (i.e., the smallest 95% confidence intervals within each material group). Error bars are not shown for the ductile specimen values due to the small number and large variation in available measurements. For all other groups, at least 4 tests were averaged for each measurement.

**Table 3-1: Compressive Properties for Filled Blends**

	Modulus	Yield Strength	Flow Stress
	MPa	MPa	MPa
Neat Blend	2770 ± 90	77.4 ± 1.0	48.7 ± 1.5
5 vol%	2920 ± 70	80.1 ± 1.3	53.7 ± 1.4
10 vol%	2720 ± 120	64.7 ± 2.0	50.9 ± 1.4
20 vol%	2240 ± 100	45.3 ± 1.2	41.3 ± 1.5

Figure 3-4: Compression Results for Filled Blends

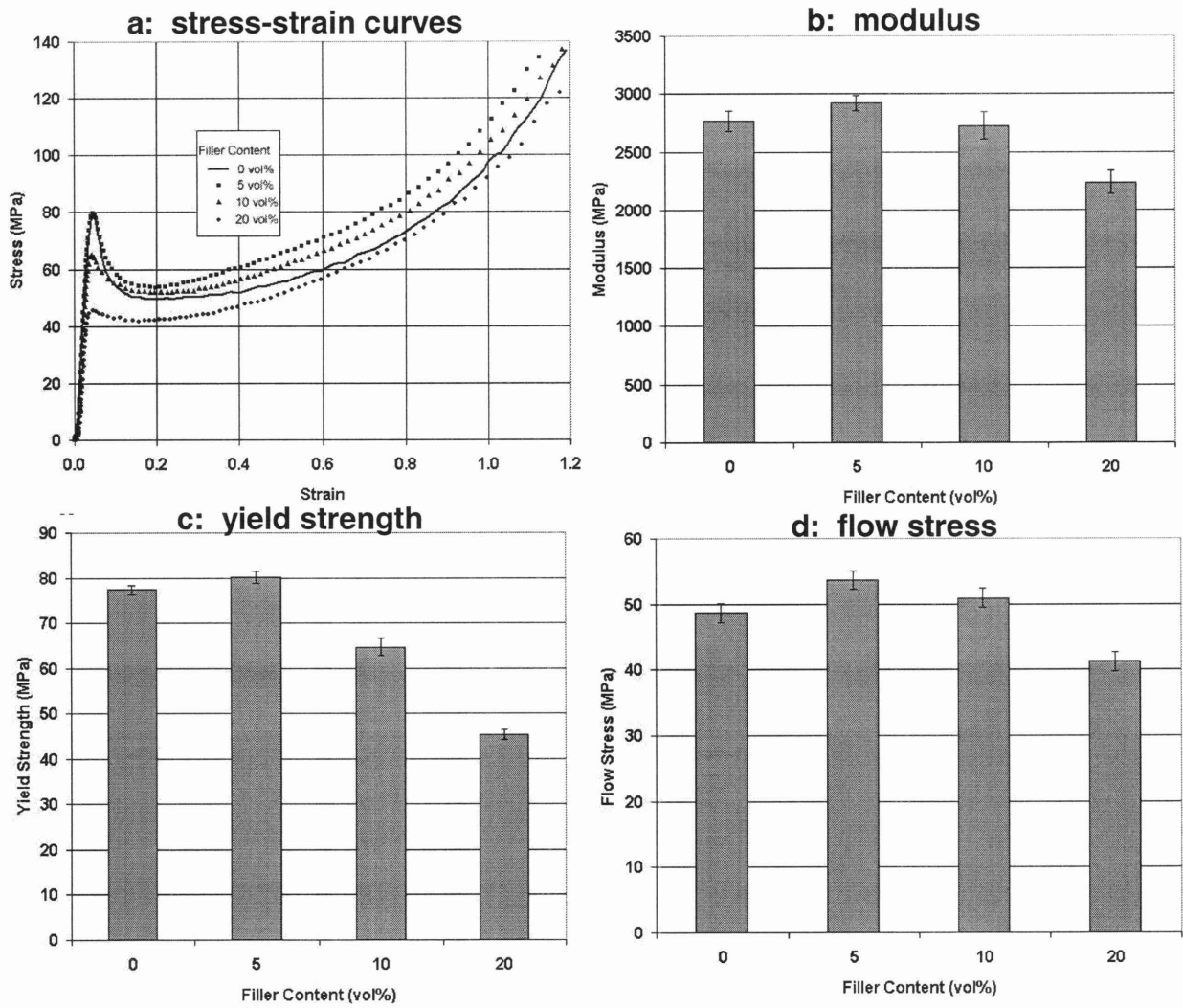
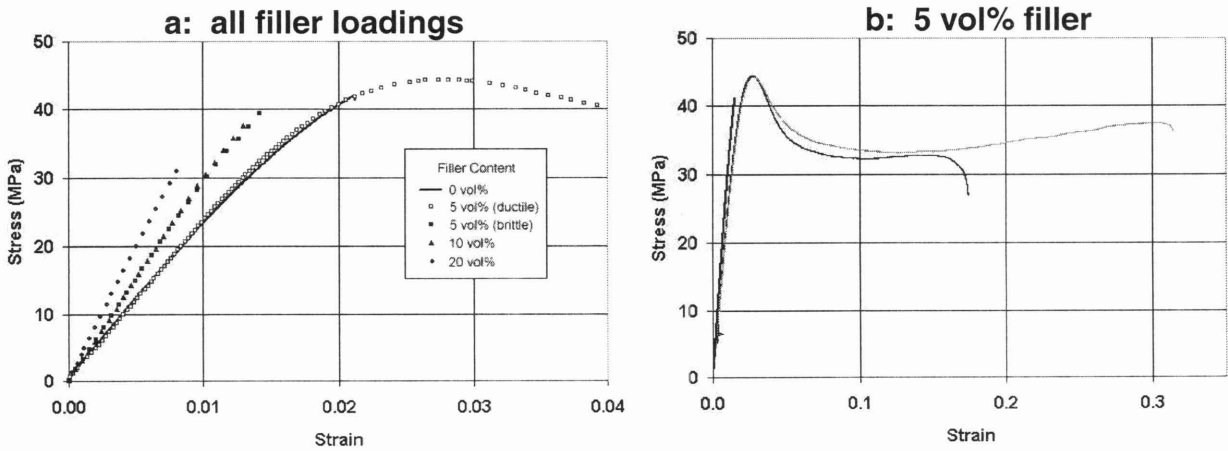
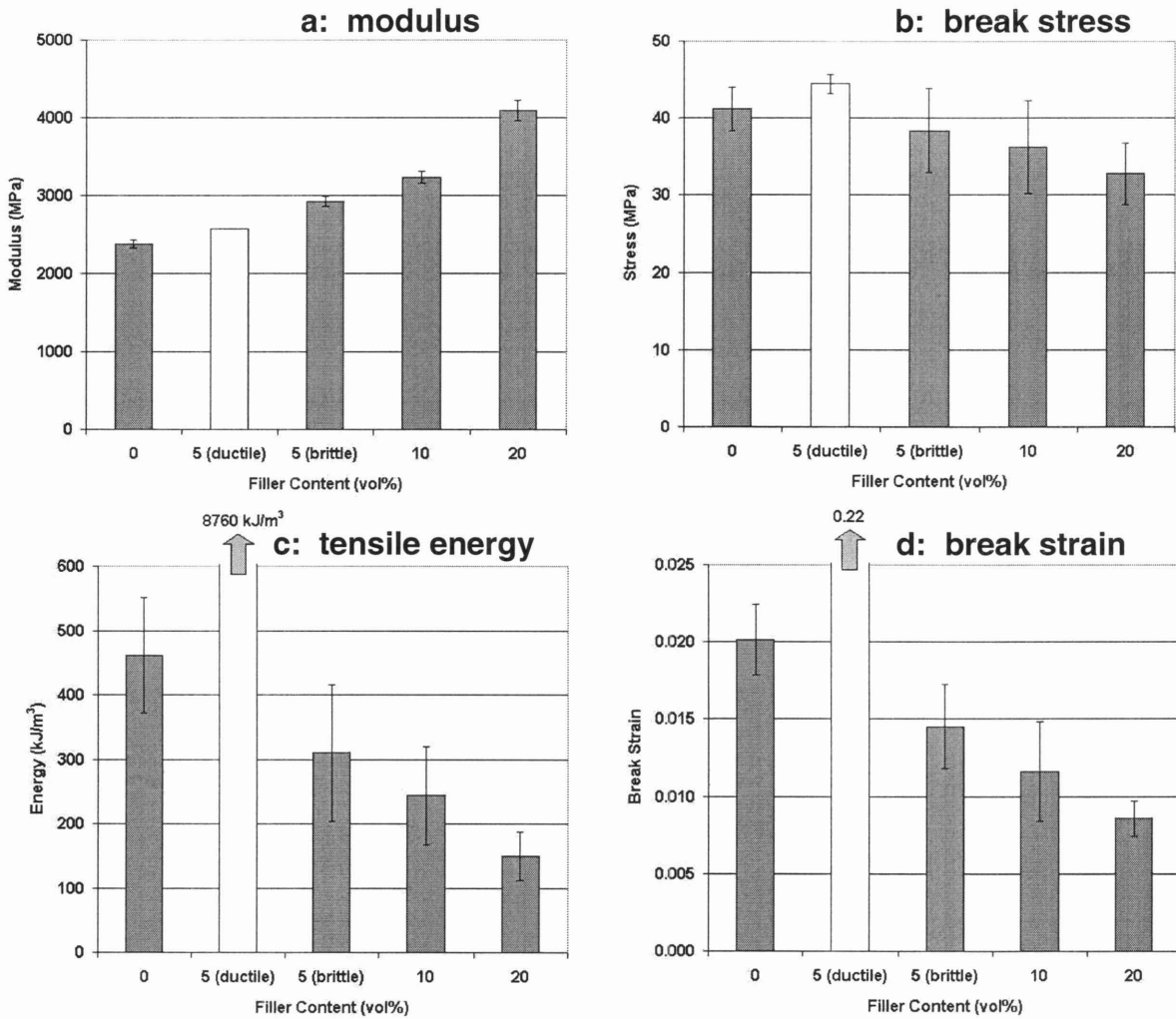


Figure 3-5: Tension Curves for Filled Blends



**Figure 3-6: Tensile Properties for Filled Blends**



**Table 3-2: Tensile Properties for Filled Blends**

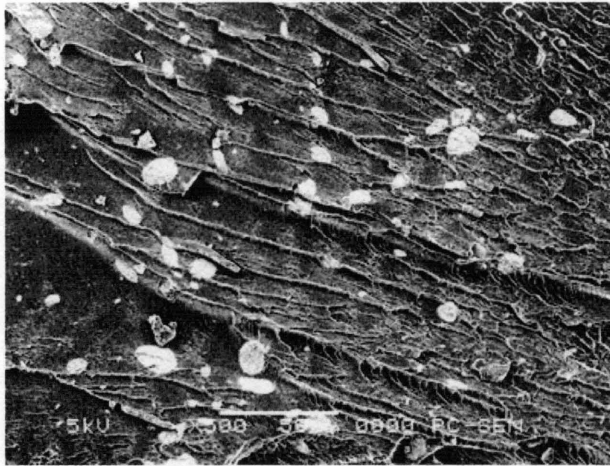
	Modulus	Break Stress	Break Strain	Energy
	MPa	MPa	%L <sub>0</sub>	kJ/m <sup>3</sup>
Neat Blend	2370 ± 50	41.1 ± 2.8	2.0 ± 0.2	462 ± 90
5 vol% (ductile)	2570	44.4 (yield)	22	8760
5 vol% (brittle)	2920 ± 70	38.4 ± 5.5	1.5 ± 0.3	310 ± 106
10 vol%	3230 ± 80	36.2 ± 6.1	1.2 ± 0.3	244 ± 76
20 vol%	4100 ± 130	32.8 ± 4.0	0.9 ± 0.1	149 ± 38

### 3.3.3 Electron Microscopy and Particle Size Analysis

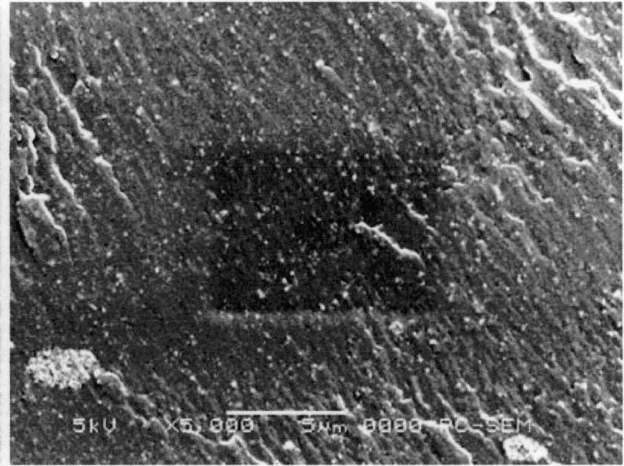
Figure 3-7 shows SEM photos of an extruded strand specimen of the 5 vol% composite. The low-magnification image (Fig 3-7a) shows agglomerates permeating the material with sizes ranging from tens of microns to fractions of microns. The high-magnification image (Fig 3-7b) shows that there are a large number of individual particles dispersed in the matrix. These particles appear to be roughly 100 nm in diameter, which is the expected size of the filler. The 10 vol% (Fig 3-8a) and 20 vol% (Fig 3-8b) composites show a similar structure, with an increasing prevalence of filler, as expected from the proportions of starting materials.

**Figure 3-7: SEM Images of Cryo-Fractured Strand, 5 vol% Composite**

**a: low magnification**



**b: high magnification**



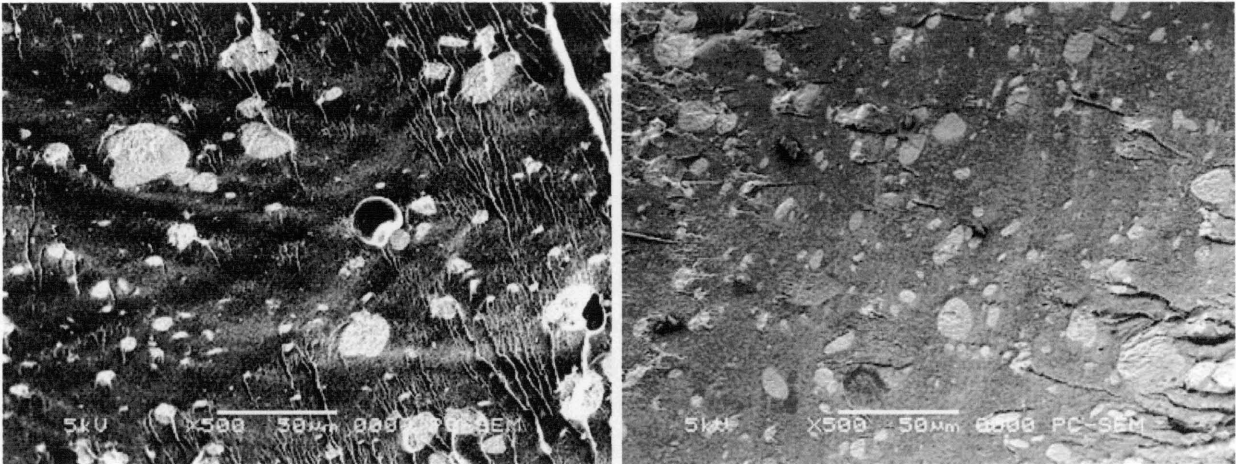
In order to characterize the well-dispersed particles in detail, agglomerate-free regions were cropped from high-magnification images and analyzed as described in Section 3.2.4. The resulting measurements are plotted in Figure 3-9. One important result is that the individual particles average 0.15  $\mu\text{m}$  in size, quite close to the expected value of 100 nm, and the measured size does not change with filler content (Fig 3-9a). As expected, the number concentration of particles (Fig 3-9b) and the area fraction occupied by the particles (Fig 3-9c) rise monotonically

with increasing filler content. There is some variation in these measurements from region to region; for example, the six individual regions used to characterize the 5 vol% composite vary as shown in Figure 3-9d. Particles from all regions analyzed were lumped together to give the measurements shown.

**Figure 3-8: SEM Images of Cryo-Fractured Composite Strands**

**a: 10 vol% filler**

**b: 20 vol% filler**



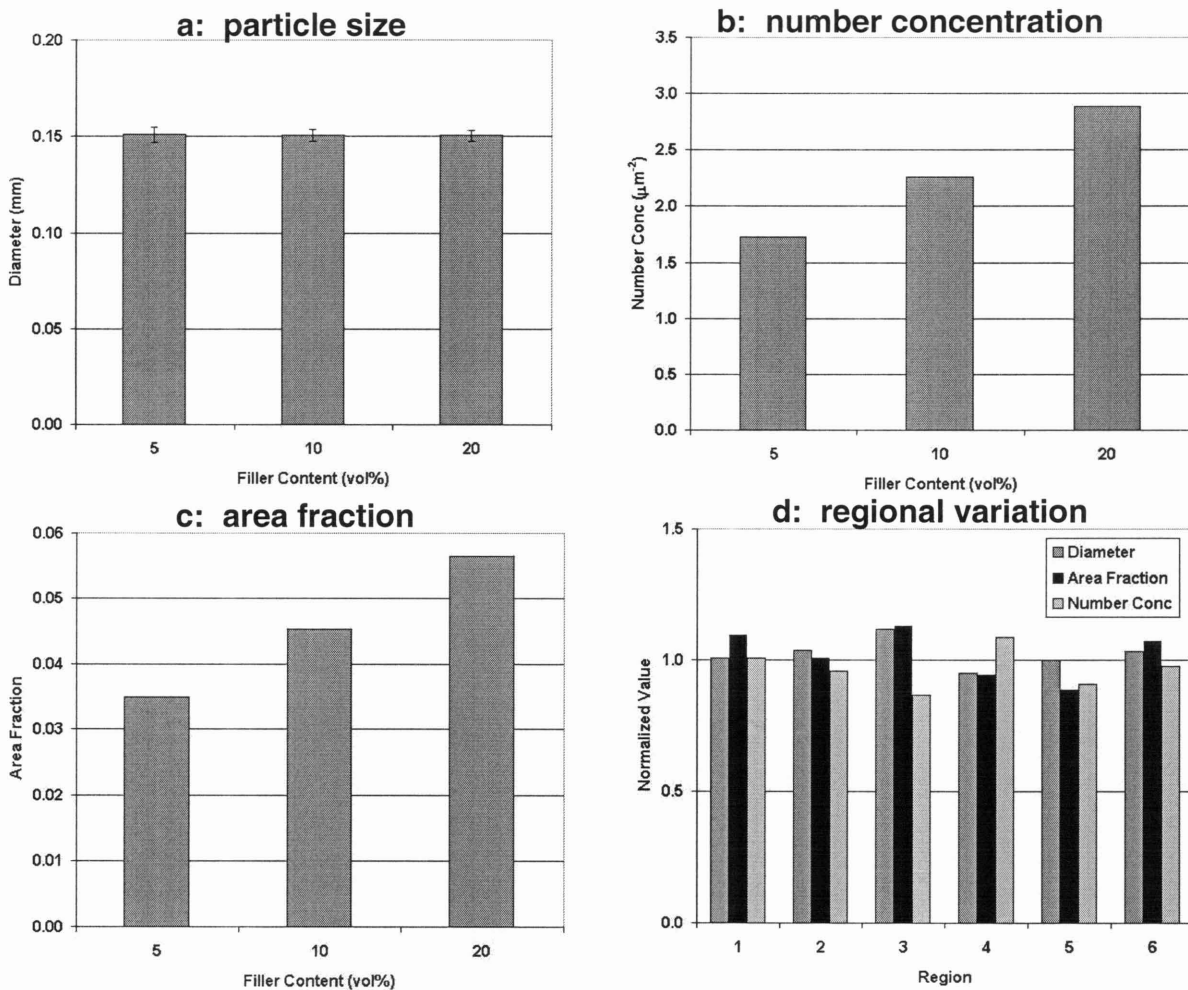
The agglomerates present in each composite were also analyzed via a similar method. A histogram of agglomerate sizes for each composite is shown in Figure 3-10. While the agglomerates range widely in size, most (approx. 90%) appear to be below 10 μm in diameter.

**Table 3-3: Characteristics of Well-Dispersed Filler Particles**

Filler Content	Particle Diameter μm	Number Concentration μm <sup>-2</sup>	Area Fraction
5 vol%	0.151	1.7	0.035
10 vol%	0.151	2.3	0.045
20 vol%	0.150	2.9	0.057



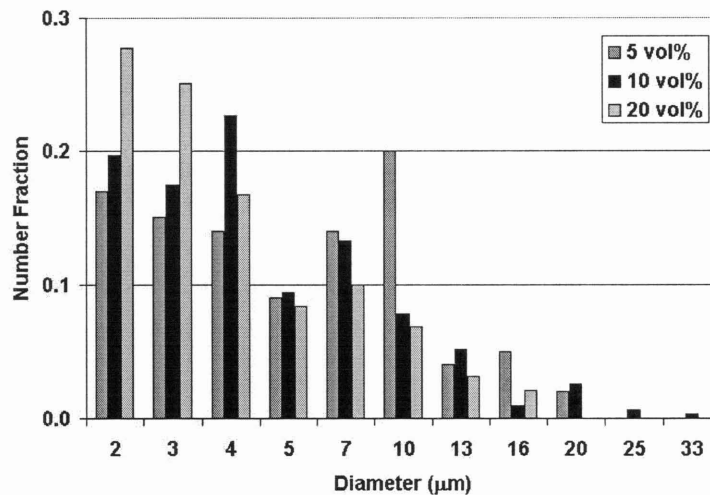
**Figure 3-9: Characterization of Well-Dispersed Filler Particles**



Post-test SEM images were also taken for tension and compression specimens. The viewing angles for each specimen type are shown in Figure 3-11. In all cases the direction of tensile deformation is to the sides, so in compression the forces acted from the top and bottom. As shown in the previous subsection, the majority of tensile specimens failed in a brittle manner. SEM photos of brittle 5 vol% composite specimens are shown in Figure 3-12. There is very little change in the morphology compared to the original extruded strands (Fig 3-7). However, a minority of 5 vol% specimens yielded and stretched to large strain values. In SEM photos of one

of these specimens (Fig 3-13), a large amount of morphological development can be seen. Some agglomerates have clearly debonded from the matrix. Others appear to have undergone internal fracture; this is shown clearly in Figure 3-13b. In contrast, almost all of the individually dispersed particles remain bonded to the matrix.

**Figure 3-10: Histogram of Agglomerate Sizes in Composite Materials**



The compression specimen (Fig 3-14) shows behavior that is quite different from either of the tensile cases. As expected from the high strain, there is a great deal of plastic deformation in the ridges surrounding the agglomerates. The agglomerates appear to have deformed to accommodate the deformation, elongating in the direction of tensile deformation (i.e. toward the sides). However, there is very little evidence of debonding or fracture of the agglomerates. The high-magnification image shows that the agglomerates may be somewhat loosened from the matrix, but the voids formed around them are not nearly as large as in the ductile tensile specimen.

**Figure 3-11: SEM Views for Mechanical Test Specimens**

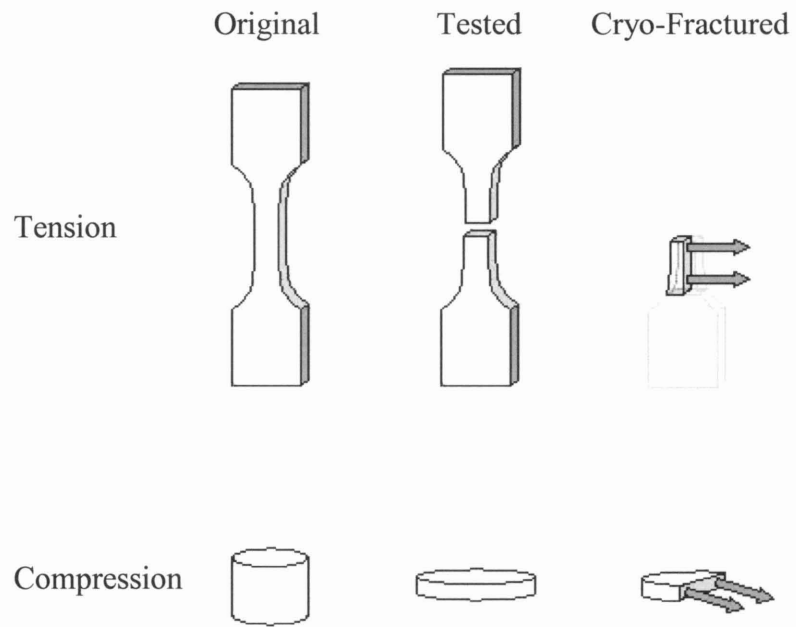
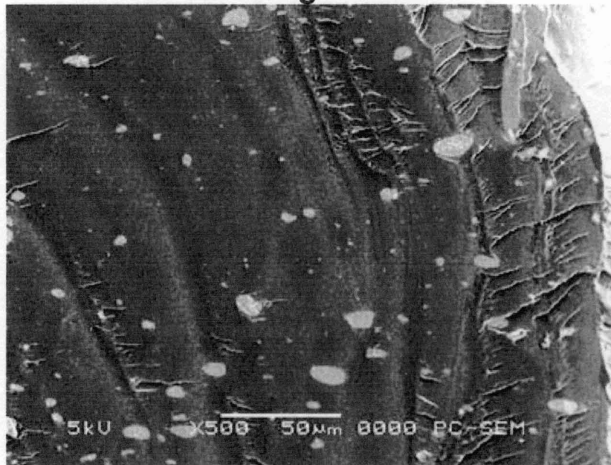


**Figure 3-12: SEM Photos of Brittle Tensile Specimens, 5 vol% Composite**

**a: low magnification**



**b: high magnification**

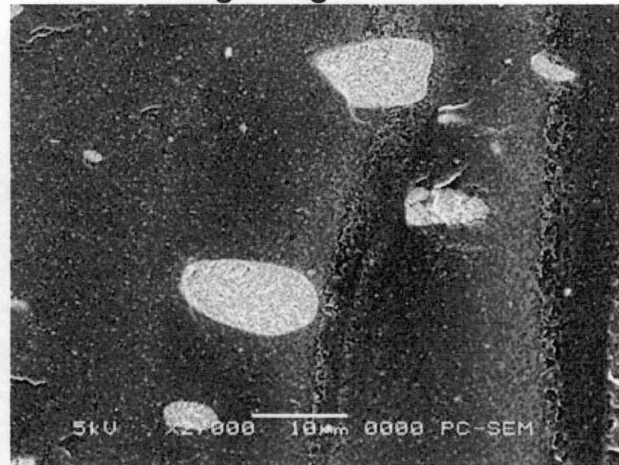
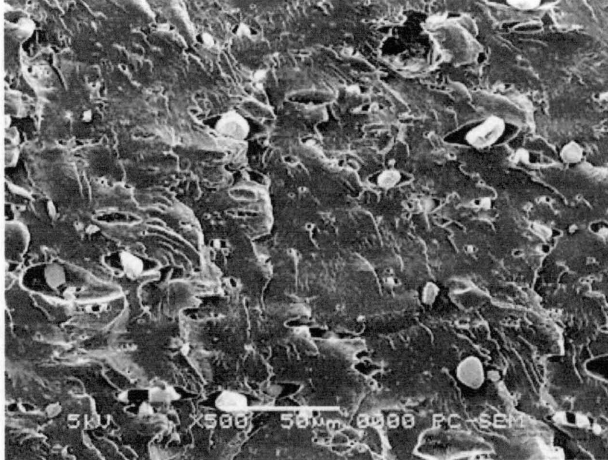


**Figure 3-13: SEM Photos of Ductile Tensile Specimens, 5 vol% Composite**

**a: low magnification**



**b: high magnification**

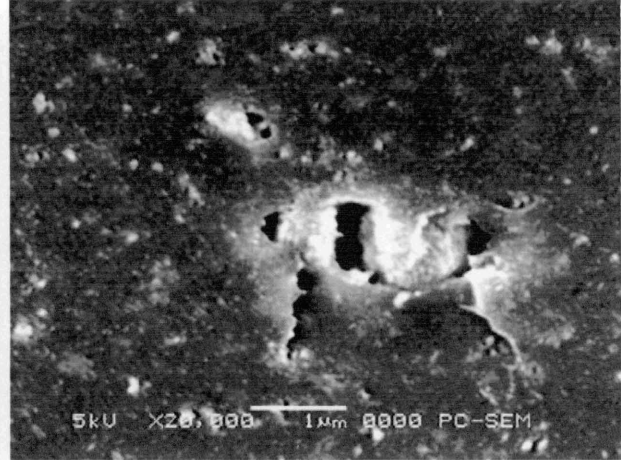
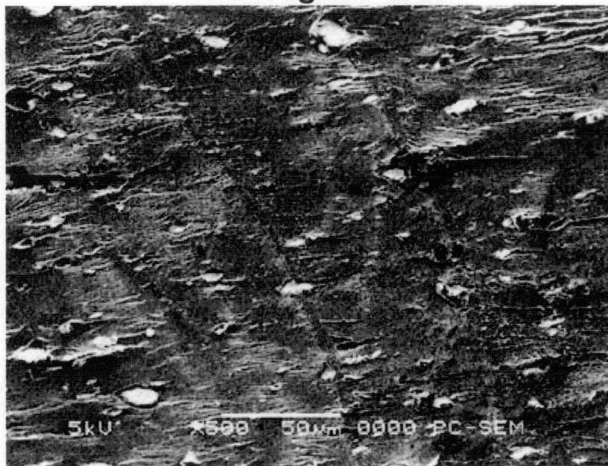
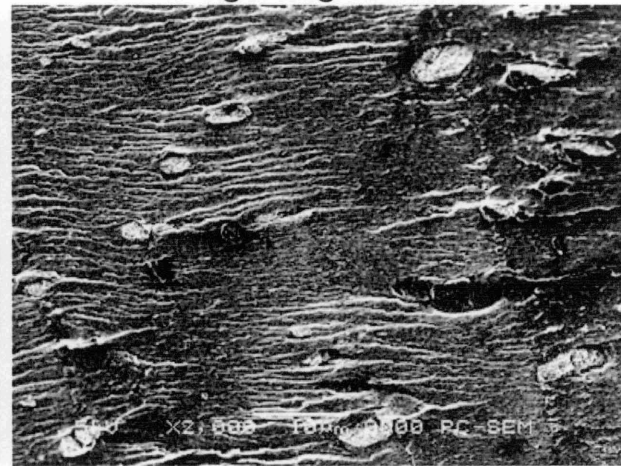


**Figure 3-14: SEM Photos of Compression Specimen, 5 vol% Composite**

**a: low magnification**



**b: high magnification**



### 3.4. Discussion

#### 3.4.1 Effect of Well-Dispersed Particles

Microscopic examination of the composite materials has shown that a large portion of the filler is present in a well-dispersed form. The concentration of these particles increases steadily with the overall volume fraction. Even in cases of large tensile deformation, these well-dispersed particles remain in contact with the surrounding matrix, implying that they adhere strongly to the polymer. Because of the intimate contact between the filler and the matrix, this fraction of the particles may be considered as a homogeneously blended additive.

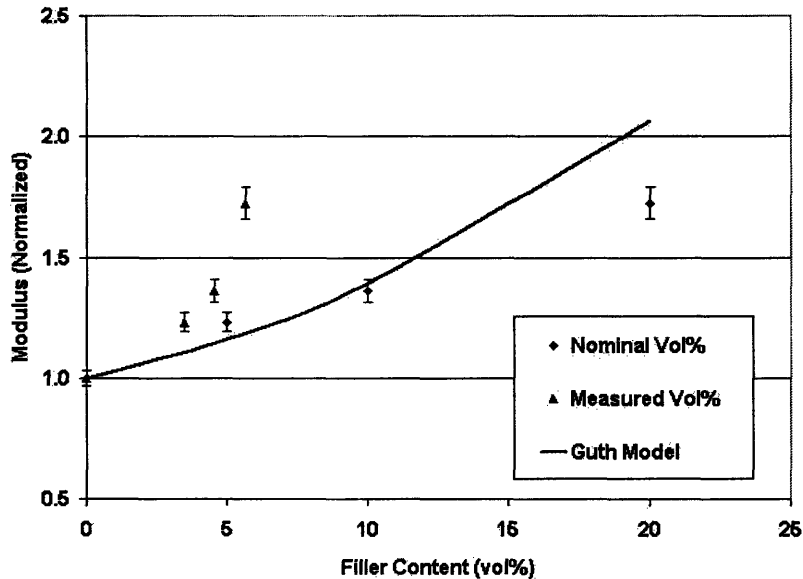
The filler particles appear to act as an anti-plasticizer in these materials. This is shown most clearly in the DSC measurements, where the  $T_g$  jumps from 45°C in the neat blend to 49°C with 5 vol% filler. The effect seems to have saturated by this point, with the  $T_g$  remaining at approximately 49°C for 10 and 20 vol% filler. Similarly, in DMA, the position of the loss tangent peak shifts from 62.5°C for the neat blend to 66.3°C for 5 vol% filler and remains roughly constant for higher loadings. These results indicate that the particles are restricting the mobility of the polymer, in effect occupying free volume that could otherwise be sampled by the chains.

The particles also reinforce the material against tensile deformation. The tensile modulus increases steadily with increasing filler content, indicating that the particles are carrying part of the load at small deformations, and that they are stiff enough and adhere strongly enough to increase the overall stiffness of the material. Several theoretical models have been derived to describe the behavior of composites containing rigid fillers, and one of the best known is the Guth-Smallwood equation [28].

$$\frac{E_{Compos}}{E_{Matrix}} = 1 + 2.5\phi + 14.1\phi^2$$

where  $\phi$  is the volume fraction of filler in the composite. This equation was derived for the case of a relatively dilute ( $\phi \leq 0.1$ ) systems of carbon black in a rubber matrix. Figure 3-15 shows the prediction from this equation plotted against the actual measurements of tensile modulus. The x-axis values are plotted for both the nominal filler content and for the measured volume fraction of well-dispersed particles.

**Figure 3-15: Tensile Moduli vs. Guth Model Predictions**



When the modulus data are plotted against nominal filler contents, the Guth model fits the data well for 5 vol% and 10 vol%. The fact that the nominal filler contents fit better than the measured filler contents implies that the agglomerates provide reinforcement as well as the well-dispersed particles. From the derivation, the equation is not expected to apply beyond 10 vol%, so the deviation at 20 vol% is not surprising.

### 3.4.2 Effect of Agglomerates

Contrary to expectations, agglomerates of filler particles do not severely reduce the fracture toughness of these materials. Agglomerates are clearly present even at the lowest filler loadings studied, and far from causing early failure, they appear to play a beneficial role in deformation.

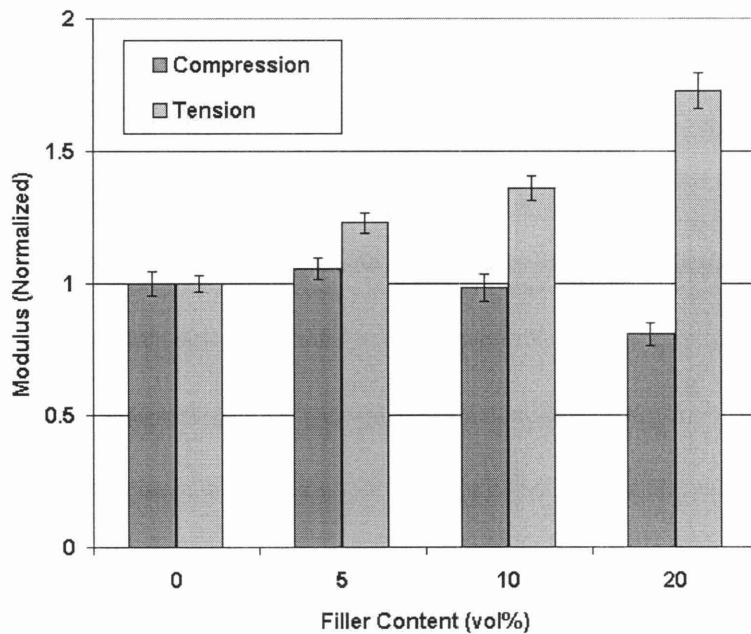
As noted above, the disposition of well-dispersed filler particles in these systems does not appear to change during deformation. Even in highly deformed specimens, they remain bonded to the matrix. In contrast, agglomerates undergo observable changes at large deformations. These changes were readily seen in SEM photos of ductile tensile specimens, where agglomerates are both debonded from the matrix and internally fractured. Either process leads to the creation of void space in the material, allowing the matrix to yield and deform more freely. Hence, it appears to be the agglomerates, and not the well-dispersed particles, that enable this system to behave in a tough manner in tension.

### 3.4.3 Contrast between Compressive and Tensile Behavior

As shown in the results, these materials show very different behavior in compression than in tension. This can be seen most clearly in the moduli. For thermoplastics, the tensile and compressive moduli are expected to be approximately equal [29]. However, the neat blend studied here has a compressive modulus 15% higher than the tensile modulus. Even more surprisingly, the moduli show very different trends as filler is added to the system. The compressive and tensile modulus, each normalized to the neat blend values, are plotted in Figure 3-16.

Differences can also be seen in the post-test SEM photographs for tension and compression specimens (Figs 3-12,13,14). The ductile tensile specimen (Fig 3-13) shows clear evidence of agglomerates debonding and fracturing. The compression specimen (Fig 3-14) shows much less such behavior, even though it reached a much higher strain (1.2 in compression vs. 0.3 in tension). The particles appear to have deformed to align in the direction of tensile deformation (the sides), but very few debonded or fractured particles are visible. This may imply that the compressive mode is unfavorable to voiding and dilatation. Rather than breaking up or debonding, the agglomerates rearrange through sliding of individual particles. Hence, the agglomerates behave more like soft particles in compression. This may also explain why the compressive modulus decreases below the neat blend value for high filler loadings.

**Figure 3-16: Comparison of Compressive and Tensile Moduli for Filled Blends**





## 4. MATRIX PROPERTY INFLUENCE

### 4.1. Effect of Matrix Properties on Toughenability

The properties of the amorphous matrix have a strong impact on the toughening behavior in composite materials. Meijer et al. [14] investigated a series of polystyrene-poly(2,6-dimethyl-1,4-phenylene ether) blends modified with non-adhering rubber particles. They showed that the entanglement density of the PS-PPE blend varies in a roughly linear fashion over the composition range, increasing for greater PPE content. As the entanglement density increased, the observed value of the critical ligament thickness increased as well, meaning that rubber toughening could be achieved with smaller volume fractions of rubber particles.

As one would expect, the properties of miscible polymer blends generally vary between the properties of their constituent homopolymers. However, the trend often deviates significantly from a linear mixing rule. In some unusual cases, blend properties can even exceed the bounds of the component properties. One example of this principle is the variation of entanglement network density with blend composition. As discussed in the previous subsection, entanglement density has a strong effect on the toughenability of a thermoplastic. Hence, the ability to vary it in a systematic way could provide a good handle for controlling mechanical properties of the resulting composite.

Wu [30] investigated several miscible binary polymer blends, including PMMA/PPO, PMMA/PVF2, PMMA/SAN, and PS/PPO. For each blend system, he took measurements of the rubbery plateau modulus  $G_N^0$  as a function of blend composition. Plateau modulus is related to the entanglement molecular weight through the formula [13]:

$$M_e = \frac{\rho RT}{G_N^0}$$

Various researchers have proposed linear [30], geometric [23], and power-law [31] mixing rules, often including thermodynamic terms to account for strong intermolecular interactions. Lomellini [32] tested these three possibilities against PS/PPO plateau modulus data collected by himself and others [33], and found that the latter two methods gave good agreement with experiment. Tsenoglou [23] also tested the geometric mixing rule against data for several different blends, including PS/PPO [33], an athermal blend, PS/tetramethylpolycarbonate [34], a blend with strong intermolecular attraction, and PMMA/PSAN [35], a blend with strong intermolecular repulsion. The model gave good agreement for all cases; its binary form can be expressed as:

$$\sqrt{G_{NB}^0} = v_1 \sqrt{G_{N1}^0} \left[ 1 + \varepsilon \left( \frac{v_2 \sqrt{G_{N2}^0}}{v_1 \sqrt{G_{N1}^0}} \right) \right]^{\pm 1/2} + v_2 \sqrt{G_{N2}^0} \left[ 1 + \varepsilon \left( \frac{v_1 \sqrt{G_{N1}^0}}{v_2 \sqrt{G_{N2}^0}} \right) \right]^{\pm 1/2}$$

where  $G_{NB}^0$  is the blend plateau modulus,  $v_i$  is the volume fraction,  $G_{Ni}^0$  is the pure-component plateau modulus, and  $\varepsilon$  is the interaction strength. The one-half powers are positive for attractive interactions and negative for repulsive interactions. For an athermal blend ( $\varepsilon = 0$ ), this expression collapses to the simple geometric mixing rule:

$$\sqrt{G_{NB}^0} = v_1 \sqrt{G_{N1}^0} + v_2 \sqrt{G_{N2}^0}$$

This relation was used in Chapter 2, along with result of computer simulation and entanglement theory, to predict the variation in entanglement molecular weight along a constant- $T_g$  trajectory in the PMMA-PVC-DOP ternary blend system (Table 2-7). Other properties, such as modulus and yield strength, were also shown to vary widely across the blend

series. In this chapter, the effect of these property variations on particle toughening behavior will be explored.

## 4.2. Experimental

### 4.2.1. Material Preparation

The polymers (PVC and PMMA), stabilizer (Themolite 890F), and plasticizer (DOP) are described in Section 2.2.1. Citrate-coated barium sulfate filler (grade HU-D, quoted mean size of 100 nm) was generously provided by Sachtleben. Before use, the filler was vacuum-dried and stored in a dessicator.

Composites in this study used base blends containing various proportions of PMMA, PVC, and DOP; abbreviated blend codes should be read as wt% PMMA/wt% PVC/wt% DOP. They were made by first hand-mixing PVC powder with stabilizer, hand-mixing this blend with PMMA beads and liquid DOP, hand-mixing the appropriate amount of filler, and then compounding the mixture in a bench-scale twin-screw extruder (Daca MicroCompounder with co-rotating screws, screw speed 100 RPM, 2 min mixing time, temperature approximately  $T_g + 120^\circ\text{C}$ , unless otherwise noted). The extruded strands were used directly for differential scanning calorimetry (DSC) and scanning electron microscopy (SEM). Extruded material was also compression molded into dumbbell-shaped specimens for uniaxial tension, and into plaques, which were then machined to make cylindrical plugs for uniaxial compression. Compression molding was done at approximately the extrusion temperature and 10,000 psi.

### 4.2.2. Thermomechanical Characterization

Modulated DSC (MDSC) was performed on a TA Instruments DSC Q1000; see Section 2.2.2 for a description. All runs began with an annealing step at  $140^\circ\text{C}$  for 20 min, followed by rapid cooling to sub-ambient temperature and then a temperature ramp. The ramp

rate was 2°C/min, the period of the oscillation was 60 sec, and the amplitude was automatically set to 0.32°C to maintain heat-only mode.

#### 4.2.3. Mechanical Property Measurement

Uniaxial compression was performed on a servohydraulic Zwick/Roell Z010 mechanical tester. Compression-molded, machined plugs approximately 3 mm in height and 6 mm in diameter were placed between plates lubricated with a thin layer of hydrocarbon oil, compressed at constant engineering strain rate to the maximum allowable load (9000 N), and then unloaded at the same strain rate.

Uniaxial tension testing was performed on the same instrument. An extensometer was used to monitor the length of the gauge section while the specimens were pulled at a constant engineering strain rate. The specimens were compression-molded dumbbells with a gauge section approximately 1.5 mm thick, 4 mm wide, and 13 mm long.

#### 4.2.4 Electron Microscopy and Particle Size Analysis

Scanning electron microscopy (SEM) was used to examine the morphology in extruded strand specimens, as well as for post-fracture analysis of compression and tension specimens. SEM samples were notched with a razor blade, cooled in liquid nitrogen for at least 30 minutes, and fractured at the notch using a blunt edge. Specimens were then mounted using carbon tape and sputter-coated with a thin layer of gold. The microscope used was a JEOL JSM-6060.

## 4.3 Results

The ternary blends used in this section will be denoted by a code that should be read as (wt% PMMA/wt% PVC/wt% DOP). For example, blend 7.8/80/12.2 consists of 7.8 wt% PMMA, 80 wt% PVC, and 12.2 wt% DOP.

### 4.3.1 Middle- $T_g$ Series

It was demonstrated in Chapter 2 that the mechanical properties of the PMMA-PVC-DOP ternary blend vary widely with composition even among blends having equal  $T_g$ 's. A blend series with a  $T_g$  of approximately 40°C was formulated and tested in Chapter 2, and the results are summarized in Table 4-1. One blend in this series, consisting of 90 wt% PVC and 10 wt% DOP (denoted 0/90/10), was used as a base material in Chapter 3 to study the effect of incorporating submicron barium sulfate filler. Of particular interest was the potential for toughening this blend using hard fillers. In order to test the effect of the base blend properties on toughenability, the same filler was added to several of the blends in the constant- $T_g$  series. In this section, the results for composites of blend 7.8/80/12.2 and blend 15.6/70/14.4 will be compared to those seen for blend 0/90/10 in the previous chapter; mechanical test results are summarized in Table 4-2. Blend 23.4/60/16.6 was not studied in detail, and results for blend 31.2/50/18.8 will be deferred to Section 4.3.4 due to morphological peculiarities.

**Table 4-1: Properties of Middle-T<sub>g</sub> Blends**

Mean ± 95% Confidence Interval							
F <sub>PMMA</sub>	F <sub>PVC</sub>	F <sub>DOP</sub>	T <sub>g</sub>	Tensile Modulus	Compressive Modulus	Compressive Yield Strength	Compressive Flow Stress
wt%	wt%	wt%	°C	MPa	MPa	MPa	MPa
0	90	10	43.5	2370 ± 50	2870 ± 320	78.2 ± 2.9	48.5 ± 2.7
7.8	80	12.2	43.9	2100 ± 40	2490 ± 170	71.1 ± 1.6	44.2 ± 1.6
15.6	70	14.4	42.0	1620 ± 90	2620 ± 340	62.1 ± 2.5	41.5 ± 1.1
23.4	60	16.6	43.3	1210 ± 80	1800 ± 110	50.6 ± 1.7	37.1 ± 2.1
31.2	50	18.8	42.7	870 ± 170	1110 ± 130	35.6 ± 2.3	30.7 ± 2.4

**Table 4-2: Mechanical Properties of Middle-T<sub>g</sub> Composites**

Mean ± 95% Confidence Interval					
Material	Tensile Modulus	Tensile Energy	Compressive Modulus	Compressive Yield Strength	Compressive Flow Stress
	MPa	kJ/m <sup>3</sup>	MPa	MPa	MPa
Blend 0/90/10	2370 ± 50	462 ± 90	2870 ± 320	78.2 ± 2.9	48.5 ± 2.7
5 vol% filler	2920 ± 70	310 ± 106	2920 ± 70	80.1 ± 1.3	53.7 ± 1.4
10 vol% filler	3230 ± 80	244 ± 76	2720 ± 120	64.7 ± 2.0	50.9 ± 1.4
20 vol% filler	4100 ± 130	149 ± 38	2240 ± 100	45.3 ± 1.2	41.3 ± 1.5
Blend 7.8/80/12.2	2100 ± 40	249 ± 53	2490 ± 170	71.1 ± 1.6	44.2 ± 1.6
5 vol% filler	2100 ± 50	431 ± 61	2810 ± 100	80.7 ± 0.7	51.7 ± 0.7
10 vol% filler	2540 ± 50	788 ± 190	2280 ± 20	77.5 ± 1.2	53.0 ± 1.0
20 vol% filler	3610 ± 120	202 ± 42	-	-	-
Blend 15.6/70/14.4	1620 ± 90	249 ± 71	2620 ± 340	62.1 ± 2.5	41.5 ± 1.1
5 vol% filler	1820 ± 50	304 ± 78	2390 ± 70	71.7 ± 0.5	48.5 ± 0.1
10 vol% filler	2250 ± 20	425 ± 151	2380 ± 130	73.9 ± 1.6	50.6 ± 0.6
20 vol% filler	3050 ± 180	151 ± 129	-	-	-

Tensile stress-strain curves for composites based on blend 7.8/80/12.2 are plotted in Figure 4-1a. Figure 4-1b shows only results for the 10 vol% composite, for which most specimens (“Normal Behavior”) broke at the yield point, but one (“Best Specimen”) deformed significantly before breaking. When examined via SEM (Fig 4-2), the ductile specimen shows a significantly different morphology (for a sketch of the viewing angle, see Fig 3-11). The white arrows on the photographs point toward the tensile fracture surface, which is less than 100 μm away in both cases. The agglomerates in the ductile specimen appear to have voids forming

around their edges, as well as showing some signs of internal fracture. Although not nearly as pronounced or widespread as in the 0/90/10 composite (5 vol%, Fig 3-13), the behavior appears qualitatively similar. The brittle specimen, which broke at the yield point, shows very little of this morphology, indicating that the voids probably form after yield. For this series of composites, the modulus increases steadily with filler content, as expected for the addition of hard particles. In contrast to blend 0/90/10, for which the average tensile energy drops with filler addition, these composites on average become tougher for 5 and 10 vol%.

**Figure 4-1: Tensile Results for Composites of Blend 7.8/80/12.2**

Nominal strain rate =  $0.001 \text{ sec}^{-1}$

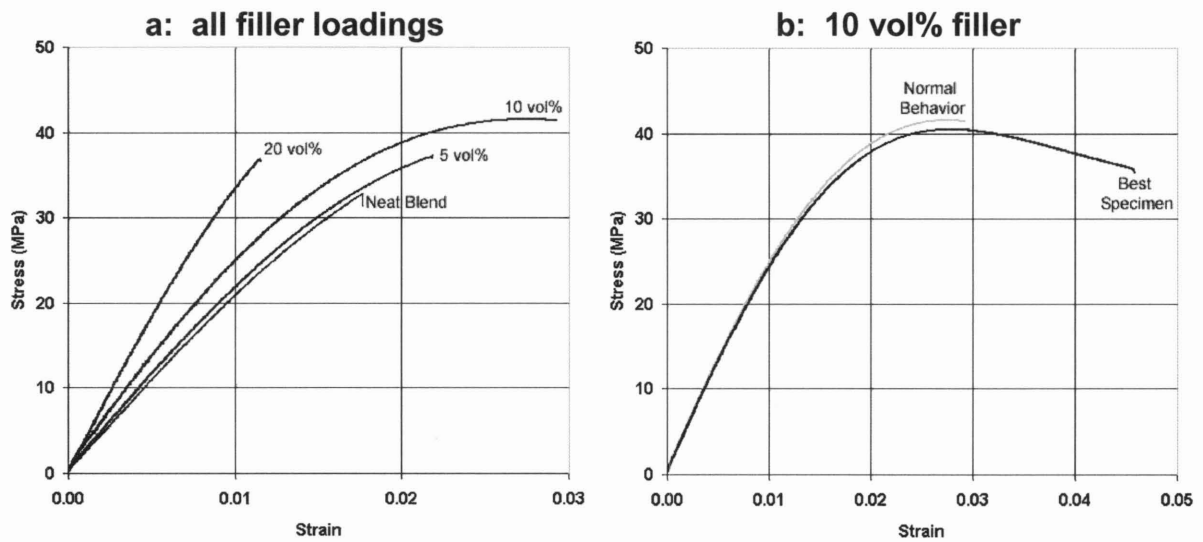
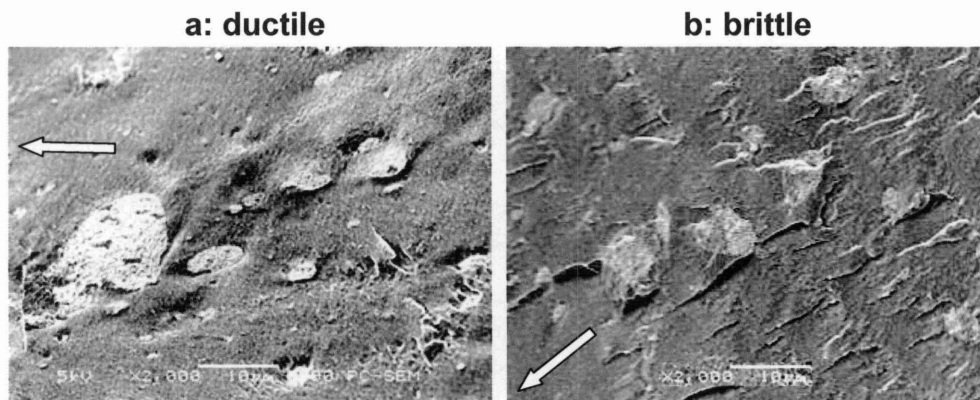


**Figure 4-2: SEM of Tensile Specimens – 10 vol% Composite of Blend 7.8/80/12.2**

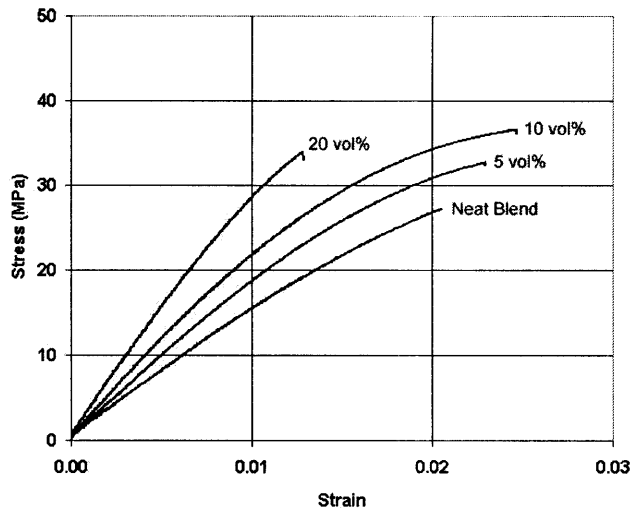
White arrows point toward tensile fracture surface, less than  $100 \mu\text{m}$  away.





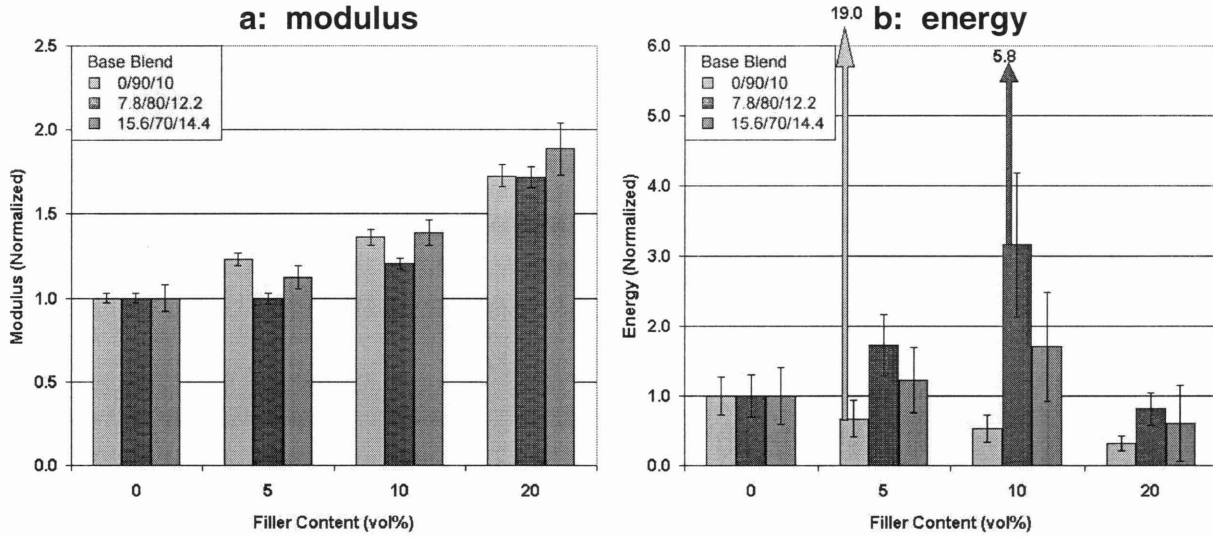
Tensile results for composites based on blend 15.6/70/14.4 are plotted in Figure 4-3. Again, the modulus increases steadily as filler is added. The toughness also appears to increase for 5 and 10 vol%, although the differences are small relative to scatter.

**Figure 4-3: Tensile Results for Composites of Blend 15.6/70/14.4**  
Nominal strain rate =  $0.001 \text{ sec}^{-1}$



The tensile properties for each series of composites, normalized to base blend values, are plotted in Figure 4-4. In all three cases, the tensile modulus either holds constant or increases with filler content. Both blend 0/90/10 and blend 7.8/80/12.2 showed isolated cases of highly toughened composites at 5 vol% (19-fold increase) and 10 vol% (5.8-fold increase), respectively. However, the behavior of the remaining specimens is very different for the two base blends. The tensile energy values for the composites of blend 0/90/10 drop monotonically with filler content, while blend 7.8/80/12.2 is toughened for small to moderate filler fractions. The tensile energy for blend 15.6/70/14.4 also appears to rise somewhat, although the trend is much weaker.

**Figure 4-4: Tensile Properties for Middle-T<sub>g</sub> Composites**  
 Block arrows show normalized tensile energy for the best specimen.



Compression behavior for composites based on blend 7.8/80/12.2 is shown in Figure 4-5, and for blend 15.6/70/14.4 in Figure 4-6. As was seen for blend 0/90/10, the compressive modulus drops for moderate filler contents, contrary to the behavior in tension. The normalized compressive properties for the three composite series are plotted in Figure 4-7.

**Figure 4-5: Compressive Properties for Composites of Blend 7.8/80/12.2**

Nominal strain rate = 0.001 sec<sup>-1</sup>

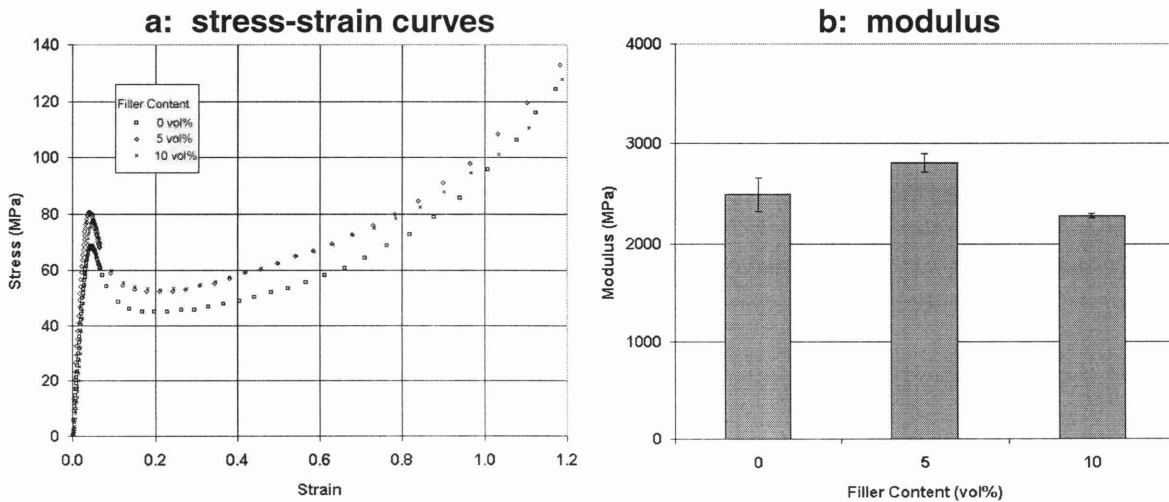


**Figure 4-6: Compressive Properties for Composites of Blend 15.6/70/14.4**

Nominal strain rate = 0.001 sec<sup>-1</sup>

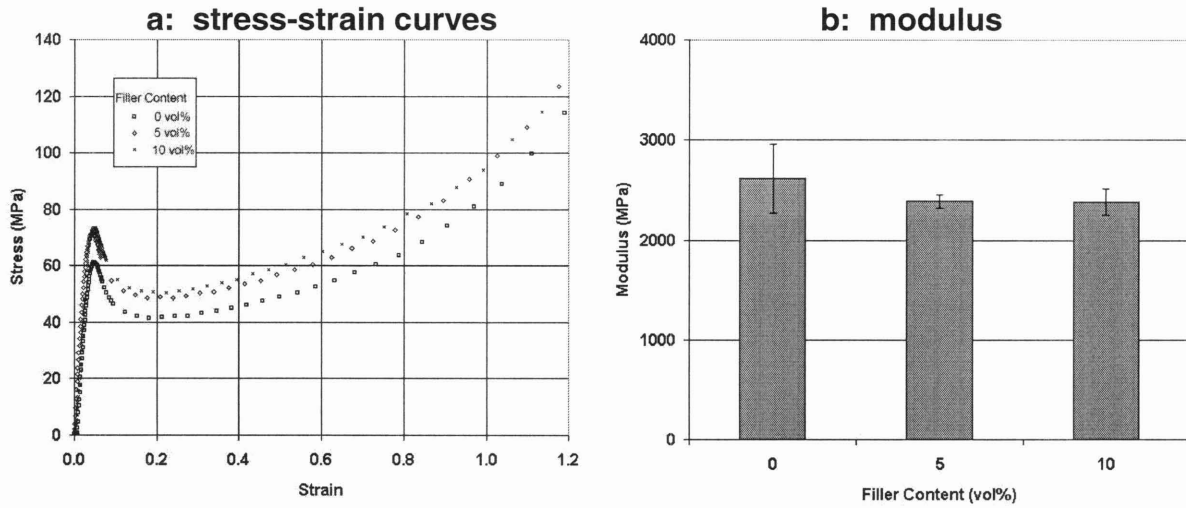
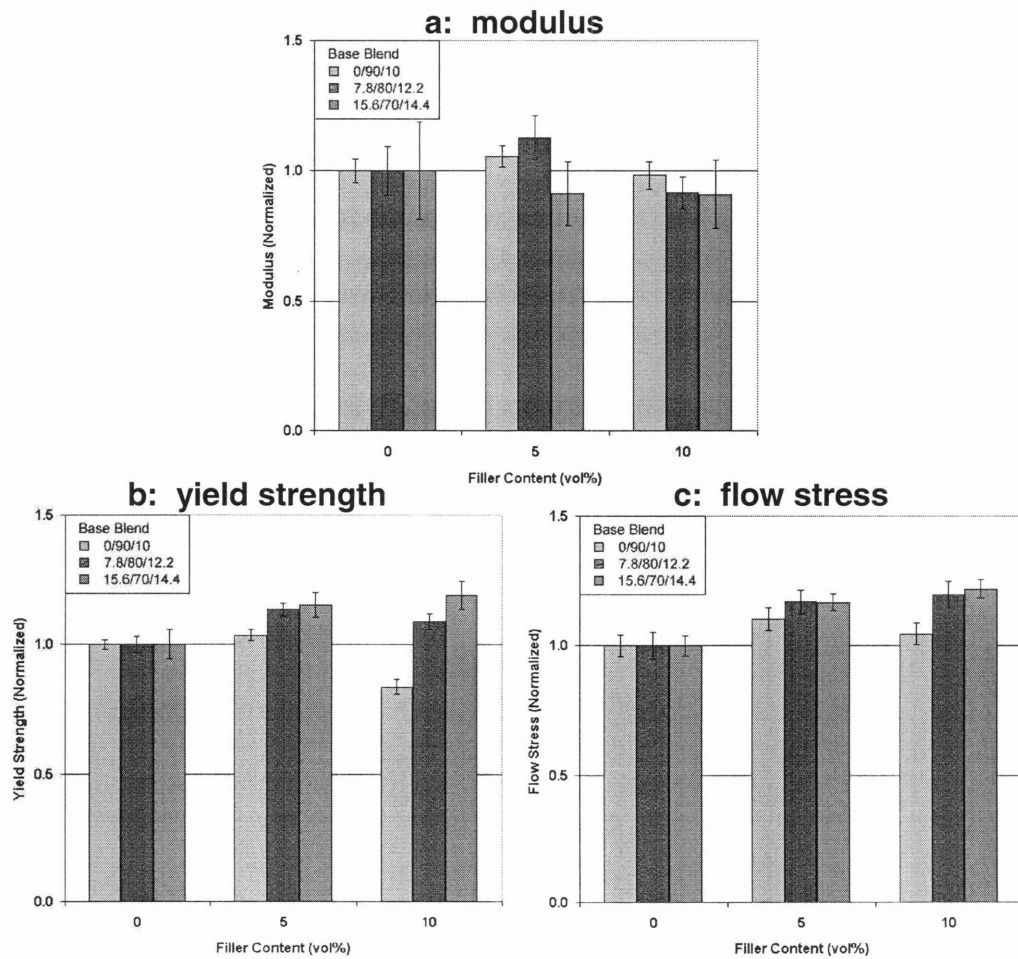


**Figure 4-7: Compressive Properties for Middle-T<sub>g</sub> Composites**



### 4.3.2 High- $T_g$ Series

A series of blends was formulated to match the  $T_g$  of neat PVC, approximately 70°C. The compositions and properties of these blends are shown in Table 4-3. By changing the glass transition temperature of the system, we are effectively testing the material at a different fictive temperature, or difference of the ambient temperature from  $T_g$ . For the filler toughening study, neat PVC and blend 36/57.5/6.5 were used as matrix materials.

**Table 4-3: Properties of High- $T_g$  Blends**

Mean $\pm$ 95% Confidence Interval							
$F_{PMMA}$	$F_{PVC}$	$F_{DOP}$	$T_g$	Tensile Modulus	Compressive Modulus	Compressive Yield Strength	Compressive Flow Stress
wt%	wt%	wt%	°C	MPa	MPa	MPa	MPa
0	100	0	74.6	2810 $\pm$ 70	2730 $\pm$ 100	73.9 $\pm$ 1.3	61.3 $\pm$ 0.7
17.7	79.3	3	73.5	-	2790 $\pm$ 140	87.4 $\pm$ 0.7	66.8 $\pm$ 0.5
36	57.5	6.5	72.9	2840 $\pm$ 100	2920 $\pm$ 140	87.2 $\pm$ 1.0	61.7 $\pm$ 0.5

Composites based on these materials were produced at 5, 10, and 20 vol% of filler and subjected to mechanical testing. Results are listed in Table 4-4. Degradation appears to be a serious problem in heavily filled composites of PVC. Processing of the 20 vol% composite was very difficult, and the extrudate came out blackened and rough. The material did not consolidate well in compression molding, and this is reflected in the poor mechanical performance of its specimens, so any statements regarding the property trends will ignore this composite.

The tensile properties for PVC-based composites are shown in Figure 4-8, and compressive properties are shown in Figure 4-9. Most neat PVC specimens broke before the yield point, but one, shown in Figure 4-8b, yielded and stretched to a strain of 0.08. This suggests that PVC has significant potential for ductility, but is highly sensitive to specimen flaws. When filler is added, the tensile modulus is increased and ductility is reduced. In

compression, addition of 5 vol% of filler increases the compressive properties, while 10 vol% causes the properties to drop.

**Table 4-4: Mechanical Properties of High-T<sub>g</sub> Composites**

Mean ± 95% Confidence Interval

Material	Tensile Modulus MPa	Tensile Energy kJ/m <sup>3</sup>	Compressive Modulus MPa	Compressive Yield Strength MPa	Compressive Flow Stress MPa
PVC	2810 ± 70	803 ± 136	2730 ± 100	73.9 ± 1.3	61.3 ± 0.7
5 vol% filler	3340 ± 180	267 ± 102	2920 ± 180	78.2 ± 1.6	64.8 ± 0.3
10 vol% filler	3510 ± 170	300 ± 49	2620 ± 150	61.8 ± 2.3	56.9 ± 2.1
20 vol% filler	*3300 ± 290	*95 ± 224	*1030 ± 170	*24.8 ± 2.0	*24.8.3 ± 2.0
Blend 36/57.5/6.5	2840 ± 100	115 ± 16	2920 ± 140	87.2 ± 1.0	61.7 ± 0.5
5 vol% filler	3410 ± 80	130 ± 90	3170 ± 80	92.2 ± 3.1	72.2 ± 2.4
10 vol% filler	3900 ± 40	155 ± 61	2750 ± 90	72.5 ± 0.8	61.2 ± 1.2
20 vol% filler	4790 ± 220	70 ± 35	2350 ± 100	76.2 ± 2.7	69.1 ± 2.1

\* The 20 vol% composite of PVC was extremely degraded.

**Figure 4-8: Tensile Properties for Composites of PVC**

Nominal strain rate = 0.001 sec<sup>-1</sup>

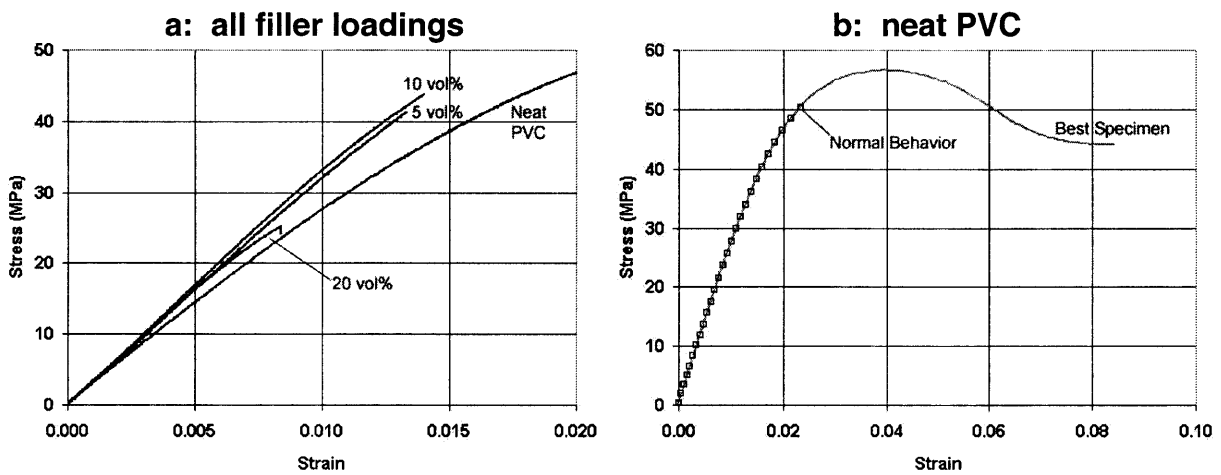
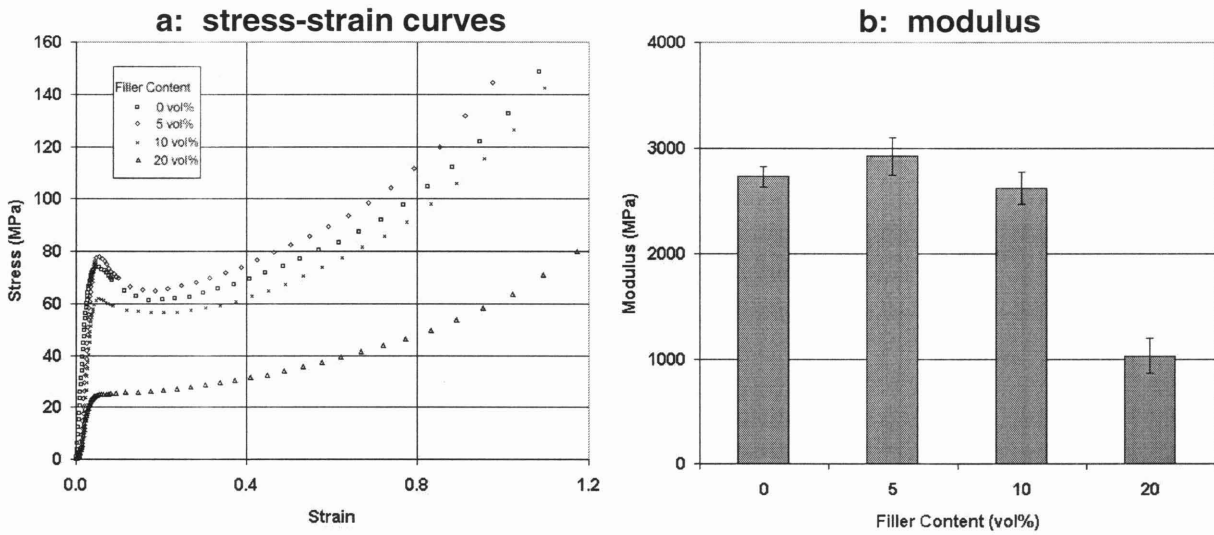


**Figure 4-9: Compressive Properties for Composites of PVC**

Nominal strain rate =  $0.001 \text{ sec}^{-1}$



Tensile curves for composites based on blend 36/57.5/6.5 are shown in Figure 4-10, and compressive properties are shown in Figure 4-11. The neat blend and its composites are quite brittle in tension, all breaking at a strain of less than 0.01. The tensile modulus increases steadily with filler content. The compressive behavior is similar to the PVC-based series, with properties increasing slightly for 5 vol% and then dropping for higher loadings.

**Figure 4-10: Tensile Properties for Composites of Blend 36/57.5/6.5**

Nominal strain rate =  $0.001 \text{ sec}^{-1}$

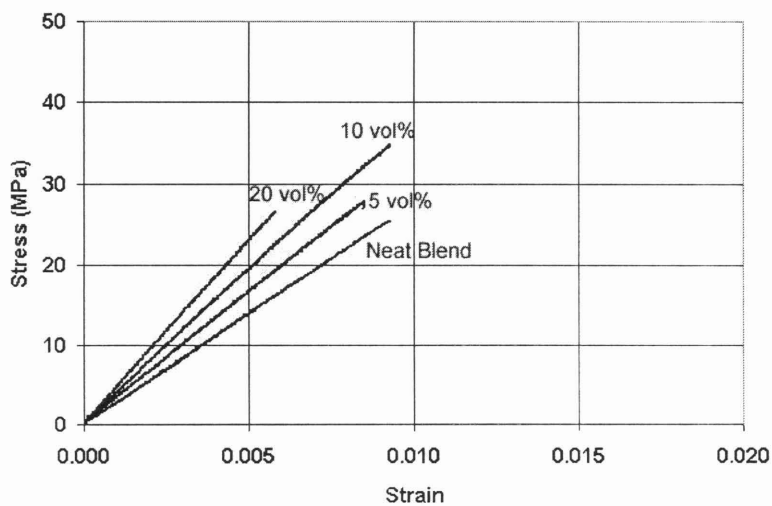
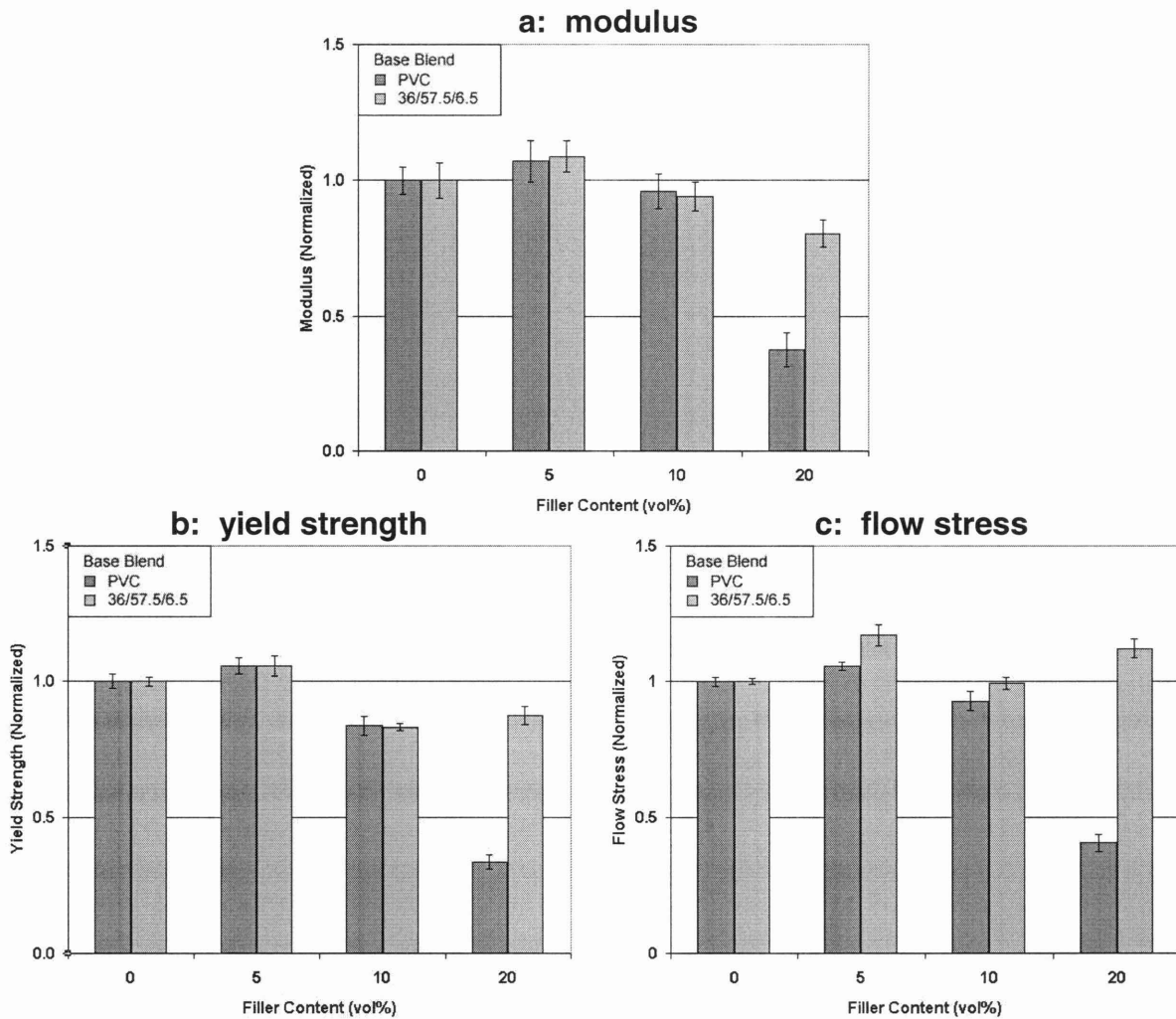


**Figure 4-11: Compressive Properties for Composites of Blend 36/57.5/6.5**

Nominal strain rate =  $0.001 \text{ sec}^{-1}$



Normalized tensile and compressive properties for the high- $T_g$  composites are shown in Figures 4-12 and 4-13, respectively.

**Figure 4-12: Tensile Properties for High-T<sub>g</sub> Composites**

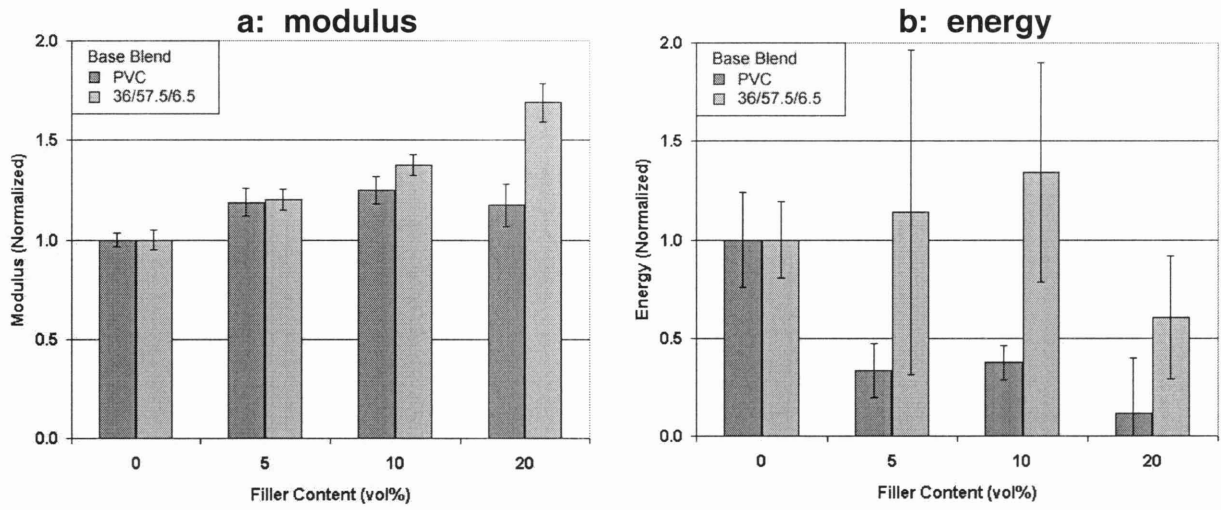
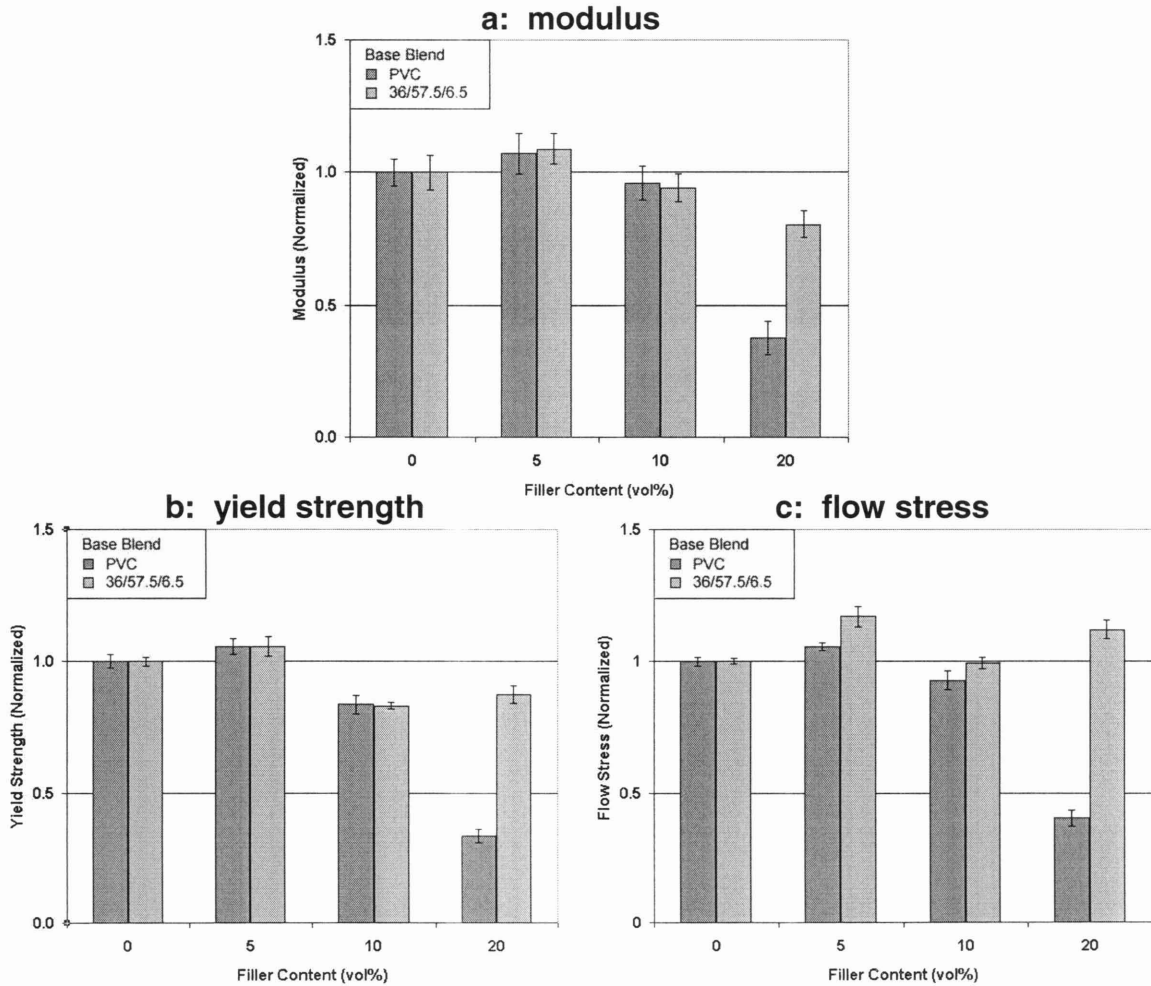


**Figure 4-13: Compressive Properties for High-T<sub>g</sub> Composites**





### 4.3.3 Low- $T_g$ Series

Similarly to the previous section, a series of blends was formulated with a  $T_g$  of approximately 30°C. Compositions and properties of the blends are shown in Table 4-5. Blend 0/85/15 and blend 30/48.1/21.9 were chosen for the filler toughening study, but only results for the former will be presented here. The latter will be discussed in the next section due to its morphological peculiarities.

**Table 4-5: Properties of Low- $T_g$  Blends**

Mean $\pm$ 95% Confidence Interval								
$F_{PMMA}$	$F_{PVC}$	$F_{DOP}$	$T_g$	Tensile Modulus	Tensile Energy	Compr Modulus	Compr Yield Strength	Compr Flow Stress
wt%	wt%	wt%	°C	MPa	kJ/m <sup>3</sup>	MPa	MPa	MPa
0	85	15	33.3	920 $\pm$ 60	21,800 $\pm$ 6200	1220 $\pm$ 110	39.0 $\pm$ 1.7	33.8 $\pm$ 2.0
30	48.1	21.9	31.6	390 $\pm$ 60	4980 $\pm$ 1000	600 $\pm$ 60	*15.2 $\pm$ 1.6	*15.2 $\pm$ 1.6

\* Blend 30/48.1/21.9 did not show a stress peak in compression, so the yield strength and flow stress were computed using the 0.2% offset method.

**Table 4-6: Properties of Composites Based on Blend 0/85/15**

Mean $\pm$ 95% Confidence Interval					
Filler Content	Tensile Modulus	Tensile Energy	Compressive Modulus	Compressive Yield Strength	Compressive Flow Stress
vol%	MPa	kJ/m <sup>3</sup>	MPa	MPa	MPa
0	920 $\pm$ 60	21,800 $\pm$ 6200	1220 $\pm$ 110	39.0 $\pm$ 1.7	33.8 $\pm$ 2.0
5	830 $\pm$ 100	16,000 $\pm$ 4000	1160 $\pm$ 120	33.4 $\pm$ 0.8	31.1 $\pm$ 0.1
10	1160 $\pm$ 50	4450 $\pm$ 1410	1340 $\pm$ 80	35.9 $\pm$ 1.0	33.3 $\pm$ 0.6
20	1860 $\pm$ 180	1490 $\pm$ 810	1690 $\pm$ 40	40.1 $\pm$ 2.3	37.9 $\pm$ 1.7

Tensile results for composites based on blend 0/85/15 are plotted in Figure 4-14. This blend has a  $T_g$  quite close to room temperature ( $\sim$ 33°C), and the increasing chain mobility is reflected in the greater ductility it exhibits in tension. The neat blend is by far the toughest

material tested in this study. Regrettably, the addition of filler leads to a steady decrease in the tensile energy (Fig 4-15).

**Figure 4-14: Tensile Curves for Composites of Blend 0/85/15**  
Nominal strain rate = 0.001 sec<sup>-1</sup>

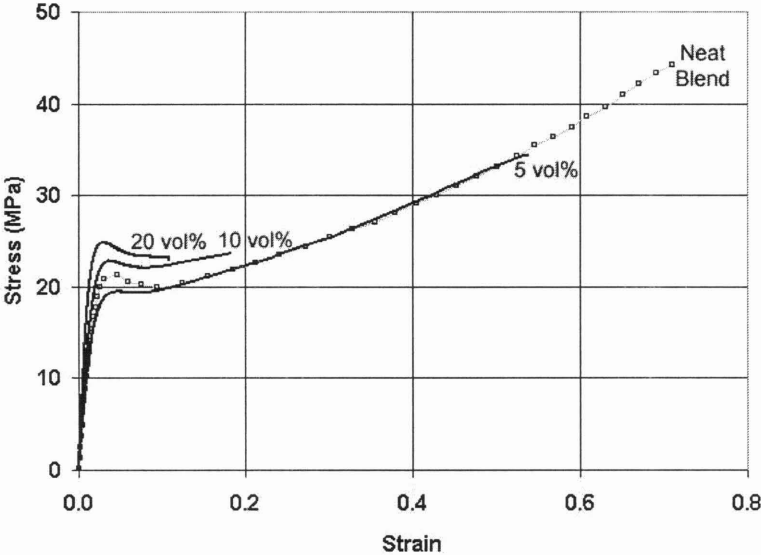
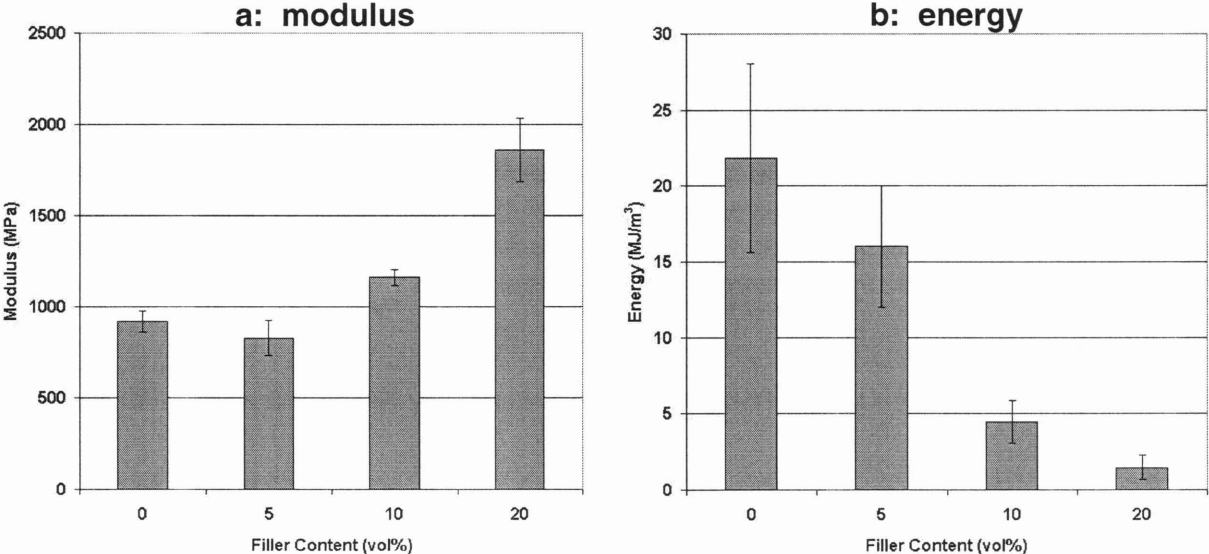


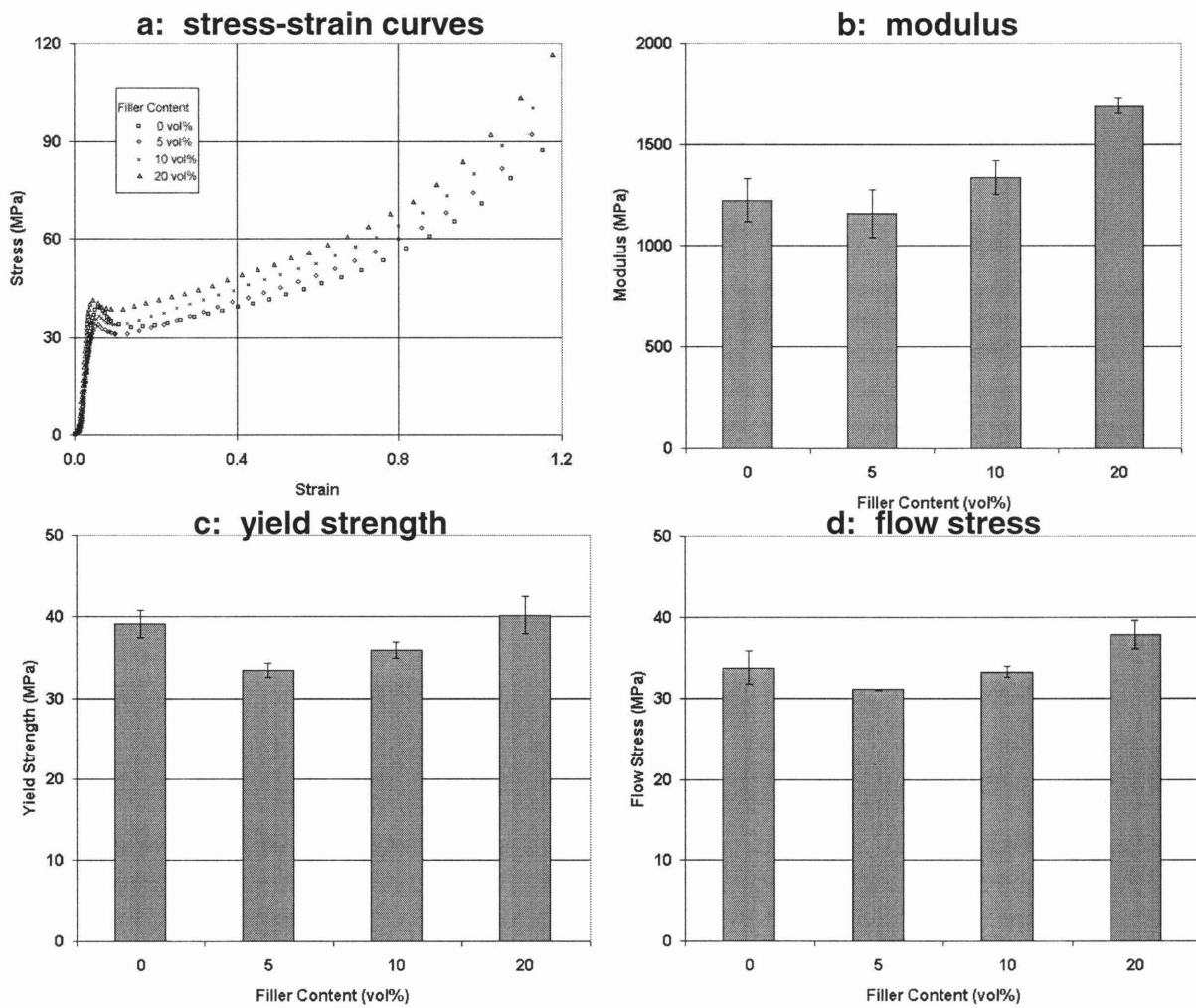
**Figure 4-15: Tensile Properties for Composites of Blend 0/85/15**



Compressive properties for this series of composites are plotted in Figure 4-16. The property trends for this system are opposite to those seen in the middle- and high- $T_g$  blends. Properties hold constant or decrease for 5 vol% filler, and then rise for higher loadings.

**Figure 4-16: Compressive Properties for Composites of Blend 0/85/15**

Nominal strain rate =  $0.001 \text{ sec}^{-1}$



#### 4.3.4 Peculiarities of High-PMMA Ternary Blends

Two of the blends chosen for this filler toughening study were blend 31.2/50/18.8 ( $T_g \sim 40^\circ\text{C}$ ) and blend 30/48.1/21.9 ( $T_g \sim 30^\circ\text{C}$ ). The former was studied in Chapter 2, and

appeared to be homogeneous in TEM. However, examination on a larger scale in SEM showed morphological features that did not appear to be filler. Similar features appeared in the latter blend. SEM photos of these two blends are shown in Figure 4-17. The same type of feature appears in most composites based on these two blends (with one notable exception that will be discussed below). For example, photos of the 10 vol% composite based on blend 31.2/50/18.8 are shown in Figure 4-18. The high-magnification photo focuses on one of the dark areas, and shows that these regions are devoid of filler particles.

**Figure 4-17: Morphology of High-PMMA Blends**

**a: blend 31.2/50/18.8**

**b: blend 30/48.1/21.9**

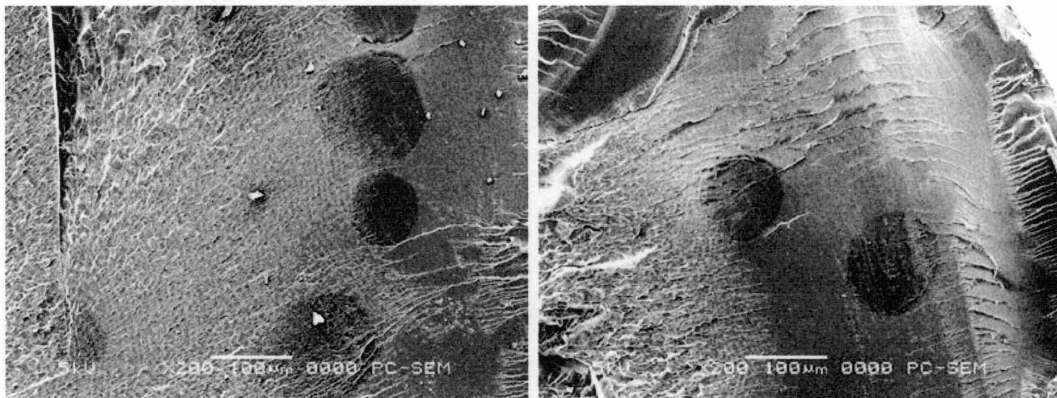
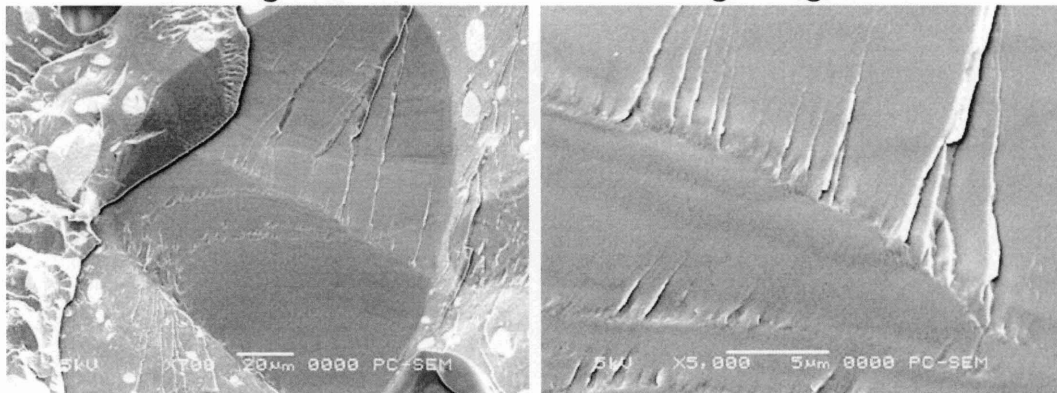


**Figure 4-18: Morphology of High-PMMA Composite**

**a: low magnification**

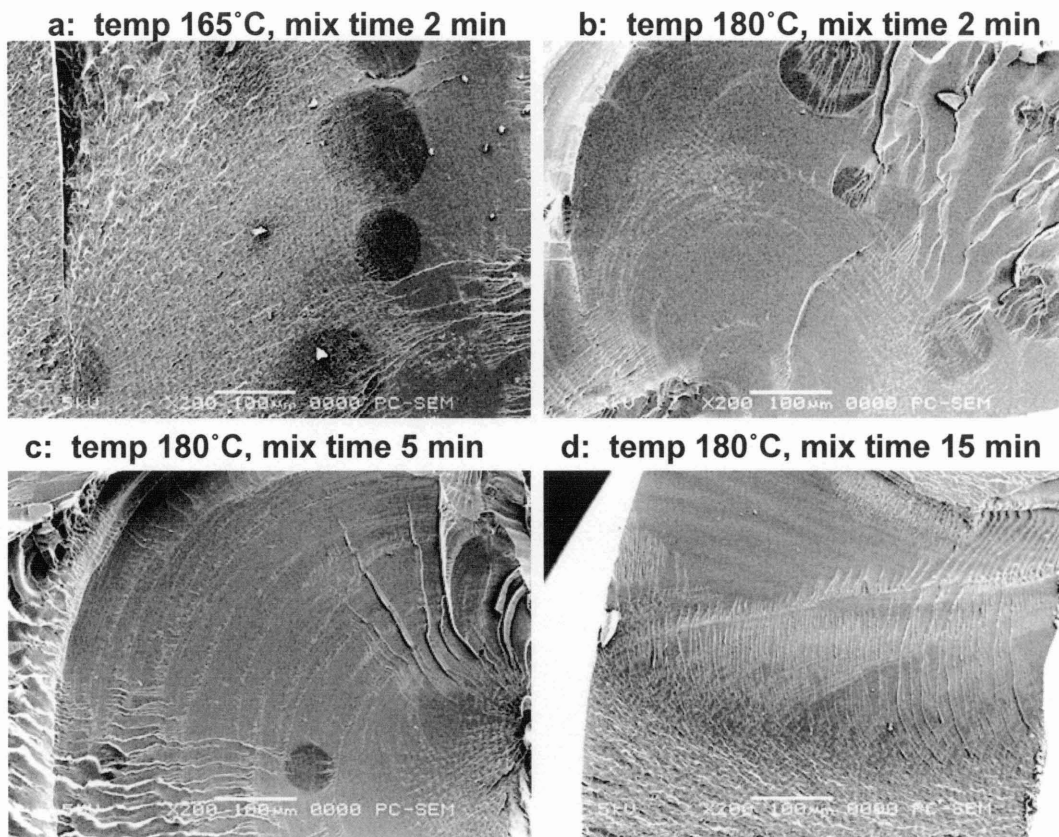
**b: high magnification**



The exclusion of filler particles suggests that these moieties occur due to insufficient mixing during the extrusion step. To test this hypothesis, a series of processing runs were performed at higher temperature (180°C, where 165°C was the prior standard) and longer mix times (5 min and 15 min, as well as the standard 2 min). As the mixing time was increased, extruded strand specimens became visibly smoother in texture. When viewed in SEM (Fig 4-19), these specimens show a steadily diminishing occurrence of dark spots. For a mixing time of 15 min, no dark spots were visible on the viewed surface. Particle size analysis, analogous to the method used in Chapter 3 to characterize filler particles, gave the results shown in Figure 4-20. As well as decreasing in area occupied, the particles decrease in diameter.

**Figure 4-19: Effect of Processing Conditions on Morphology**

Blend 31.2/50/18.8



There are two reasonable explanations for the presence of the dark moieties. First, they could indicate the formation of a second, thermodynamically stable phase within the blend. Second, they could be grains that were present from the beginning of the mixing process, unblended due to insufficient kinetic driving forces. There are several difficulties with the first case. The sparse and uneven distribution of the moieties would be unlikely to form during such short mixing times. The nucleation of the moieties would have to be highly disfavored, and the growth very fast, to show such a coarse phase structure. Also, one would expect increased processing temperature and time to lead to further nucleation and coarsening in this case; we see just the opposite. Finally, in order to explain the exclusion of filler particles from the moieties, one would need to stipulate that the surface energy of the particles in these areas be much higher than in the surrounding matrix.

The second explanation, that the moieties were present initially and failed to mix in, fits the results much better. The coarse distribution would be expected in this case, and one would expect material to be gradually stripped away as processing conditions intensify, as indicated by the decreasing diameter. The exclusion of filler would also be a natural consequence of this case.

Given these arguments, it seems probable that the dark moieties found in these systems are actually unmelted PMMA beads. An SEM photograph of the neat PMMA used in this study is shown in Figure 4-20. As shown in the particle characterization (Fig 4-21), the moieties are similar in size to the beads, and the somewhat smaller size could be explained by partial mixing of the outermost bead material. This is further supported by the variation in DSC behavior with changing processing conditions (Fig 4-22). The  $T_g$  of the blend rises with increased mixing

intensity, indicating that the fraction of high- $T_g$  material is increasing. Also, the appearance of features around the  $T_g$  of PMMA ( $\sim 117^\circ\text{C}$ ) diminishes with mixing time.

**Figure 4-20: PMMA Beads**

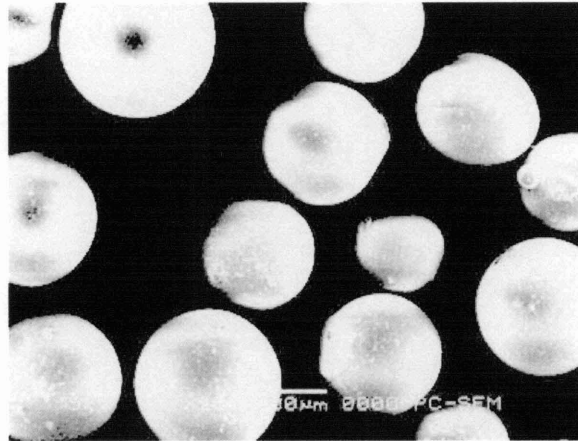


**Figure 4-21: Characterization of Dark Regions**  
From SEM image analysis

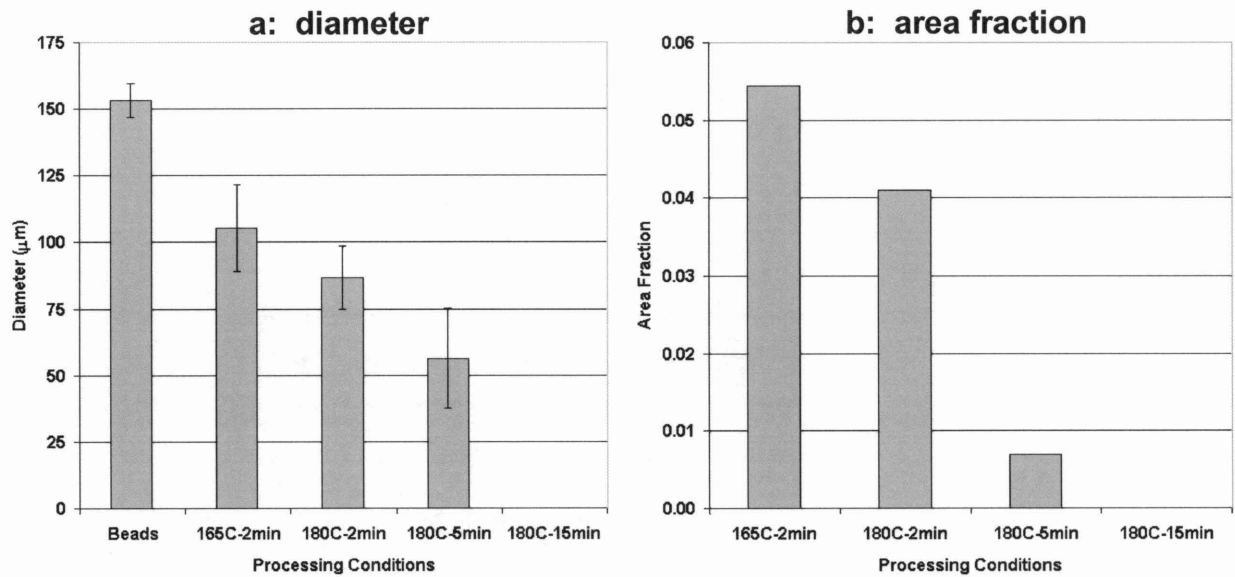
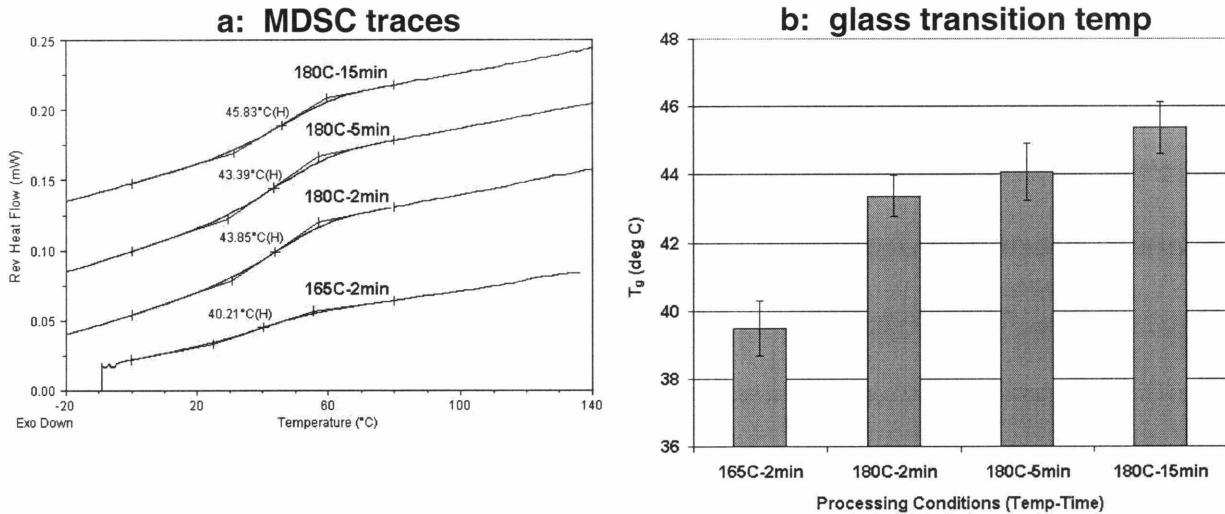


Figure 4-22: Effect of Processing Conditions on MDSC Behavior



Addition of filler appears to intensify mixing in these materials, as evidenced by the lack of unmixed beads in the 20 vol% composite based on blend 31.2/50/18.8 (Fig 4-23a). This is presumably due the increased viscosity of the mixture as filler is added, which forces the extruder motor to exert more torque in order to maintain screw speed, and hence imparting more specific mechanical energy to the material. Unmixed beads do appear in the 20 vol% composite based on blend 30/48.1/21.9 (Fig 4-23b), possibly due to the lower processing temperature (160°C) used for this material. It is interesting to note that when tested in tension, the 20 vol% composite based on blend 31.2/50/18.8 exhibited much greater ductility than those based on the other middle-T<sub>g</sub> blends (Fig 4-24). This suggests that the other composites of this blend, when mixed at appropriate conditions, may show even tougher behavior.



### Figure 4-23: Morphology of Heavily-Filled Composites

Tensile specimens of 20 vol% composites

a: base blend 31.2/50/18.8

b: base blend 30/48.1/21.9

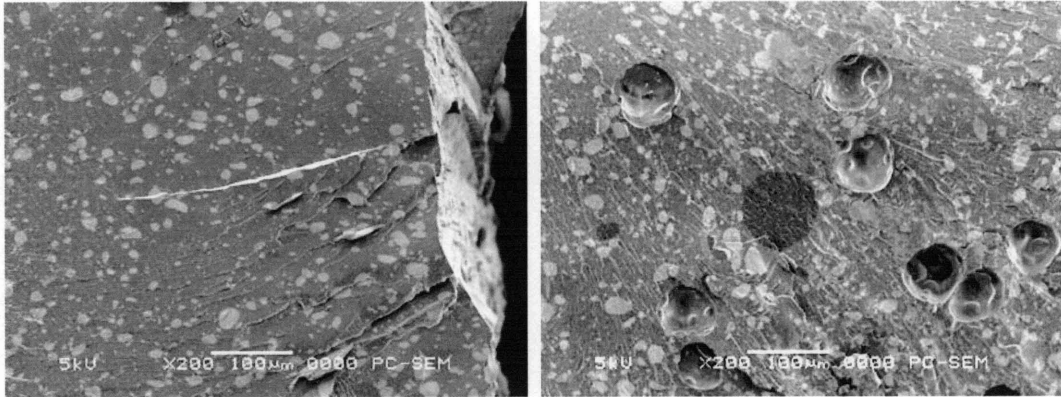
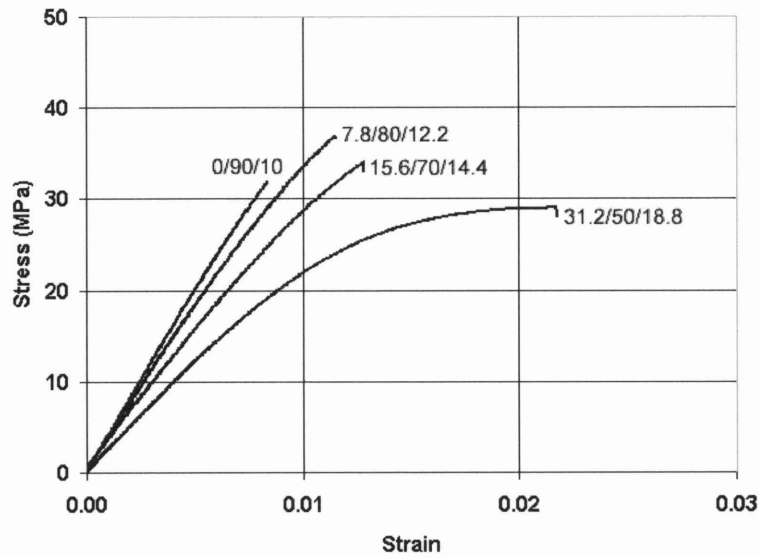


### Figure 4-24: Tensile Behavior of Heavily-Filled Composites

Filler content 20 vol%



Although the blends in question appear to be miscible in principle, in practice their homogeneity is highly dependent on the intensity of mixing during extrusion. The major factors affecting the mixing process are the temperature, mixing time, and filler content.

#### 4.4 Discussion

In this study, the middle- $T_g$  ( $\sim 40^\circ\text{C}$ ) blend series was the only one that showed successful hard-particle toughening. The low- $T_g$  ( $\sim 30^\circ\text{C}$ ) blends were quite ductile in tension when unfilled but were embrittled by the addition of filler. The high- $T_g$  ( $\sim 70^\circ\text{C}$ ) blends were generally brittle in tension, and were not afforded any additional ductility by the filler.

Within the middle- $T_g$  series, blend 0/90/10 delivered the greatest improvements due to filler. At 5 vol% of filler, several tensile specimens showed a large increase in ductility and a 19-fold increase in tensile energy. The tough macroscopic behavior coincided with debonding and internal fracture of the filler agglomerates in the material (as seen via SEM), phenomena that were not discernable in brittle specimens of the same material or for higher filler loadings. This type of behavior was also seen in a 10 vol% composite specimen based on blend 7.8/80/12.2. The tensile energy increase was smaller for this case, roughly 6-fold over the base blend, and the degree of debonding and void formation was correspondingly lower. Minimal toughness increases were seen in the third system investigated, blend 15.6/70/14.4.

As discussed in Section 1.2, the mechanism of particle debonding and void formation has been observed in several other studies of hard-particle toughening, and is thought to have an analogous effect to the debonding or cavitation of soft particles in rubber-modified thermoplastics. As voids are formed, the matrix is divided into thin ligaments that, if below a certain critical thickness, are able to yield, stretch, and dissipate mechanical energy more readily than the bulk polymer [4]. If the deformation occurs over a significant portion of the specimen rather than being highly localized, a large improvement in macroscopic toughness can result.

It has been shown in the literature that for miscible blends, the critical thickness value increases for greater entanglement density [14]. Direct measurement of entanglement density

values could not be accomplished for these blends due to their nonlinear rheological behavior and rapid degradation at high temperature. For this reason, computer simulation and basic entanglement theory were used to predict entanglement molecular weight values for these blends (Table 2-7). Blend 0/90/10 was found to have the lowest expected  $M_e$  value, and hence the highest entanglement density. It follows that this blend should have the highest critical thickness, and that appears to be the case because 0/90/10 required a smaller amount of filler than 7.8/80/12.2 to reach the greatest increase in toughening.

From the results presented in Section 3.3.2, it appears that neat PVC has significant potential for ductility, but is highly sensitive to specimen flaws. It has been shown in the literature that PVC is notch sensitive, and fails via crazing in such cases [36]. This may explain why no toughening is seen in PVC with the addition of hard particles. The early fracture in these systems may be initiated by filler agglomerates, surface flaws in the specimens, or both. In any case, the results imply that plasticized PVC (e.g. blend 0/90/10) is less susceptible to flaw-induced failure than neat PVC. This may be simply a consequence of increased chain mobility, which allows the polymer to redistribute load around a crack tip more readily [37].

## 5. CONCLUSION

### 5.1. Summary of Thesis Contributions

The primary goal of this work is to show that a miscible polymer blend system, in this case PMMA-PVC-DOP, is a powerful tool for the study of toughening behavior in particle-filled systems. Chapter 2 shows that this blend has a significant region of miscibility in the PVC-rich domain, and that the glass transition temperatures for the miscible region fit well to a simple empirical model, facilitating prediction of a constant- $T_g$  series. Mechanical properties, such as modulus and yield strength, were shown to vary significantly across constant- $T_g$  blend series.

Chapter 3 focuses on a single blend, and shows that significant toughening can be achieved through the addition of hard particle fillers without significant loss in modulus. SEM photographs show evidence of filler agglomerates in the 1-10  $\mu\text{m}$  range both debonding from the matrix and undergoing internal fracture. Both processes give rise to void space within the material, allowing greater freedom for deformation. Well-dispersed 100 nm particles remain bonded to the matrix even at large macroscopic deformation, and do not appear to initiate void formation. Consequently, this type of filler should be considered as two separate materials: the well-dispersed particles behave as a homogeneously-blended additive, while the agglomerates behave as a second phase of non-rigid particles.

Chapter 4 demonstrates large differences in mechanical behavior of composites depending on the properties of the polymer matrix. Middle- $T_g$  ( $\sim 40^\circ\text{C}$ ) blends show the most potential for particle toughening, and toughening was achieved more readily (i.e. with a smaller amount of filler) in blends with higher entanglement density. High- $T_g$  ( $\sim 70^\circ\text{C}$ ) blends remained brittle with the addition of filler. Low- $T_g$  ( $\sim 30^\circ\text{C}$ ) blends were tough when unmodified, and

hence did not require additives for toughening. They became less ductile with increasing filler content.

## 5.2. Future Work

There are many opportunities for future work in this area. The present work should be extended to include high-rate mechanical testing, such as Izod impact and/or split Hopkinson pressure bar experiments. These methods would evaluate the robustness of the toughening in this system for harsh conditions. More filler loadings should be mixed in order to optimize toughening, especially in blends 0/90/10 and 7.8/80/12.2, which showed significant potential for toughening. In order to simplify the system, new composites should also be made using larger, more uniform filler particles that will be easier to disperse. New blend matrix space could be explored using an alternative plasticizer, such as dibutyl phthalate.

Efforts should be made to improve the dispersion of the barium sulfate filler. Treatment with polar chemicals such as methyl methacrylate may help improve the compatibility of the particles with the matrix. Longer processing times may also help. If better dispersion can be achieved, then perhaps a mixture of fillers could be used: nanoscale fillers for hardening, and microscale fillers to initiate voids.

Further toughening studies should be done on blends 31.2/50/18.8 ( $T_g \sim 40^\circ\text{C}$ ) and 30/48.1/21.9 ( $T_g \sim 30^\circ\text{C}$ ). As discussed in Chapter 4, these blends were found to be heterogeneous on a coarse scale when mixed at standard conditions. Further experiments showed the former blend to become homogeneous when mixed at higher temperature ( $180^\circ\text{C}$  instead of  $165^\circ\text{C}$ ) for a longer time (15 min instead of 2 min), or at high filler loadings. In general, blends containing significant amounts of PMMA should be processed at a temperature of  $180^\circ\text{C}$  or higher, and mixing time should be scaled relative to PMMA content. Since the filler appears to act as a mixing aid, mixing time could be reduced for highly filled blends.

Computer simulation of this system could yield a greater understanding of the governing mechanisms. Especially interesting would be a model of the deformation of filler clusters within the material, in order to compare behavior in tensile and compressive deformation modes.

## BIOGRAPHICAL NOTE

Roger Lockwood Aronow was born in San Francisco, CA, and graduated from Lowell High School in 1996. He attended the University of California at Santa Barbara from Fall 1996 through Spring 2000, earning a Bachelor of Science degree in Chemical Engineering. He served as president for the campus chapter of the Golden Key International Honor Society and vice president of Tau Beta Pi California Sigma chapter. Summer work experience included research in the Department of Chemistry (1998) and an internship at NuSil Technologies (Carpinteria, CA, 1999). He graduated with Highest Honors at class rank 1 for the College of Engineering, and was awarded Outstanding Senior Student in Chemical Engineering and the Hynes/Wood Student Activities Award.

In Fall 2000, Roger entered the doctoral program in the Department of Chemical Engineering at MIT. He attended the David H. Koch School of Chemical Engineering Practice in Fall 2001, conducting projects in process optimization at Cabot Corporation (Billerica, MA) and General Mills, Inc. (Minneapolis, MN), and received a Master of Chemical Engineering Practice degree. He subsequently began work as a graduate researcher in the laboratory of Professor Robert E. Cohen on a thesis project entitled "Toughening Mechanisms in Composites of Miscible Polymer Blends with Rigid Filler Particles".



## REFERENCES

1. Ash, B.J., R.W. Siegel, and L.S. Schadler, *Mechanical Behavior of Alumina/Poly(methyl methacrylate) Nanocomposites*. *Macromolecules*, 2004. **37**: p. 1358-1369.
2. Kontou, E. and G. Spathis, *Structural Rearrangements During Yielding of Glassy Polymers*. *Polymer Engineering and Science*, 1998. **38**(9): p. 1443-1449.
3. Treloar, L.R.G., *Stress-strain data for vulcanized rubber under various types of deformation*. *Transactions of the Faraday Society*, 1944. **40**: p. 59.
4. Wu, S., *Phase structure and adhesion in polymer blends: A criterion for rubber toughening*. *Polymer*, 1985. **26**: p. 1855-1863.
5. van der Sanden, M.C.M., H.E.H. Meijer, and P.J. Lemstra, *Deformation and toughness of polymeric systems: 1. The concept of a critical thickness*. *Polymer*, 1993. **34**(10): p. 2148-2154.
6. Bartczak, Z., et al., *Toughness Mechanism in Semi-Crystalline Polymer Blends: I. High-Density Polyethylene Toughened with Rubbers*. *Polymer*, 1999. **40**: p. 2331-2346.
7. Stricker, F., Y. Thomann, and R. Mulhaupt, *Influence of Rubber Particle Size on Mechanical Properties of Polypropylene-SEBS Blends*. *Journal of Applied Polymer Science*, 1998. **68**: p. 1891-1901.
8. Bartczak, Z., et al., *Toughness mechanism in semi-crystalline polymer blends: II. High-density polyethylene toughened with calcium carbonate filler particles*. *Polymer*, 1999. **40**: p. 2347-2365.
9. Wu, S., *A Generalized Criterion for Rubber Toughening: The Critical Matrix Ligament Thickness*. *Journal of Applied Polymer Science*, 1988. **35**: p. 549-561.
10. Muratoglu, O.K., et al., *Toughening Mechanism of Rubber-Modified Polyamides*. *Polymer*, 1995. **36**(5): p. 921-930.
11. Lin, L. and A.S. Argon, *Deformation Resistance in Oriented Nylon 6*. *Macromolecules*, 1992. **25**(15): p. 4011-4024.
12. Thio, Y.S., *Toughening Mechanisms in Polypropylene Filled with Rigid Particles*, in *Chemical Engineering*. 2003, Massachusetts Institute of Technology: Cambridge, MA.
13. Ferry, J.D., *Viscoelastic Properties of Polymers*. 1980, New York: Wiley.
14. van der Sanden, M.C.M., H.E.H. Meijer, and T.A. Tervoort, *Deformation and toughness of polymeric systems: 2. Influence of entanglement density*. *Polymer*, 1993. **34**(14): p. 2961-2970.
15. Schurer, J.W., A. de Boer, and G. Challa, *Influence of tacticity of poly(methyl methacrylate) on the compatibility with poly(vinyl chloride)*. *Polymer*, 1975. **16**: p. 201-204.
16. Vanderschueren, J., et al., *Effect of tacticity on the transition behaviour of poly(methyl methacrylate)/poly(vinyl chloride) blends. Thermally stimulated depolarization study*. *Polymer*, 1982. **23**: p. 395-400.
17. Vorenkamp, E.J., et al., *Influence of the tacticity of poly(methyl methacrylate) on the miscibility with poly(vinyl chloride)*. *Polymer*, 1985. **26**: p. 1725-1732.
18. Lemieux, E., et al., *Influence of the Tacticity of Poly(methyl methacrylate) on Its Miscibility with Chlorinated Polymers*. *Macromol*, 1988. **21**: p. 2148-2154.
19. Jager, H., E.J. Vorenkamp, and G. Challa, *LCST behaviour in blends of PMMA with PVC*. *Polym Comm*, 1983. **24**: p. 290-292.

20. Belhaneche-Bensemra, N., A. Bedda, and B. Belaabed, *Study of the Properties of Rigid and Plasticized PVC/PMMA Blends*. Macromol Symp, 2003. **202**: p. 151-165.
21. Thomas, L.C., *Use of multiple heating rate DSC and modulated temperature DSC to detect and analyze temperature-time-dependent transitions in materials*. American Laboratory, 2001. **33**(1): p. 26.
22. Razinskaya, I.N., et al., *Study of Compatibility Assessments and of the Phase State of Polymer Mixtures*. Polym Sci USSR, 1972. **14**: p. 1079-1086.
23. Tsenoglou, C., *Network Architecture and Modulus of Miscible Heteropolymer Blends*. Journal of Polymer Science: Part B: Polymer Physics, 1988. **26**: p. 2329-2339.
24. Thio, Y.S., et al., *Toughening of isotactic polypropylene with CaCO<sub>3</sub> particles*. Polymer, 2002. **43**: p. 3661-3674.
25. Lazzeri, A., Y.S. Thio, and R.E. Cohen, *Volume Strain Measurements on CaCO<sub>3</sub>/Polypropylene Particulate Composites: The Effect of Particle Size*. Journal of Applied Polymer Science, 2004. **91**: p. 925-935.
26. Hertzberg, R.W., *Deformation and Fracture Mechanics of Engineering Materials*. 4 ed. 1996, Hoboken, NJ: John Wiley & Sons, Inc. 786.
27. Zhuk, A.V., et al., *Debonding microprocesses and interfacial strength in particle-filled polymer materials*. Journal of Materials Science, 1993. **28**: p. 4595-4606.
28. Guth, E., *Theory of Filler Reinforcement*. Journal of Applied Physics, 1945. **16**: p. 20-25.
29. Spitzig, W.A. and O. Richmond, *Effect of Hydrostatic Pressure on the Deformation Behavior of Polyethylene and Polycarbonate in Tension and in Compression*. Polymer Engineering and Science, 1979. **19**(16): p. 1129-1139.
30. Wu, S., *Entanglement, Friction, and Free Volume Between Dissimilar Chains in Compatible Polymer Blends*. Journal of Polymer Science: Part B: Polymer Physics, 1987. **25**: p. 2511-2529.
31. Graessley, W.W. and S.F. Edwards, *Entanglement interactions in polymers and the chain contour concentration*. Polymer, 1981. **22**(10): p. 1329-1334.
32. Lomellini, P., *On the plateau modulus mixing rule of miscible blends*. Macromol Theory Simul, 1994. **3**: p. 567-574.
33. Prest, W.M.J. and R.S. Porter, *Rheological Properties of Poly(2,6-dimethylphenylene Oxide)-Polystyrene Blends*. Journal of Polymer Science: Part A-2, 1972. **10**: p. 1639-1655.
34. Wisniewsky, C., G. Marin, and P. Monge, *Viscoelastic behavior of compatible polymer blends: Polystyrene/tetramethylpolycarbonate*. European Polymer Journal, 1984. **20**(7): p. 691-695.
35. Wu, S., *Chain entanglement and melt viscosity of compatible polymer blends: poly(methyl methacrylate) and poly(styrene-acrylonitrile)*. Polymer, 1987. **28**(7): p. 1144-1148.
36. Narisawa, I., M. Ishikawa, and H. Ogawa, *Notch brittleness of ductile glassy polymers under plane strain*. Journal of Materials Science, 1980. **15**(8): p. 2059-2065.
37. Kramer, E.J., *Microscopic and molecular fundamentals of crazing*, in *Advances in Polymer Science*, H.H. Kausch, Editor. 1983, Springer-Verlag: Berlin. p. 1-56.

**Figure 2-2: Transmission Electron Micrographs of Binary Blends**

Labels are composition in wt% PMMA/PVC; each image shows a 1-micron square.

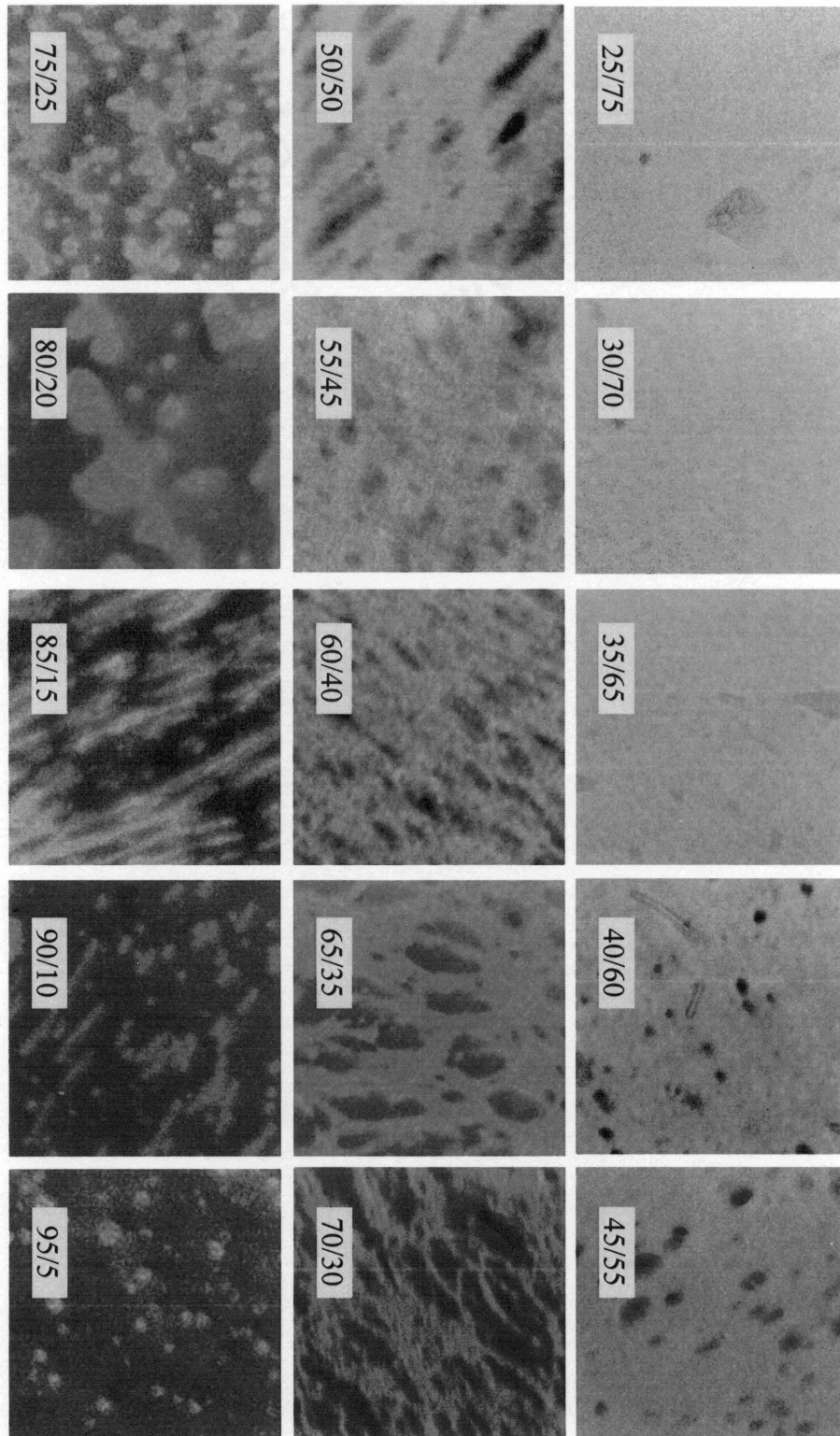
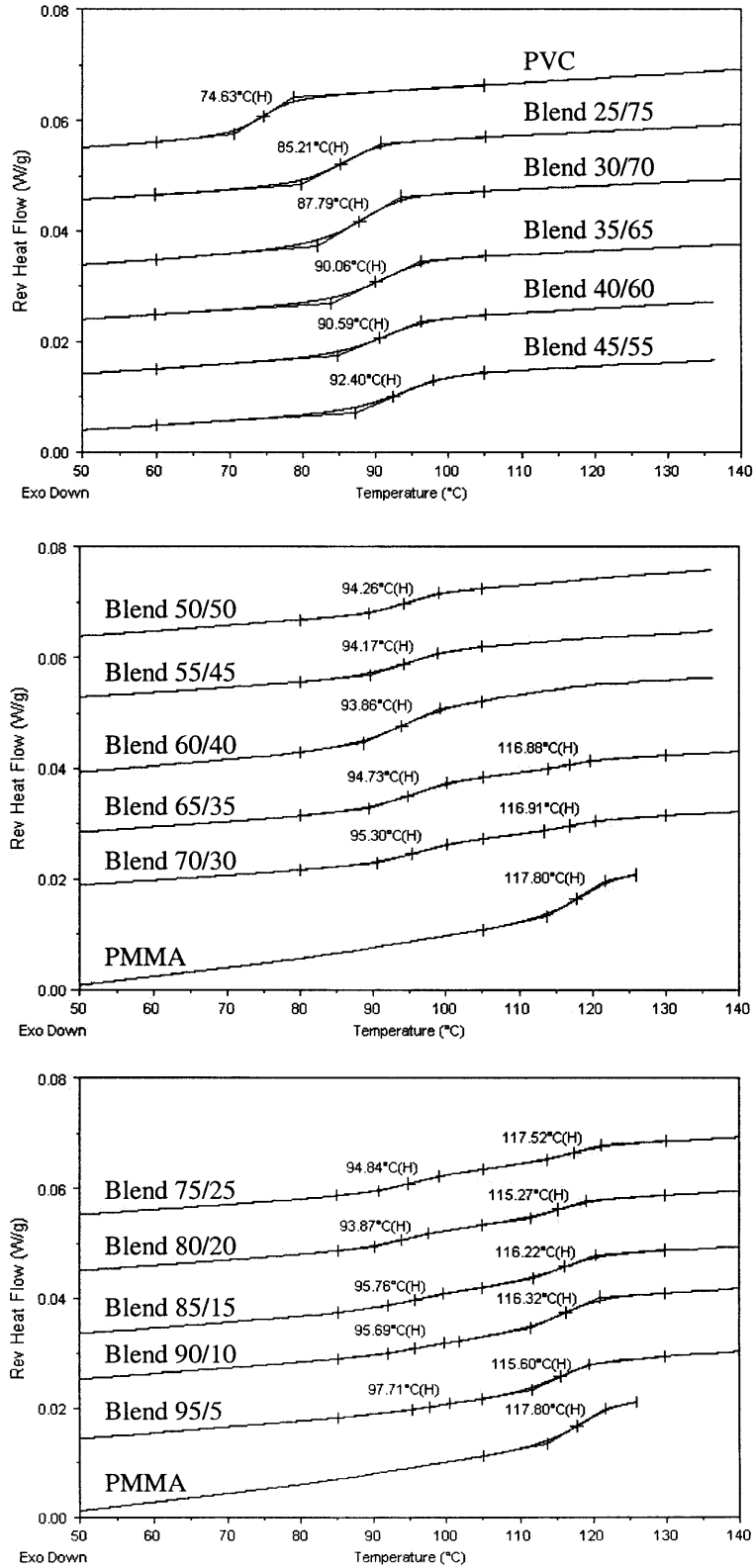


### Figure 2-3: DSC Traces for Binary Blends

Labels are composition in wt% PMMA/PVC; all tests carried out at 2°C/min, with an initial annealing step (see Methods).



Labels are composition in wt% PMMA/PVC/DOP; each image shows a 1-micron square.

